Universidade Federal do Rio Grande – FURG
Instituto de Oceanografia

Programa de Pós-Graduação em Oceanografia Física, Química e Geológica

CLIMA DE ONDAS NO OCEANO ATLÂNTICO SUL: TENDÊNCIAS, EXTREMOS E RELAÇÕES COM MODOS DE VARIABILIDADE CLIMÁTICA

NATAN ZAMBRONI MAIA

Tese apresentada ao PPGOCFQG, como parte dos requisitos para a obtenção do Título de Doutor.

Orientador: *Prof. Dr*. Lauro Calliari

Universidade Federal do Rio Grande (FURG), Brasil

Coorientador: *Prof. Dr*. Luis Pedro Almeida

Universidade Federal do Rio Grande (FURG), Brasil / CoLAB +Atlantic, Portugal

Rio Grande, RS, Brasil

Maio, 2023

CLIMA DE ONDAS NO OCEANO ATÂNTICO SUL: TENDÊNCIAS, EXTREMOS E RELAÇÕES COM MODOS DE VARIABILIDADE CLIMÁTICA

Tese apresentada ao PPGOCFQG, como parte dos requisitos para a obtenção do Título de Doutor.

por

NATAN ZAMBRONI MAIA

Rio Grande, RS, Brasil

Maio, 2023

© A cópia parcial e a citação de trechos desta tese são permitidas sobre a condição de que qualquer pessoa que a consulte reconheça os direitos autorais do autor. Nenhuma informação derivada direta ou indiretamente desta obra deve ser publicada sem o consentimento prévio e por escrito do autor

Ficha Catalográfica

M217c Maia, Natan Zambroni.
Clima de ondas no Oceano Atlântico Sul: tendências, extremos e relações com modos de variabilidade climática / Natan Zambroni Maia. – 2023.
103 f.

Tese (doutorado) – Universidade Federal do Rio Grande – FURG, Programa de Pós-Graduação em Oceanografia Física, Química e Geológica, Rio Grande/RS, 2023.
Orientador: Dr. Lauro Calliari.
Coorientador: Dr. Luis Pedro Almeida.

1. Ondas de tempestade 2. Tendências de longo termo 3. Variabilidade interanua 4. Variabilidade multidecadal 5. AMO 6. TSA 7. SAM I. Calliari, Lauro II. Almeida, Luis Pedro III. Título.

CDU 551.46

Catalogação na Fonte: Bibliotecário José Paulo dos Santos CRB 10/2344

UNIVERSIDADE FEDERAL DO RIO GRANDE - FURG
IO – INSTITUTO DE OCEANOGRAFIA
PROGRAMA DE PÓS-GRADUAÇÃ0 EM OCEANOLOGIA
E-mail: ccpofog@furg.br – home-page: www.ppgo.furg.br

ATA ESPECIAL DE DEFESA DE TESE DE DOUTORADO – 02/2023

Às treze horas do dia oito de maio do ano de dois mil e vinte e três, por videoconferência, reuniu-se a Comissão Examinadora da Tese de **DOUTORADO** intitulada **" Clima de ondas no Oceano Atlântico Sul: tendências, extremos e relações com Modos de Variabilidade Climática"**, do **Acad. Natan Zambroni Maia**. A Comissão Examinadora foi composta pelos seguintes membros: Prof. Dr. Lauro Júlio Calliari – Orientador (IO/FURG – *in memoriam*), Prof. Dr. Luis Pedro Almeida – Orientador (PPGO-IO/FURG/CoLAB+Atlantic-PORTUGAL), Profa. Dra. Salette Amaral de Figueiredo (IO/FURG), Prof. Dr. João Luiz Nicolodi (IO/FURG), Prof. Dr. Bruno Castelle (*Université de Bordeaux*-FRANÇA) e Prof. Dr. Pedro de Souza Pereira (UFSC). Dando início à reunião, a Coordenadora Adjunta do Programa de Pós-Graduação em Oceanologia (PPGO), Profa. Dra. Elisa Helena Fernandes, agradeceu a presença de todos e fez a apresentação da Comissão Examinadora. Logo após, esclareceu que o Candidato teria um tempo de 45 a 60 min para explanação do tema, e cada membro da Comissão Examinadora, um tempo máximo de 30 min para perguntas. A seguir, passou à palavra ao Candidato que apresentou o tema e respondeu às perguntas formuladas. Após ampla explanação, a Comissão Examinadora reuniu-se em reservado para discussão do conceito a ser atribuído ao Candidato. Foi estabelecido que as sugestões de todos os membros da Comissão Examinadora, que seguem em pareceres em anexo, foram aceitas pelo Orientador/Candidato para incorporação na versão final da Tese, que deverá ser entregue num prazo máximo de 30 dias após a defesa. Finalmente, a Comissão Examinadora considerou o candidato **APROVADO**, por unanimidade. Nada mais havendo a tratar, foi lavrada a presente ATA, que após lida e aprovada, será assinada pela Comissão Examinadora, pelo Candidato e pela Coordenadora do Programa de Pós-Graduação em Oceanologia.

Prof. Dr. Luis Pedro Almeida

Documento assinado digitalmente
gov.br JOAO LUIZ NICOLODI
Data: 08/05/2023 17:40:22-0300
Verifique em https://validar.iti.gov.br

Profa. Dra. Salette Amaral de Figueiredo

Prof. Dr. João Luiz Nicolodi

Prof. Dr. Bruno Castelle

Prof. Dr. Pedro de Souza Pereira

Profa. Dra. Elisa Helena Leão Fernandes
Coordenadora Adjunta PPGO

Documento assinado digitalmente
gov.br ELISA HELENA LEAO FERNANDES
Data: 09/05/2023 08:29:30-0300
Verifique em https://validar.iti.gov.br

Acad. Natan Zambroni Maia

Documento assinado digitalmente
gov.br NATAN ZAMBRONI MAIA
Data: 08/05/2023 17:51:16-0300
Verifique em https://validar.iti.gov.br

Ao amor, à música e ao mar. Sempre.

Ao meu amigo Lauro Calliari, que por décadas formou e inspirou centenas de oceanógrafos e entusiastas das Ciências do Mar.

Índice

Agradecimentos....8
Lista de Figuras....10
Lista de Tabelas....12
Lista de Equações....13
Lista de Acrônimos, Abreviações e Símbolos....14
Resumo....16
Abstract....17
Capítulo I: Introdução....18
1.1 Ondas de superfície oceânica....18
1.2 Modos de Variabilidade Climática....24
1.2.1 Oscilação Multidecadal do Atlântico (AMO)....26
1.2.2 Modo Anular do Sul (SAM)....29
1.2.3 Índice do Atlântico Sul Tropical (TSA)....30
Capítulo II: Hipótese....33
Capítulo III: Objetivos.... 34
3.1. Objetivo geral....34
3.2. Objetivos específicos....34
Capítulo IV: Material e Métodos.... 35
4.1 Reanálise de ondas – ERA5....35
4.2 Índices Climáticos…….....37
4.3 Estatísticas de tendências e correlações....38
4.4 Definições de “Eventos Extremos”....38
4.5 Parâmetros de Eventos Extremos....39
Capítulo V: Artigo 1. “Wave climate trends and breakpoints during the Atlantic Multidecadal Oscillation (AMO) in southern Brazil”....40
Capítulo VI: Artigo 2. “Long-term trends and wave climate variability in the South Atlantic Ocean: the influence of climate indices”……..……..63
Capítulo VII: Síntese da Discussão e Conclusões....82

7.1 Síntese da Discussão do Artigo 1.....82
7.1.1 Variações e tendências do *WEF*.....82
7.1.2 Relações entre o *WEF* e o AMO.....84
7.2 Síntese da Discussão do Artigo 2.....86
7.2.1 Tendências do clima de ondas e Eventos Extremos.....86
7.2.2 Correlações entre clima de ondas e índices Climáticos.....87
7.2.3 Clima de ondas e mudanças climáticas.....88
7.3 Conclusões.....89
7.4 Considerações finais e perspectivas para trabalhos futuros.....90
Capítulo VIII: Referências Bibliográficas.....91

I

AGRADECIMENTOS

Inicialmente agradeço a Deus pelo presente da vida e pela oportunidade de viver momentos e experiências maravilhosas.

Agradeço à minha querida família de Volta Redonda, em especial a meus pais, irmão e cunhada pelo incondicional apoio, força, incentivo e estímulo ao longo de minha jornada acadêmica. A distância por vezes nos priva de algumas coisas, mas o amor de vocês sempre me nutriu para ir atrás de meus objetivos. Eu amo vocês.

Agradeço também aos meus familiares de Belém que sempre me apoiaram ao longo do doutorado e me deram incontáveis palavras de incentivo e força. Também amo vocês.

Aos colegas do Laboratório de Oceanografia Geológica (LOG-FURG), obrigado pela convivência ao longo destes anos.

De igual forma, agradeço aos amigos do "velho e isolado prédio B18" no Paléoenvironnements Océaniques et Continentaux da Université de Bordeaux (EPOC-UB, França). O ano que passamos juntos foi simplesmente mágico e eu tenho todos vocês no meu coração. Obrigado por me receber tão bem na França. Vocês são incríveis! *"De même, grâce aux amis du ' bâtiment ancien et isolé B18' des Paléoenvironnements Océaniques et Continentaux de l'Université de Bordeaux (EPOC-UB, France). L'année que nous avons passée ensemble a été juste magique et je vous porte tous dans mon cœur. Merci de m'avoir si chaleureusement accueilli en France. Vous êtes incroyable!"*

Obrigado ao João pela parceria dentro e fora da Universidade. Foram boas discussões sobre o trabalho em plena pandemia no quintal de casa!

Obrigado ao Pedro pela inestimável força para a realização desta Tese. Aprendi muito com você! Obrigado pelo convívio dentro e fora da FURG e pelas discussões acerca deste tema. Esta Tese não teria saído da forma como está sem você.

Obrigado ao Dr. Bruno Castelle por me receber em seu grupo de trabalho na França e pelos seus ensinamentos e suas brilhantes contribuições no segundo artigo da Tese. Você colocou este trabalho em outro patamar! *"Merci au Dr. Bruno Castelle pour m'avoir dans son groupe de*

travail en France et pour ses enseignements et ses brillantes contributions dans le deuxième article de la Thèse. Vous avez amené ce travail à un autre niveau!"

Obrigado aos amigos do Cassino, local que tanto amo. Vocês fazem toda a diferença nos confins do Brasil!

Àqueles que tive o prazer de dividir um palco, obrigado. A música tem um poder transformador e foi (é) essencial na minha caminhada. Em especial, obrigado ao "Bando de Coirana" pelas explosões de energia e alegria.

Obrigado mais que especial à Monique, minha amada esposa. Obrigado por dividir sua vida comigo e por aceitar dividir a minha com você. Mais uma vez, como sempre, estivemos juntos em uma caminhada. Obrigado por seu apoio, incentivo, força, amizade e amor. Você tem o dom de transformar as coisas e seu sorriso me ilumina. Você sempre me amparou e nunca me deixou desistir. Vivemos incríveis experiências ao longo de nossos doutorados e tenho certeza que Deus ainda nos reserva excelentes momentos. Que sorte a minha ter você ao meu lado. Eu te amo!

De forma também especial agradeço ao meu orientador e amigo Lauro Calliari. Estivemos juntos na graduação, no mestrado e também no doutorado. Obrigado por me orientar e por me incentivar a viver a oceanografia em todas as suas vertentes. Você sempre será umas das minhas melhores referências! Seus ensinamentos são atemporais.

Agradeço à CAPES pela bolsa de estudos ao longo do doutorado e também ao CAPES-PrInt pela bolsa de doutorado sanduíche. De igual forma, obrigado à equipe PrInt-FURG pelo suporte e por viabilizar minha ida à França em um cenário de pandemia.

Por fim, agradeço à oceanografia, que transformou a minha vida, me permitiu viver experiências incríveis e me levou para lugares nos quais nunca imaginei estar. Você me fascina.

Esta Tese não é só minha, é de todos nós.

II

Lista de Figuras

Entende-se por: Figura A.B, onde “A” se refere ao capítulo e “B” se refere ao número da figura no referido capítulo.

Figura 1.1. Geração de ondas do tipo “sea” e “swell” sob o efeito do vento 19

Figura 1.2. Fluxograma para geração de ondas sob a influência de Modos de Variabilidade Climática.....20

Figura 1.3. Correlações significativas inter-regionais entre SST e o *WEF* entre 1948–2008.....21

Figura 1.4. Variabilidade global na energia das ondas.....22

Figura 1.5. Média espacial anual da Potência das Ondas calculada globalmente e por bacia oceânica.....23

Figura 1.6. Alterações espaciais na energia média das ondas.....24

Figura 1.7. Principais Modos de Variabilidade Climática atuantes no globo.....26

Figura 1.8. Série temporal do índice AMO normalizado.....28

Figura 1.9. Distribuição espacial de correlação do índice AMO com a energia das ondas ao longo do globo.....28

Figura 1.10. Série temporal do índice SAM normalizado.....30

Figura 1.11. Série temporal do índice TSA normalizado.....31

Figura 4.1. Área de estudo compreendida no Artigo 1 (ponto preto) e Artigo 2 (todo o domínio).....36

Figura 5.1. Locations of the Rede Ondas waverider, ERA-5 validation point and ERA-5 analyzed point……...45

Figura 5.2. Time series of overlapping *Hs* (A), T (B) and θ (C) from ERA-5 and Rede Ondas waverider data during 2016……48

Figura 5.3. *WEF* variation between 1979–2019……..50

Figura 5.4. Segmented linear model of the normalized residuals from *WEFm* linear models. Continuous lines indicate subperiods with significant variations and segmented lines indicate subperiod without significant variations. *WEFm*=mean wave energy flux……..…51

Figura 5.5. Segmented linear model of the normalized residuals from *WEF98* linear models. The segmented lines indicate subperiods without significant variations. *WEF98*= extreme wave energy flux (98th percentile)……...52

Figura 5.6. *WEFm* variation per quadrant. Continuous lines indicate subperiods with significant variations, and segmented lines indicate subperiods without significant variations. *WEFm*=mean wave energy flux……...53

Figura 5.7. *WEF98* variation per quadrant. Segmented lines indicate subperiods without significant variations. *WEF98*= extreme wave energy flux (98th percentile)……54

Figura 5.8. Comparison between the AMO index (red line), 10-year running mean *WEFm* (blue line, A) and 10-year running mean *WEF98* (blue line, B). AMO = Atlantic Multidecadal Oscillation; *WEFm* = mean wave energy flux; *WEF98*= extreme wave energy flux (98th percentile)……..54

Figura 5.9. Comparison between the AMO index (red line) and 10-year running mean *WEFm* values per quadrant (blue lines). AMO= Atlantic Multidecadal Oscillation; *WEF* = mean wave energy flux……..55

Figura 6.1. Spatial domain for wave field. The locations of the North (Nt), Central (Ct) and South (St) virtual buoys are indicated by the colored stars……67

Figura 6.2. Time-average (left-hand panels) and trend (right-hand panels) of *Hs* and extreme event parameters between 1950 and 2021: (a,e) *Hs*; (b,f) cumulative Intensity; (c,g) cumulative Duration; (d,h) Frequency……69

Figura 6.3. Left-hand panels: spatial distribution of correlations between *Hs* and (a) AMO, (b) TSA and (c) SAM, respectively. The hatched areas show locations where correlation is not statistically significant. The locations of the North (Nt), Central (Ct) and South (St) virtual buoys are indicated by the colored stars. Right-hand panel: corresponding time series of *Hs* anomaly (solid line) and (d) AMO (Nt), (e) TSA (Ct) and (f) SAM (St) (colored bars) with indication of computed correlations……..71

Figura 6.4. Spatial distribution of correlations between extreme events parameters and climate indices considering the entire analyzed period. (a-c) Intensity; (d-f) Duration; (g-i) Frequency. The hatched areas show locations where correlation is not statistically significant…….72

Figura 6.5. Mean *Hs* and *WEF* and corresponding anomalies over the 5 most (left-hand panels, positive phase) and less (right-hand panels, negative phase) intense years of each climate index……...73

III

Lista de Tabelas

Entende-se por: Tabela A.B, onde "A" se refere ao capítulo e "B" se refere ao número da tabela no referido capítulo.

Tabela 1.1. Principais Modos de Variabilidade Climática e suas variabilidades temporais aproximadas.....25

Tabela 5.1. Statistical results of the comparison between ERA-5 reanalysis data and Rede Ondas waverider data using nine mont*Hs* of records from 2016 (n=5575 for each parameter). *Hs*= significant wave height; Tp= peak period; θ= mean wave direction; R= Pearson's correlation coeffcient; RMSE= root mean square error……..….47

Tabela 5.2. Statistical validation parameters found in the current work and by other authors, including the database and locations of each study. *Hs*= significant wave height; T= mean period; θ= mean wave direction; R= Pearson's correlation coeffcient; RMSE= root mean square error……..49

Tabela 5.3. P-values from regression analyses of *WEFm* and *WEF98* from the ERA-5 database tendency analysis. *WEFm*=mean wave energy flux; *WEF98*= extreme wave energy flux (98th percentile)……..49

Tabela 5.4. *WEFm* and *WEF98* associated with each quadrant. *WEFm*=mean wave energy flux; *WEF98*= extreme wave energy flux (98th percentile)……..50

Tabela 5.5. NOVA for the *WEFm* and *WEF98* of all wave incidence quadrants. *WEFm*=mean wave energy flux; *WEF98*= extreme wave energy flux (98th percentile); F= F-statistics……....50

Tabela 5.6. *WEFm* values for the subperiods defined by the breakpoints identified using the Muggeo method. *WEFm*=mean wave energy flux……..52

Tabela 5.7. *WEF98* means for the subperiods defined by the breakpoints identified using the Muggeo method. *WEF98*= extreme wave energy flux (98th percentile)……..….52

Tabela 6.1. Correlation coefficients (r) between climate indices……70

Tabela 6.2. Correlation coefficients r between climate indices, *Hs* and extreme event parameters at North (Nt), Central (Ct) and South (St) points. The values in parentheses indicate the percentage of parameter variance explained by the climate index.……72

IV

Lista de Equações

Entende-se por: Equação A.B, onde "A" se refere ao capítulo e "B" se refere ao número da equação no referido capítulo.

Equação 4.1. Fluxo de energia de onda.....36

Equação 4.2. Intensidade de eventos extremos integrada no tempo.....39

Equação 5.1. Wave energy flux.....46

Equação 5.2. Wave energy period.....46

Equação 5.3. Modelo linear de Muggeo (genérico 1).....46

Equação 5.4. Modelo linear de Muggeo (genérico 2).....46

Equação 6.1. Wave energy flux.....67

Equação 6.2. Intensity of extreme events integrated in time……..68

V

Lista de Acrônimos, Abreviações e Símbolos

A

AMO: Oscilação Multidecadal do Atlântico (*Atlantic Multidecadal Oscillation*)

AAO: Oscilação Antártica (*Antarctic Oscillation*)

APM: Anticiclone Polar Migratório

C

cm: centímetro

D

D: Duração de evento extremo

F

F: Frequência de evento extremo

E

ENSO: El Nino Oscilação Sul (*El Nino Southern Oscillation*)

ECMWF: Centro Europeu de Previsões Meteorológicas de Médio Prazo (*European Centre for Medium-Range Weather Forecasts*)

H

HN: Hemisfério Norte

HS: Hemisfério Sul

Hs: Altura significativa de onda

Hs95: Altura significativa extrema de onda (percentil 95)

hr: hora

I

I: Intensidade de evento extremo

IPCC: Painel Intergovernamental sobre Mudanças Climáticas (I*ntergovernmental Panel on Climate Change*)

K

kW: kilowatt

M

m: metro

N

NAO: Oscilação do Atlântico Norte (*North Atlantic Oscillation*)

NOAA: Administração Oceânica e Atmosférica Nacional (*National Oceanic and Atmospheric Administration*)

R

RCP: Rota de Concentração Representativa (*Representative Concentration Pathway*)

S

SST: Temperatura da Superfície do Mar (*Sea Surface Temperature*)

SAM: Modo Anular Sul (*Souther Annular Mode*)

SAR: Radar de Abertura Sintética

SLP: Pressão ao Nível do Mar (*Sea Level Pressure*)

SSE: sul-sudeste

SSW: sul-sudoeste

SW: sudoeste

T

TSA: Índice do Atlântico Sul Tropical (*Tropical South Atlantic Index*)

TNA: Índice do Atlântico Norte Tropical (*Tropical North Atlantic Index*)

Tp: Período de pico de onda

W

WHWP: Piscina Quente do Hemisfério Ocidental (*Western Hemisphere Warm Pool*)

WEF: Fluxo de Energia de Onda (*Wave Energy Flux*)

WEFm: Fluxo médio de Energia de Onda

WEF98: Fluxo extremo de Energia de Onda (percentil 98)

WAM: Wave Modelling

Θ: Direção de incidência de onda

ρ: Densidade da água

g: Aceleração da gravidade

VI

Resumo

Compreender como a variabilidade e as tendências do clima das ondas mudam ao longo do tempo são análises cruciais para mitigar os potenciais impactos induzidos pelas ondas e adaptar as áreas costeiras a tais efeitos. Para este fim, é importante relacionar a variabilidade e tendências do clima de ondas com Índices Climáticos para melhor compreender e prever padrões de variabilidade de ondas em larga escala temporal e espacial. Este estudo investiga tais links no Oceano Atlântico Sul usando 72 anos de reanálise de onda do ERA5. Diferentes parâmetros de onda são calculados, incluindo estatísticas de ondas de tempestade sendo analisados em termos de tendências de longo prazo e mudanças interanuais. Os resultados indicam que, ao longo das últimas décadas, o fluxo de energia das ondas aumentou tanto em condições normais (29,4%) como em condições extremas (12,6%), bem como a altura das ondas tem aumentado significativamente em todo o domínio, enquanto os eventos extremos estão se tornando mais intensos, prolongados e frequentes, embora com variabilidade espacial mais complexa, com taxas de incremento de até 350 m^2hr, 10h e 0,25 eventos por ano, respectivamente. Os resultados sugerem que o comportamento das ondas no Oceano Atlântico Sul é influenciado por alguns Índices Climáticos em escalas interanuais a multidecadais. As variações dessas propriedades ondulatórias são correlacionadas principalmente, de baixas a altas latitudes, com a Oscilação Multidecadal do Atlântico (AMO), Índice do Atlântico Sul Tropical (TSA) e Modo Anular Sul (SAM), com diferentes graus de correlação e escalas de tempo preferidas. Uma melhor compreensão e previsão da evolução destes índices climáticos, incluindo no âmbito das mudanças climáticas, será fundamental para antecipar perigos costeiros nesta região subsidiando o desenvolvimento de planos de gestão costeira.

Palavras-Chave: Ondas de tempestade; tendências de longo termo; variabilidade interanual; variabilidade multidecadal; AMO, TSA, SAM.

VII

Abstract

Understanding how wave climate variability and trends change over time are crucial analyzes needed to mitigate potential wave-induced impacts and adapt coastal areas to such effects. To this end, it is important to relate wave climate variability and trends to climate indices to better understand and predict large-scale patterns of temporal and spatial wave variability. This study investigates such links in the South Atlantic Ocean using 72 years of ERA5 wave hindcast. Different wave parameters are computed, including storm wave statistics, and are further analyzed in terms of long-term trends and interannual changes. The results indicate that, over the last decades, the wave energy flux is increasing both normal (29,4%) and extreme conditions (12,6%), as well the wave height has been significantly increasing across the entire domain, while extreme events are getting stronger, longer and more frequent, although with more complex spatial variability, with growth rates up to 350 m^2hr, 10h e 0,25 events per year, respectively. The results suggest that the wave behavior in the South Atlantic Ocean is influenced by some Climate Indices either in interannual to multidecadal scales. The variations of these wave properties are primarily correlated, from low to high latitudes, with the Atlantic Multidecadal Oscillation (AMO), Tropical Southern Atlantic Index (TSA) and Southern Annular Mode (SAM), with different correlations degrees and preferred timescales. The better understanding and predicting the evolution of these climate indices, including under climate change, will be critical to anticipate coastal hazards in this region subsidizing the development of coastal management plans.

Keywords: Storm waves; long term trends; interannual variability; multidecadal variability, AMO, TSA, SAM.

Capítulo I: Introdução

1. Introdução

1.1 Ondas de superfície oceânica

A evolução das ondas oceânicas geradas pelo vento é um dos fenômenos mais complexos da geofísica e possui grande significado prático para a sociedade e ecossistemas marinhos, sendo responsável por processos erosivos, transporte sedimentar e inundações além de moldar a costa e determinar onde e como as infraestruturas costeiras e offshore são construídas incluindo portos e usinas de geração de energia ondomotriz [Reguero et al., 2013; 2019; Babanin et al., 2019]. Além disso, as ondas são um componente proeminente de riscos costeiros uma vez que em condições extremas transferem grandes quantidades de energia para o continente aplicando enormes tensões às instalações costeiras e estruturas de proteção [Oumeraci, 1994; Van der Meer et al., 2016; Mentaschi et al., 2017]. Assim, mudanças no clima de onda são cada vez mais reconhecidas como tendo amplas implicações para a engenharia oceânica e o gerenciamento de riscos de desastres e, à medida que aumentam em altura e

energia, seus efeitos podem se tornar mais profundos [Barnard et al., 2015; Mentaschi et al., 2017; Marshall et al., 2015; Reguero et al., 2019].

As ondas de gravidade são o resultado da importante troca de energia e momento na interface oceano-atmosfera e se propagam pelas bacias oceânicas transportando a energia acumulada obtida do vento [Hemer et al., 2010; Reguero et al., 2012] (Figura 1.1). Logo, processos que incluem modificações na temperatura da superfície do mar (SST), nos padrões de vento e pressão atmosférica levam a mudanças no clima de onda que por sua vez impactam a costa de diferentes formas [Garner et al., 2017; Castelle et al., 2017; Rasmussen et al., 2018; Vousdoukas et al., 2018a; Oliveira et al., 2019]. Segundo Morin et al. [2019], aproximadamente 50% do litoral mundial está em risco devido às mudanças no clima de ondas, com cerca de 40% revelando mudanças robustas em suas propriedades. Portanto, entender como as características das ondas mudam ao longo do tempo e suas tendências de longo prazo é crucial para o desenvolvimento de políticas de gestão costeira eficientes no âmbito da adaptação às mudanças climáticas [De Leo et al., 2021].

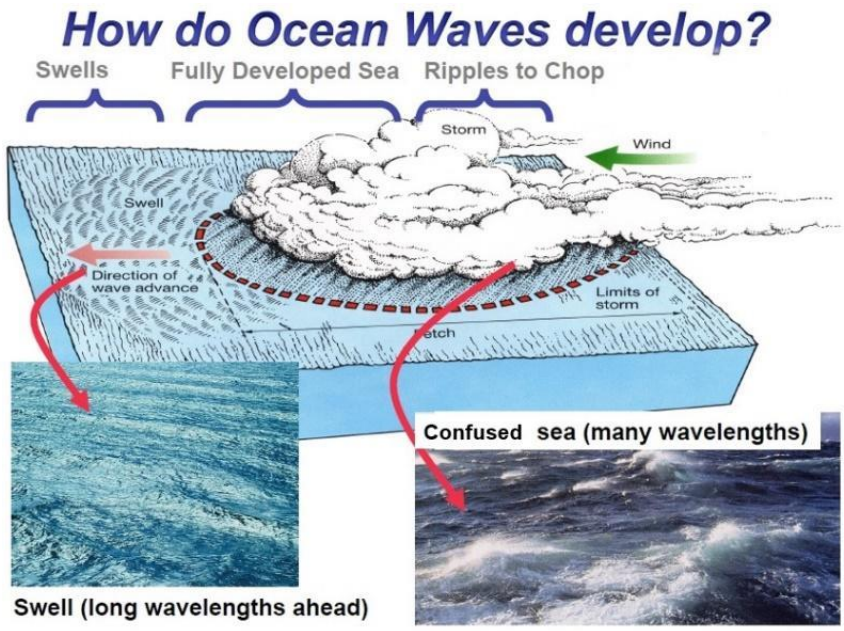


Figura 1.1. Geração de ondas do tipo “sea” e “swell” sob o efeito do vento.
Fonte: http://danangadventures.com/2022/03/how-are-waves-formed/

O clima global tem padrões preferenciais de variabilidade, chamados Modos de Variabilidade Climática. Estes padrões climáticos possuem características identificáveis, efeitos regionais específicos e comportamento oscilatório conhecido. Modos de Variabilidade Climática são representados por Índices Climáticos a exemplo do Modo Anular Sul (Souther Annular Mode - SAM), Índice do Atlântico Sul Tropical (Tropical South Atlantic Index - TSA), Índice do Atlântico Norte Tropical (Tropical North Atlantic Index - TNA), Piscina Quente do Hemisfério Ocidental (Western Hemisphere Warm Pool - WHWP) e Oscilação Multidecadal do Atlântico (Atlantic Multidecadal Oscillation - AMO). Devido a sua gênese se relacionar diretamente a processos que ocorrem entre o oceano e a atmosfera, o comportamento das ondas ao redor do globo é influenciado por um ou uma associação de diferentes Índices Climáticos [Castelle et al., 2017] (Figura 1.2).

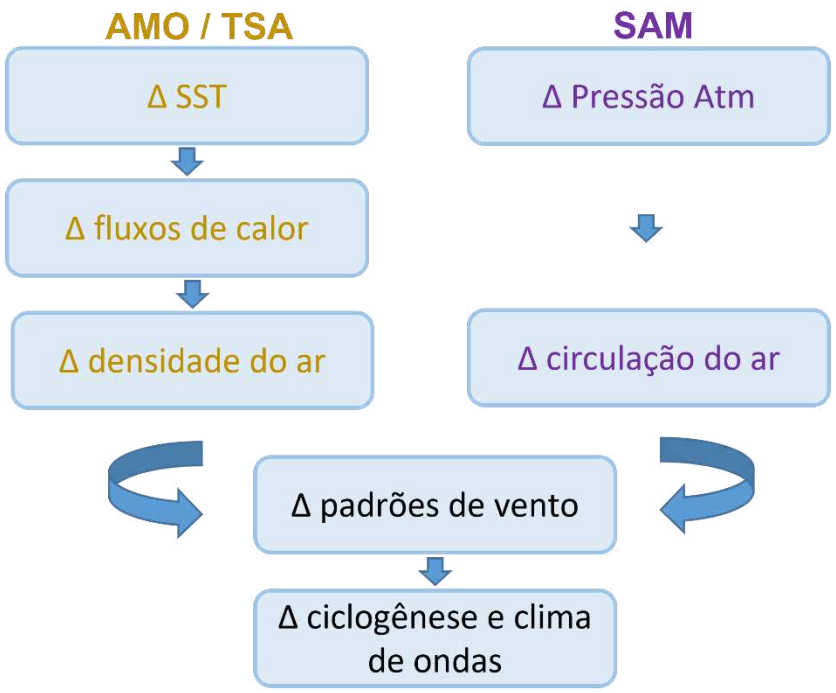


Figura 1.2. Fluxograma para geração de ondas sob a influência de Modos de Variabilidade Climática. Fonte: do autor

Associado a estas variabilidades há os Padrões de Teleconexão, que correlacionam condições meteorológicas em regiões distantes e diferentes,

que não estão ligadas fisicamente e que transportam e distribuem propriedades atmosféricas ao longo do globo. Portanto, mudanças na atmosfera podem levar a alterações no clima de ondas em ambos os hemisférios [Oliveira et al., 2019]. Nas últimas décadas, por exemplo, foram obtidas correlações positivas entre a SST do Atlântico tropical e norte e a energia das ondas nos extratrópicos austrais, sugerindo a intensificação da transferência de energia dos campos de vento para geração de ondas nessas regiões como resultado das tendências de aquecimento dos oceanos [Silva et al., 2020]. Diferentes estudos [Hemer et al., 2010; Castelle et al., 2017; Mentaschi et al., 2017; Marshall et al., 2018; Oliveira et al., 2019; Reguero et al., 2019; Silva et al., 2020] investigaram o clima de ondas ao redor do globo e relataram a existência de correlações significativas em diferentes oceanos entre a variabilidade de SST, índices climáticos e a variabilidade em propriedades como direção, altura e Fluxo de Energia de Ondas (*WEF*) em condições médias e extremas (Figura 1.3).

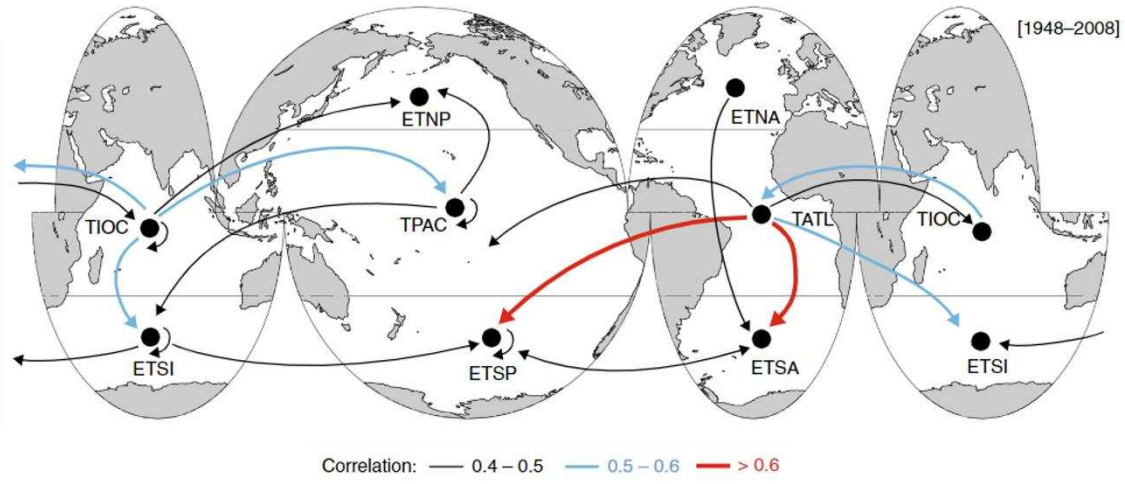


Figura 1.3. Correlações significativas inter-regionais entre SST e o *WEF* entre 1948–2008. O tamanho e a cor das setas indicam o coeficiente de correlação máximo entre a temperatura regional da superfície do mar na região de origem com a potência das ondas sazonal na região de destino. As sub-bacias oceânicas correspondem a: Pacífico Norte extratropical (ETNP), Pacífico tropical (TPAC), Pacífico Sul extratropical (ETSP), Atlântico Norte extratropical (ETNA), Atlântico tropical (TATL), Atlântico Sul extratropical (ETSA), Oceano Índico tropical (TIOC) e Oceano Índico Sul extratropical (ETSI). Retirado de Reguero et al. [2019].

Segundo Silva et al. [2020] e Reguero et al. [2019] nas últimas décadas o clima predominante de ondas de vento tem mudado tanto em direção quanto em

magnitude nos Hemisférios Norte (*HN*) e Sul (*HS*), um fenômeno provavelmente em resposta às dinâmicas atmosféricas alteradas e teleconexões inter-hemisféricas em associação com o aumento da temperatura global (Figura 1.4). Estudos anteriores no Oceano Atlântico mostraram um consenso de que o Atlântico Norte apresenta uma tendência de aumento nas condições de tempestade e nas alturas significativas das ondas [Kushnir et al., 1997; Wang e Swail, 2000; Swail et al., 2000; Wang et al., 2003; Dodet et al., 2010; Mentaschi et al., 2017]. Mais ao norte, no Oceano Ártico, Waseda et al. [2018] também encontraram tendência de aumento da altura das ondas nas últimas quatro décadas. Já no *HS*, Reguero et al. [2013] e Oliveira et al. [2019a] identificaram tendências crescentes nas alturas significativa de onda no oeste do Atlântico Sul nos últimos 60 e 32 anos, respectivamente.

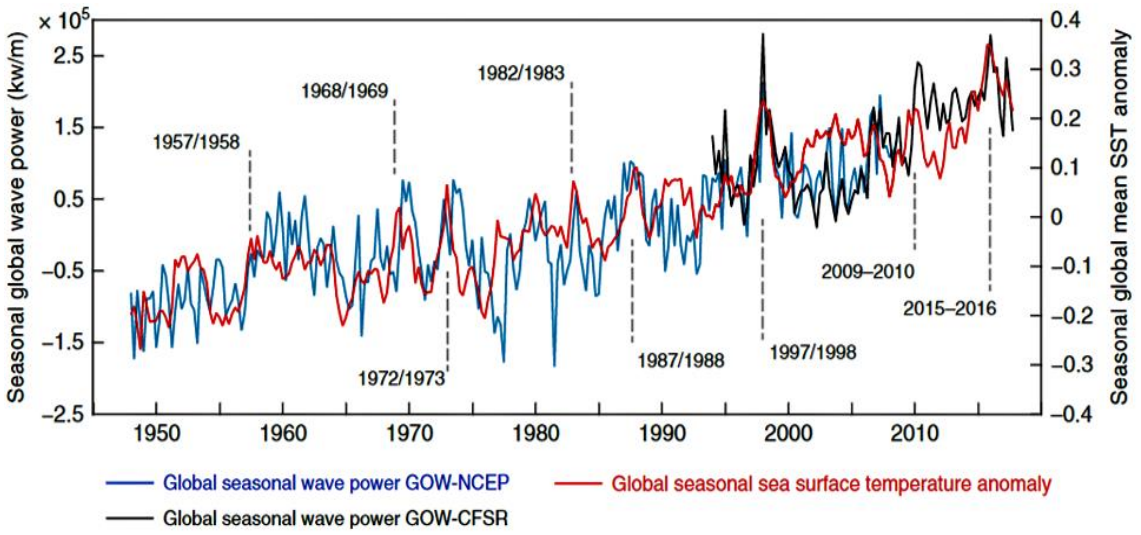


Figura 1.4. Variabilidade sazonal histórica no forçamento oceanográfico e variabilidade global sazonal na energia das ondas (azul: GOW-NCEP; preto: GOW-CFSR; eixo vertical esquerdo) e anomalias da temperatura da superfície do mar (linha vermelha; eixo vertical direito). Anos correspondentes a fortes eventos de El Niño, ou seja, aqueles com valor do Índice Niño Oceânico superior a 1,5, são anotados e sobrepostos no gráfico. Retirado de Reguero et al. [2019].

Em cenários futuros, as projeções do clima de ondas para o final do século XXI também indicam que o aquecimento da SST como resultado de mudanças no clima levará a um aumento na altura e nos níveis de energia das ondas de diferentes maneiras ao redor do globo [Morim et al., 2019; Meucci et al., 2020;

O'Grady et al., 2021]. Além disso, as tendências de aquecimento da SST induzirão uma intensificação a longo prazo de alguns índices climáticos como SAM, ENSO, AMO e NAO, que por sua vez, também influenciarão o comportamento das ondas [Mentaschi et al., 2017; Reguero et al., 2019] além de convecção mais intensa e tempestades mais frequentes [Grassi et al., 2005], forçada, principalmente, pelas emissões de gases de efeito estufa e destruição do ozônio antártico [Cai et al., 2003; Wang e Cai, 2013].

Os processos meteoceanográficos que ocorrem no *HS* têm relevante importância para a dinâmica da atmosfera e dos oceanos ao redor do globo. Sendo o oceano mais energético de todos [Reguero et al., 2019] (Figura 1.5), além de apresentar o crescimento mais rápido de ventos e ondas tanto em percentis médios quanto em percentis extremos em comparação com os demais oceanos [Babanin et al., 2019] (Figura 1.6), o swell gerado no Oceano Austral pela ação de intensos ciclones extratropicais se propaga ao longo dos oceanos do mundo, impactando quase todas as costas do globo [Hemer et al., 2010]. De acordo com Sterl e Caires [2005], 15% da variabilidade global das ondas é devido à propagação do swell da região de tempestades no *HS* e governa a variabilidade de sua média global. Dada a importância do Oceano Austral no contexto global, é necessário um esforço concentrado para determinar a variabilidade e tendências do clima de ondas do *HS* e, em particular, em altas latitudes [Hemer et al., 2010].

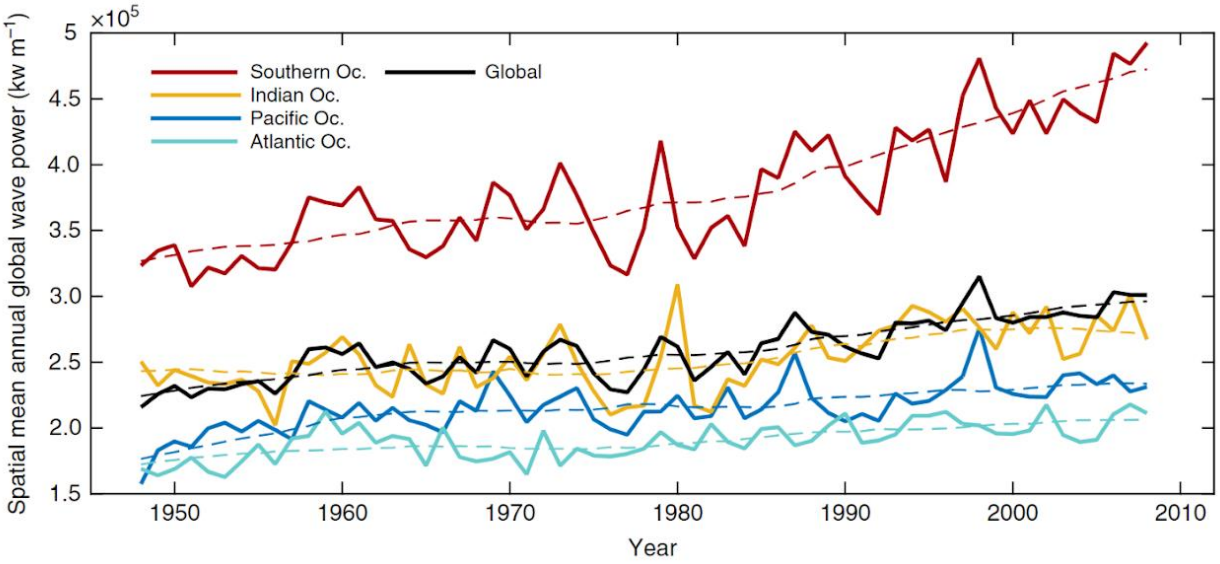


Figura 1.5. Média espacial anual da Potência das Ondas calculada globalmente e por bacia oceânica. As linhas tracejadas representam as médias móveis de 10 anos. O Oceano Austral é definido entre as latitudes de 40°S e 80°S. A potência de onda regional média é calculada como a média espacial de cada série histórica de potência de onda. As linhas sólidas indicam cada série temporal. Retirado de Reguero et al. [2019].

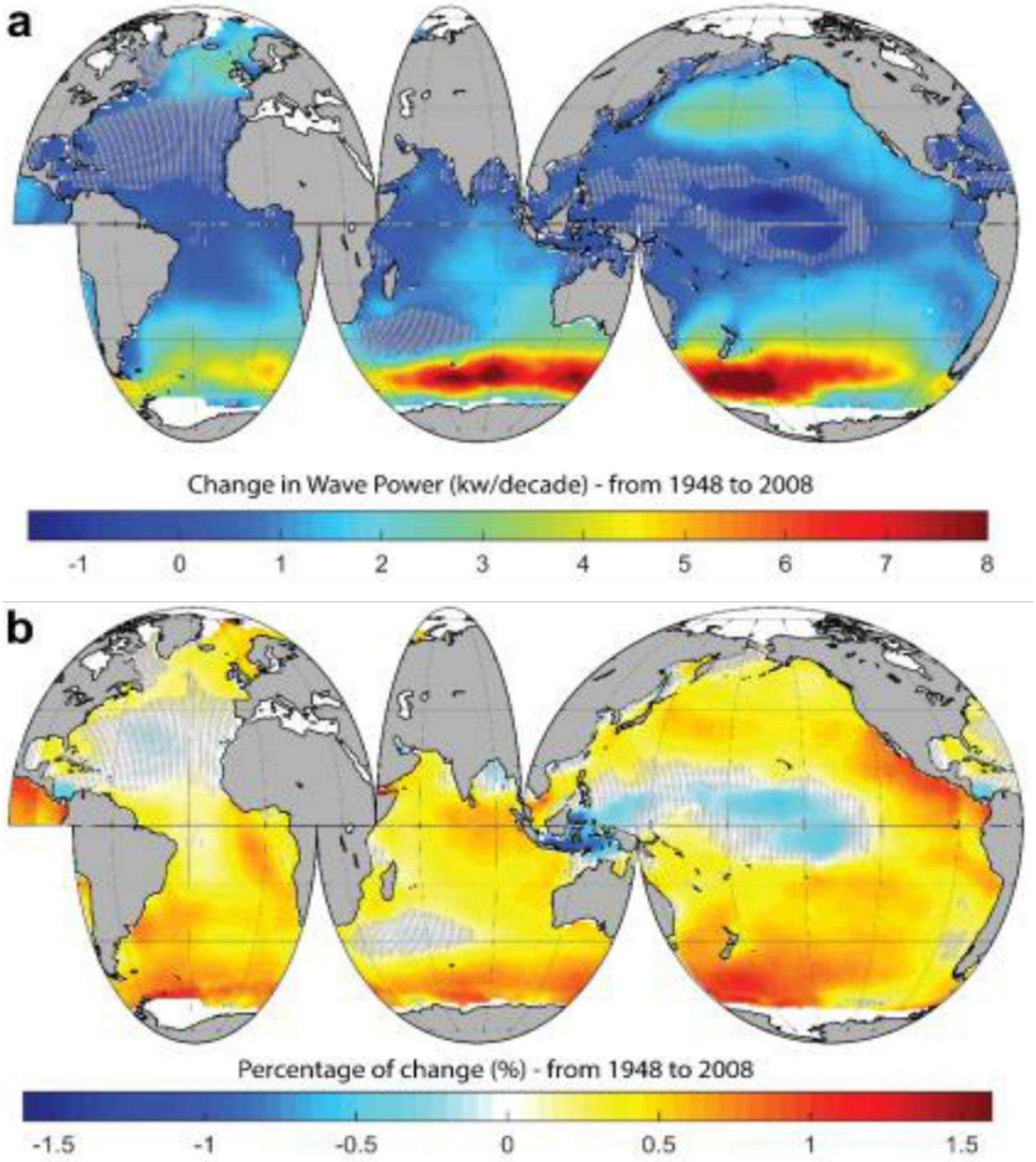


Figura 1.6. Alterações espaciais na energia média das ondas. Mudança média na potência da onda ao longo do intervalo de tempo histórico (1948-2008) expressa em valores absolutos por década (a) e porcentagem por ano (b). As áreas hachuradas marcam regiões que não são significativas no nível de 95%. Retirado de Reguero et a. [2019].

1.2 Modos de Variabilidade Climática

Índices Climáticos são amplamente considerados associados à variabilidade climática natural típica em escalas interanuais a multidecadais (Tabela 1.1) e são geralmente caracterizados em termos de oscilação em torno

da média nos padrões e distribuições da pressão ao nível do mar (SLP), vento e SST [Thompson e Wallace, 1998; Kerr, 2000; Trenberth et al., 2002; Hurrell et al., 2003; Hemer et al., 2010; Silva et al., 2020]. A variabilidade do clima de ondas em diferentes partes do globo é modulada por um ou uma combinação de vários Modos Climáticos (Figura 1.7); assim, o entendimento da variabilidade do comportamento das ondas requer uma compreensão profunda destes processos atuantes na interface oceano-atmosfera.

Tabela 1.1. Principais Modos de Variabilidade Climática e suas variabilidades temporais aproximadas.

Índice Climático	Acrônimo	Escala temporal aproximada
Atlantic Meridional Mode	AMM	Interanual
Atlantic Nino	-	Interanual
Artic Oscillation	AO	Decadal
North Atlantic Oscillation	NAO	Decadal
East Atlantic Pattern	EAP	Decadal
Atlantic Multidecadal Oscillation	AMO	Multidecadal
El Nino Southern Oscillation	ENSO	Interanual
Pacific Decadal Oscillation	PDO	Decadal
North Pacific Gyre Oscillation	NPGO	Decadal
Indian Ocean Dipole Mode	IOD	Interanual
Southern Annular Mode (Antarctic Oscillation)	SAM (AAO)	Interanual

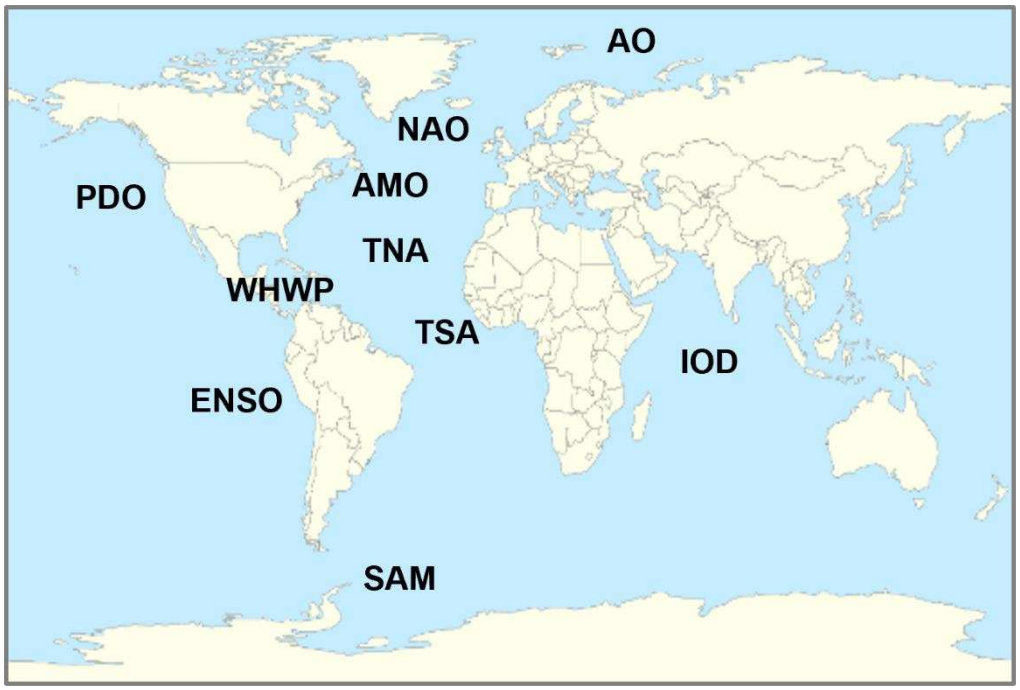


Figura 1.7. Principais Modos de Variabilidade Climática atuantes no globo. AO: Oscilação Ártica; AMO: Oscilação Multidecadal do Atlântico; ENSO: El-Nino Oscilação Sul; IOD: Dipolo do Oceano Índico; NAO: Oscilação do Atlântico Norte; PDO: Oscilação Decadal do Pacífico; SAM: Modo Anular do Sul; TNA: Índice do Atlântico Norte Tropical; TSA: Índice do Atlântico Sul Tropical; WHWP: Piscina Quente do Hemisfério Ocidental. Fonte: do autor.

1.2.1 Oscilação Multidecadal do Atlântico (AMO)

Descrito por Kerr [2000], o AMO é visto como um indicador de mudanças globais na circulação termohalina [Biastoch et al. 2015] sendo identificado como um modo de variabilidade natural que ocorre no Oceano Atlântico com base nas anomalias médias de SST na bacia do Atlântico Norte, tipicamente entre 0°-70°N. Denomina-se por variações multidecadais com menos de 0,4°C de faixa de magnitude alternando entre as fases quente (positiva) e fria (negativa) com uma periodicidade de aproximadamente 70 anos e 0,4°C de anomalia para SST global [Wang et al., 2009; Frajka-Williams et al., 2017; Kayano et al., 2019; Trenberth e Shea, 2006; Trenberth et al., 2021] (Figura 1.8). Desde 1995, o AMO tem sido positivo em uma nova fase quente [Ortega et al., 2013; Alexander et al., 2014]. As impressões do AMO nos campos de SST e SLP, embora centradas no Atlântico Norte, estendem-se bem além desta área e têm influências pronunciadas sobre o tempo e o clima em todo o mundo. O AMO afeta amplamente as mudanças no clima global [Yang et al., 2020] e diferentes efeitos

são observados em todo o mundo, como variações de temperatura e pressão no Atlântico Sul, Pacífico e Oceano Antártico [Lyu e Yu, 2017; Odériz et al., 2020]. Como um dos mais importantes Modos de Variabilidade Climática, o AMO tem sido amplamente associado a anomalias climáticas regionais proeminentes que podem modular a atividade de furacões e ciclones tropicais no Atlântico [Goldenberg et al., 2001; McCabe et al., 2004; Wang et al., 2008] e o fluxo de energia de ondas no Oceano Antártico [Reguero et al., 2019]. Os efeitos do AMO são sentidos em todo o Oceano Atlântico, conferindo um comportamento dipolo em que a fase quente apresenta aquecimento anômalo no Atlântico Norte e resfriamento anômalo nos oceanos Atlântico Sul e Antártico, com fortes gradientes meridionais na faixa de 40°-70°S, enquanto a fase fria do AMO mostra um padrão de anomalia SST de sinal quase reverso [Timmermann et al., 2007; Wang et al., 2008; Latif, 2013; Lyu e Yu, 2017; Kayano et al., 2019; Reguero et al., 2019]. Segundo Crowley e Kim [1993], mudanças decadais a multidecadais na circulação termohalina devem afetar principalmente as temperaturas dos Oceanos Atlântico e Antártico, com uma assinatura clara no campo de SST no Mar de Weddell e na Passagem de Drake.

No Oceano Atlântico Sul, estudos anteriores baseados em dados de reanálise de ondas e SST [Ortega et al., 2013; Alexander et al., 2014; Biastoch et al., 2015; Kayano et al., 2019] revelaram fortes interações entre mudanças nas interações oceano-atmosfera e o índice AMO. Kayano et al. [2019] observaram relações entre o AMO e a variabilidade multidecadal da atividade de ciclones tropicais no Atlântico, que aumentaram amplamente em frequência e intensidade desde o final da década de 1980 quando se iniciou a fase positiva do AMO. Wang et al. [2008] indicam que a variação multidecadal da atividade de furacões no Oceano Atlântico coincide com as fases quentes e frias do AMO. Segundo estes autores, os comportamentos dos ciclones e furacões no Oceano Atlântico são modulados pelas oscilações do AMO. Reguero et al. [2019] identificaram fortes correlações entre o fluxo de energia das ondas (*WEF*) e o comportamento do AMO respectivamente no *HS* e no oeste do Oceano Atlântico Sul (Figura 1.9). Durante as fases negativas e positivas do AMO, os fluxos de calor nas interações oceano-atmosfera induzem mudanças no potencial de energia cinética disponível na atmosfera, nos ciclones extratropicais de baixo

nível, nos padrões de vento e, consequentemente, no clima de ondas do Oceano Atlântico [Escobar et al., 2004; Ortega et al., 2013; Kayano et al., 2019] e também além, como mudanças no Ártico, Pacífico e outras partes do globo [Enfield et al., 2001; Knight et al., 2005; Zhang e Delworth, 2007; Chylek et al., 2009 ; Alexander et al., 2013].

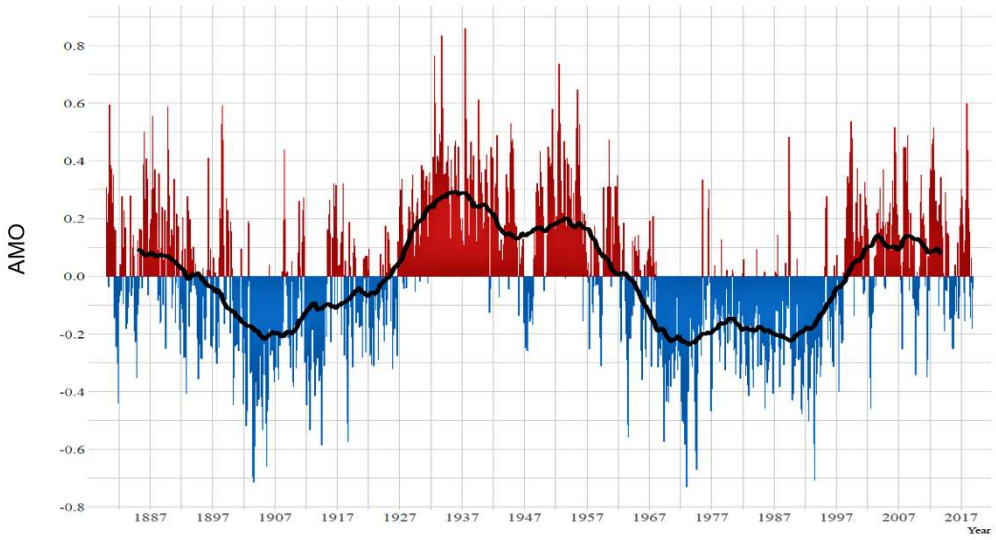


Figura 1.8. Série temporal do índice AMO normalizado. Fase positiva (negativa) em vermelho (azul) e linha de tendência em preto.
Fonte:https://upload.wikimedia.org/wikipedia/commons/b/b4/Atlantic_Multidecadal_Oscillation.svg

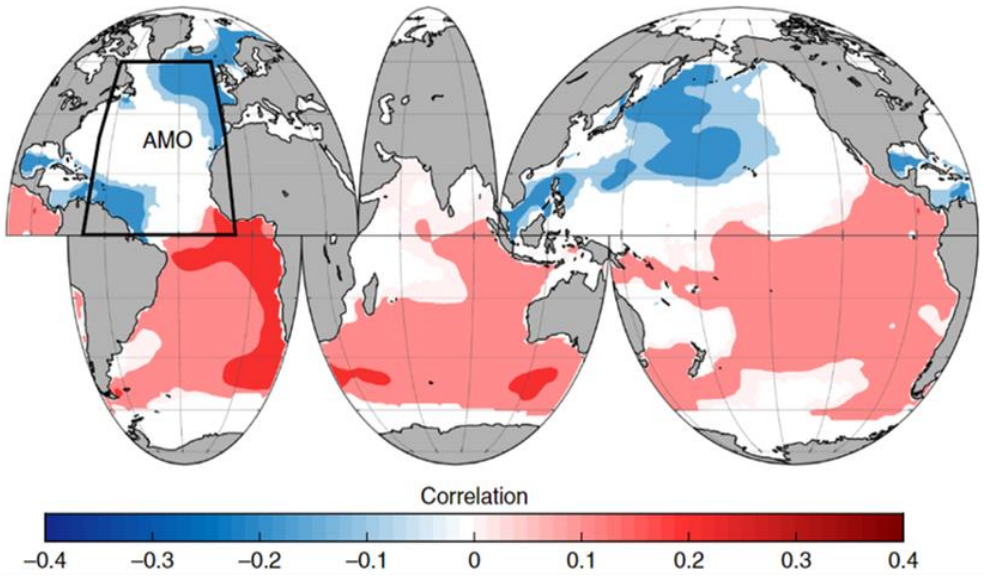


Figura 1.9. Distribuição espacial de correlação do índice AMO com a energia das ondas ao longo do globo. Somente as correlações a 95% de significância são mostradas. Retirado de Reguero et al. [2019]

1.2.2 Modo Anular do Sul (SAM)

O SAM [Trenberth, 1979; Rogers e Van Loon, 1982; Mo e White, 1985], também conhecido como Oscilação Antártica [AO - Thompson e Wallace, 1998] é o principal modo de variabilidade na circulação atmosférica extratropical e de altas latitudes no *HS* [Marshall, 2003]. Esta oscilação é caracterizada por perturbações de altura geopotencial zonalmente simétricas com sinais opostos entre a Antártica e as latitudes a cerca de 45°S, sendo representado por uma oscilação nos valores dos sistemas de pressão superficial entre médias e altas latitudes com escala temporal que pode variar de semanas a meses [Thompson e Wallace, 2000; Reboita et al., 2009; Fogt e Marshall, 2020]. Sen Gupta e England [2006] mostraram que a fase positiva do SAM é caracterizada por anomalias negativas de temperatura e anomalias positivas de vento zonal ao longo da Antártica, com condições opostas próximo à latitude média de 45ºS. Condições reversas são identificadas na fase negativa do SAM. Em sua fase positiva, o cinturão de vento de oeste de latitude média muda para os polos e o transporte e dispersão de massas de ar antárticas são inibidas. Por outro lado, uma mudança para o equador nos ventos de oeste de latitude média e a dispersão de massas de ar e frentes frias para o norte (fluxos meridionais) caracterizam a fase negativa do SAM [Marshall et al, 2018].

Devido à sua dinâmica, o SAM é o principal modo que influencia a altura, a variabilidade direcional e o fluxo de energia das ondas no sul do *HS* [Hemer et al., 2010; Marshall et al., 2018], induzindo variações no tempo e clima nesta região e impulsionando variações na circulação do Oceano Austral em uma ampla gama de escalas de tempo (diária a sazonal) com contribuição relativa das ondulações de sul de alta energia para o fluxo médio efetivo de energia das ondas que se propagam particularmente ao longo da costa sul-americana [Silva et al., 2020]. Especialmente em altas latitudes, a fase positiva do SAM tem correlação positiva com alturas de onda significativas e está associada à geração de tempestades e ventos extremos relacionados a ondas extremas [Hemer et al., 2010; Mentaschi et al., 2017]. O SAM também exerce forte e significativa influência na ocorrência de condições de alta e baixa alturas de onda, definidas quando as anomalias de *Hs* estão abaixo do percentil 5 e acima do percentil 95 [Marshall et al., 2018].

No entanto, a assinatura do SAM em ondas de superfície oceânica se estende além do forçamento local gerado pelo vento nos extratrópicos do *HS* até o forçamento remoto nos extratrópicos com o sinal atmosférico associado semelhante a um trem de ondas de Rossby e, por consequência, influenciando o regime de ondas também no HN [Marshall et al., 2018], uma vez que os resultados das tempestades do Oceano Antártico irradiam para todas as principais bacias oceânicas [Babanin et al., 2019]. Ao longo das últimas décadas, o SAM apresenta tendência geral positiva (Figura 1.10) [Thompson e Wallace, 2000; Thompson e Solomon, 2002; Marshall, 2003; Cai et al., 2005; Cai e Cowan, 2007; Hemer et al., 2010; Marshall et al., 2018] que segundo Cai et al. [2003], Gillet et al. [2003], Thompson e Solomon [2002] e Marshall e Connolley [2006] é resultado do aumento induzido pelas mudanças climáticas nos gradientes de temperatura meridionais na estratosfera e na superfície dos oceanos.

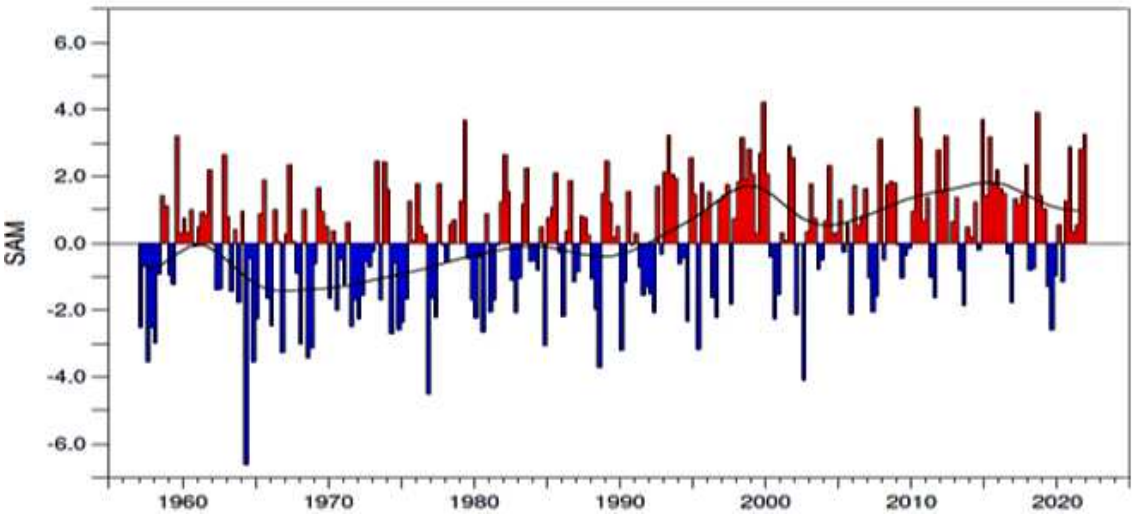


Figura 1.10. Série temporal do índice SAM normalizado. Fase positiva (negativa) em vermelho (azul) e linha de tendência em preto. Retirado de Trenberth et al. [2007].

1.2.3 Índice do Atlântico Sul Tropical (TSA)

O TSA é um indicador das temperaturas da superfície no leste do Oceano Atlântico Sul tropical. É um componente importante da variabilidade da SST nesta região, caracterizado por anomalias quentes ou frias da SST medidos entre 0º-20ºS e 10ºE-30ºW (Figura 1.11). Enfield et al. [1999] definiram o índice

TSA utilizando padrões dipolares de SST no Atlântico Sul tropical onde foram encontrados uma periodicidade de 8 a 12 anos para a primavera-inverno e de 2 a 3 anos para a primavera-verão. Os valores positivos do índice indicam que a temperatura da superfície do mar é anomalamente quente e valores negativos indicam anomalia fria sobre a região sul do Oceano Atlântico. Segundo Reguero et al. [2013] o TSA está associado a aumento na altura, fluxo de energia e mudanças na direção das ondas na zona equatorial do Oceano Atlântico e também na região do Rio da Prata. Tais alterações são principalmente provocadas pelo reforço dos ventos alísios de sudeste e de leste no Atlântico equatorial ocidental devido a uma migração para norte da zona de convergência intertropical.

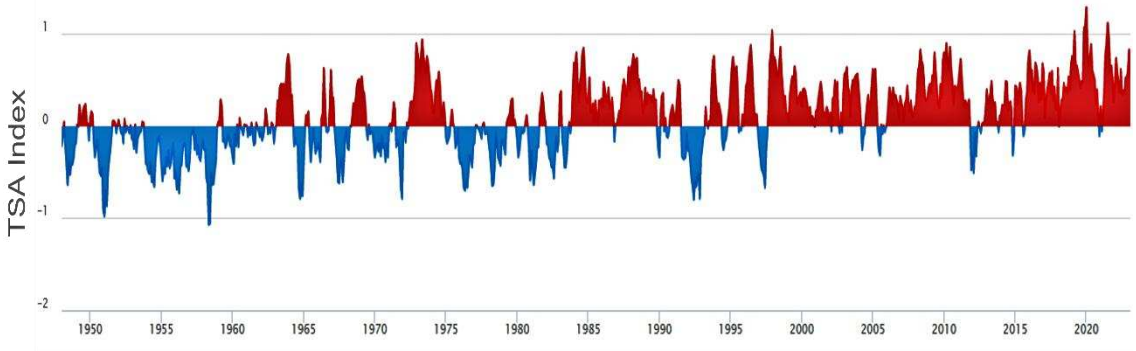


Figura 1.11. Série temporal do índice TSA normalizado. Fase positiva (negativa) em vermelho (azul).
Fonte: https://meteorologia.unifei.edu.br/teleconexoes/indice?id=tsa

Esta tese investiga o comportamento das ondas no Oceano Atlântico Sul ao longo das últimas décadas e sua relação com os principais Modos de Variabilidade Climática atuantes nesta bacia oceânica. Foram usadas longas séries temporais de reanálise baseadas em conjuntos de dados históricos de ondas compreendida entre os anos 1950 e 2021. O comportamento das ondas e os Índices Climáticos em questão foram analisados com base na correlação das séries temporais, análise de regressão e tendências de longo prazo, tanto em condições médias quanto em condições extremas. Do ponto de vista marinho e costeiro, a interação entre o comportamento das ondas e os Índices Climáticos

é importante se esta relação servir de base para o desenvolvimento de políticas marinhas e planos de gestão costeira, principalmente considerando as condições médias e extremas a médio e longo prazo das tendências das ondas. Os resultados apresentam novas perspectivas e contribuições sobre o papel da variabilidade climática de ondas e seus drivers de longo prazo no Oceano Atlântico Sul e seus fatores relacionados principalmente com condições extremas.

Capítulo II: Hipótese

A presente tese possui como hipótese a seguinte proposição:

"Ao longo das últimas décadas o Fluxo de Energia de Ondas e o padrão comportamental dos eventos meteo-oceanográficos extremos no Oceano Atlântico Sul foi alterado em função da oscilação de Modos de Variabilidade Climática."

Capítulo III: Objetivos

A presente tese possui os seguintes objetivos:

3.1 Objetivo geral

Analisar as tendências e extremos do clima de ondas e suas relações com Modos de Variabilidade Climática ao longo das últimas décadas no Oceano Atlântico Sul.

3.2 Objetivos específicos

i. Investigar as variações de longo termo do Fluxo de Energia de Ondas no sul do Brasil.

ii. Investigar as relações entre a variabilidade do clima de ondas e Modos de Variabilidade Climática no Oceano Atlântico Sul.

iii. Investigar a variabilidade da duração, frequência e intensidade dos eventos meteoceanográficos extremos e suas relações com Modos de Variabilidade Climática no Oceano Atlântico Sul.

Capítulo IV: Material e Métodos

4. Material e Métodos

4.1 Reanálise de ondas – ERA5

Dada a escassez de longas e contínuas séries temporais, os modelos globais de onda fornecem uma alternativa útil para abordar a variabilidade espacial e temporal bem como as tendências das condições das ondas que se propagam ao longo do *HS* [Hemer et al., 2010]. No Artigo 1 foram utilizados 41 anos (1979-2019) e no Artigo 2 72 anos (1950-2021) de reanálise de ondas globais com resolução temporal de 3 horas produzido pelo Centro Europeu de Previsões Meteorológicas de Médio Alcance (ECMWF) - ERA 5 [Hersbach et al., 2020], a partir do qual a altura significativa (*Hs*), o período de pico (Tp) e a direção de incidência de ondas (θ) foram extraídos, a partir dos quais o fluxo de energia da onda (*WEF*) foi calculado (Equação 1) [Antolínez et al., 2016; Mentaschi et al., 2017; Marshall et al., 2018; Reguero et al., 2019; Odériz et al., 2020a; Odériz et al., 2020b]. O *WEF* representa a taxa de energia total transportada em uma direção ortogonal à propagação da crista de onda durante um período de tempo.

No Artigo 1 foram utilizados os resultados de reanálise de um único ponto localizado nas coordenadas 32°30'S e 50°W a 1000 m de profundidade (águas profundas). Já no Artigo 2, as saídas do modelo foram extraídas em uma grade regular com resolução espacial de 0,5° cobrindo o Oceano Atlântico Sul entre 5°N-60°S e 69,5°W-20°E, totalizando 23.580 pontos de grade individuais (Figura 4.1).

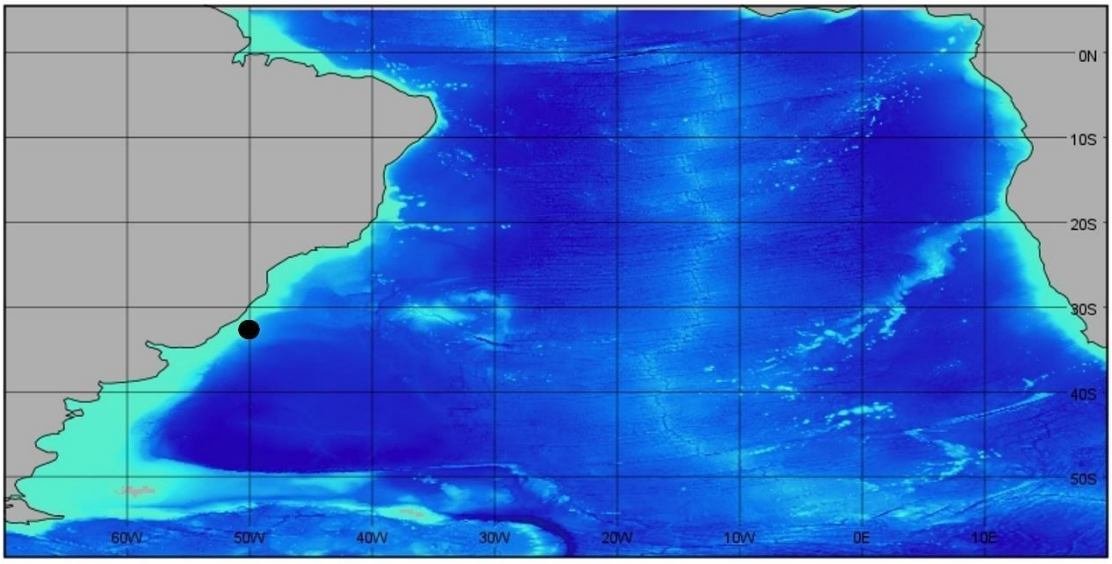


Figura 4.1. Área de estudo compreendida no Artigo 1 (ponto preto) e Artigo 2 (todo o domínio).

A diferença do comprimento das séries entre os artigos se deve ao fato de, após a finalização do Artigo 1, a base de dados do ECMWF ter sido ampliada iniciando então em 1950, permitindo assim desenvolver o Artigo 2 com 31 anos a mais de dados.

$$WEF = \frac{\rho\, g^2\, Hs^2\, T}{64\,\pi} \qquad \text{Eq. 4.1}$$

Equação 4.1. Fluxo de energia de onda. (ρ) densidade da água; (g) aceleração da gravidade; (*Hs*) altura significativa de onda; (T) período de pico.

A reanálise ERA-5 é um sistema global de assimilação de dados atmosféricos, de ondas e de gelo que fornece produtos desde 1950 até o presente em um esquema quase em tempo real e é mantido pelo Centro Europeu de Previsões Meteorológicas de Médio Prazo – ECMWF. Os dados de onda ERA-5 são gerados pelo WAM, um modelo de 3ª geração que integra a equação básica de transporte que descreve a evolução de um espectro bidimensional de

ondas oceânicas sem suposições adicionais não planejadas em relação à forma espectral. O WAM usa a altura da onda de altímetros e observações avançadas de SAR como fonte na assimilação do modelo e possui o ETOPO2 como um banco de dados de batimetria do Centro Nacional de Dados Geofísicos (NGDC/NOAA). Existem três funções de fonte explícitas que descrevem a entrada do vento, a transferência não linear e a dissipação do whitecapping. Há uma função de fonte de dissipação de fundo adicional e os termos de refração estão incluídos na versão de profundidade finita do modelo, por isso leva em consideração a física básica de águas rasas, ou seja, a energia máxima das ondas e o deslocamento de frequência para baixo são controlados pela profundidade da água. O modelo é executado em uma grade esférica de latitude e longitude e pode ser usado em qualquer região oceânica. O WAM prevê espectros direcionais junto com propriedades de onda, como a altura significativa, direção e frequência média das ondas e campos de tensão do vento corrigidos incluindo a tensão induzida pela onda e o coeficiente de arrasto em cada grade ponto em tempos de saída escolhidos [The Wamdi Group 1988; Dee et al. 2011]. A atenuação lenta das ondulações de longo período e o impacto das águas rasas na entrada do vento são introduzidos com o retorno geral do nível de dissipação devido ao whitecapping. Levando em consideração que o modelo utiliza assimilação de dados em águas intermediárias, seus produtos consideram as transformações das ondas induzidas pela variação de profundidade e interação com o fundo. Porém, vale ressaltar que devido à resolução da grade de 0,5° do modelo, variações batimétricas menores que esta escala podem não ser bem representadas e causar incertezas em alguns resultados, como a direção da onda em áreas costeiras. Uma descrição detalhada do ERA5 pode ser encontrada em Hersbach et al. [2020].

4.2 Índices Climáticos

Com base em suas influências no Oceano Atlântico, os índices AMO [Enfield et al., 2001], WHWP (Wang et al., 2001), TSA [Einfield et al., 1999], TNA [Einfield et al., 1999] e SAM [Marshall, 2003] foram usados para representar processos de grande escala que podem influenciar as condições climáticas no

Oceano Atlântico Sul. Os índices mensais de teleconexão disponíveis desde janeiro de 1950 foram baixados do Laboratório de Ciências Físicas da National Oceanic and Atmospheric Administration (NOAA) [www.psl.noaa.gov], nominalmente AMO, WHWP, TSA e TNA. O SAM foi obtido do British Antarctic Survey [www.bas.ac.uk/], disponível desde 1957.

4.3 Estatísticas de tendências e correlações

As tendências lineares de longo prazo foram calculadas usando um modelo de regressão linear com um nível de confiança de 95%. A significância estatística das tendências foi verificada por meio de análise de variância (ANOVA) com nível de confiança de 95%, indicando assim se as variáveis analisadas são significativamente diferentes umas das outras (crítico $F < F$; $P < 0,05$).

As séries temporais anuais de todos os parâmetros de onda foram usadas para abordar a variabilidade e tendências do clima de onda. Em cada ponto da grade, cada Índice Climático foi usado para calcular as correlações com os parâmetros das ondas, que também foram regredidos linearmente para calcular as tendências de longo prazo. A relação entre as propriedades das ondas e os Índices Climáticos foi avaliada por meio do coeficiente de correlação de Pearson (r), que é uma medida da força e direção da relação linear entre duas variáveis [Reguero et al., 2019]. A significância estatística foi calculada por meio do teste t de Student ao nível de confiança de 95% [Almeida et al., 2011; Reguero et al., 2019]. Para realizar estas análises, foram usadas as séries temporais normalizadas de todos os parâmetros entre todos os pares possíveis de pontos de grade dentro de todo o domínio da área em questão. A normalização faz-se necessária para usar uma escala comum, sem distorcer as diferenças nos intervalos de valores nem perder informações das séries temporais de cada propriedade e torna-las comparáveis.

4.4 Definição de “Eventos Extremos”

Embora os impactos de eventos meteo-oceanográficos extremos em regiões costeiras sejam bastante conhecidos e estudados, não existe consenso

na bibliografia sobre a definição de “condições extremas”. Logo, esta definição é dada de diferentes maneiras e abordagens. Nesta tese, para caracterizar “Evento Extremo” o método do “pico acima do limite” definido por Dorsch et al. [2008] foi aplicado em *Hs*. Seguindo a definição de Masselink et al. [2014] e posteriormente utilizada em outros estudos [Castelle et al., 2015; Angnuureng et al., 2017], para cada ponto da grade do domínio no Oceano Atlântico Sul um “Evento Extremo” foi definido como um evento onde *Hs* excedeu o percentil 95 (*Hs95*). Além disso, um único evento extremo foi definido como um período contínuo de *Hs* excedendo o *Hs95* por pelo menos 12 horas [Sénéchal et al., 2015; Agnuureng et al., 2017]. Adicionalmente, a individualização dos eventos extremos foi feita através de um critério de independência definido como o intervalo de 30 horas entre registos consecutivos de *Hs* com base em Almeida et al., [2011].

4.5 Parâmetros de Eventos Extremos

Para estudar o comportamento dos Eventos Extremos três parâmetros foram definidos: duração (D), frequência (F) e intensidade (I). Para a duração, em cada ano calculamos o número de horas em condições extremas. Para a frequência de ocorrência, consideramos o número de Eventos Extremos registrados em cada ano e, por fim, a intensidade [Karunarathna et al., 2014; Sénéchal et al., 2015; Angnuureng et al., 2017] foi calculada seguindo Mendoza et al. [2011]:

$$I = \int_{t1}^{t2} Hs(t)^2 dt \qquad \text{Eq. 4.2}$$

Equação 4.2. Intensidade de eventos extremos integrada no tempo.

onde a duração do Evento Extremo em questão inicia e termina em t1 e t2, respectivamente, representando assim a integral das alturas de onda ao longo de todo o período sob condições extremas.

Capítulo V: Artigo 1

"Wave climate trends and breakpoints during the Atlantic Multidecadal Oscillation (AMO) in southern Brazil"

5.1 Artigo 1

O primeiro manuscrito originado desta Tese é de autoria de Natan Zambroni Maia, Luis Pedro Almeida, Leonardo Emmendorfer, João Luiz Nicolodi e Lauro Calliari e é intitulado ***"Wave climate trends and breakpoints during the Atlantic Multidecadal Oscillation (AMO) in southern Brazil"***, publicado em 2022 no periódico *"**Ocean and Coastal Research**"* e disponível no link https://www.scielo.br/j/ocr/a/R6pyb7ZXZ7Gppb6sQzxrM6b/?format=pdf&lang=en.

Ocean and Coastal Research

ORIGINAL ARTICLE

http://doi.org/10.1590/2675-2824070.21086nzm
ISSN 2675-2824

Wave climate trends and breakpoints during the Atlantic Multidecadal Oscillation (AMO) in southern Brazil

Natan Zambroni Maia[1,*], Luis Pedro Almeida[1,2], Leonardo Emmendorfer[3], João Luiz Nicolodi[1], Lauro Calliari[1]

[1] Universidade Federal do Rio Grande- Instituto de Oceanografia - Laboratório de Oceanografia Geológica - Campus Carreiros (Av. Itália - Carreiros, Rio Grande - 96201-900 - RS - Brazil)
[2] CoLAB +Atlantic - LACS Building (Estrada da Malveira da Serra, 920 - 2750-834 - Cascais Portugal)
[3] Universidade Federal do Rio Grande - Centro de Ciências Computacionais (Rodovia, RS-734, s/n - Carreiros, Rio Grande - 96203-900 - RS - Brazil)

* Corresponding author: natanzambroni@gmail.com

ABSTRACT

Understanding how wave climate variability and its trends change over time are crucial analyses required to mitigate potential wave-induced impacts and adapt coastal areas to such effects. The long-term trends and breakpoints of the wave energy flux (WEF) and its relationship with teleconnection patterns in southern Brazil were studied using ERA-5 wave reanalysis with validation using a waverider. We determined that the interannual mean WEF (WEFm) and extreme WEF (WEF98) that reaches the southern Brazil have increased over the past four decades, with a increment of 0.063 and 0.17 kW/m/year, respectively 0.63 and 0.29% per year. By the Muggeo method we determined that subperiods with increasing WEFm trends are related to the SSE and SSW quadrants and that these are also the most energetic ones and with the highest annual increment rates of WEFm and WEF98. Our results also suggest that the positive trends observed in interannual WEF values are likely related to the long term transition of cold to warm Atlantic Multidecadal Oscillation (AMO) phase in the western South Atlantic Ocean. From a coastal risk perspective, it is important to understand the relationship between climatic indices and the wave climate to support long-term coastal management policies.

Descriptors: Wave hindcast, ERA-5 reanalysis data, Western South Atlantic Ocean, Wave energy flux, Climate indices.

INTRODUCTION

Climate changes, including modifications in wind patterns, will lead to changes in the wave climate that could affect coastal erosion and flooding processes (Mentaschi et al. 2017; Garner et al. 2017; Rasmussen et al. 2018; Vousdoukas et al. 2018; Oliveira et al. 2019a). Understanding how wave characteristics (e.g., the wave height, period, direction and energy) change over time and their long-term trends is crucially required to mitigate potential hazards and allow low-lying coastal areas to adapt to such threats. Therefore, the evaluation of trends in future wave climates is fundamental for the development of efficient policies within the framework of climate change adaptation and mitigation measures (De Leo et al. 2021). Previous studies in the Atlantic Ocean have shown a consensus that the northern part of the North Atlantic Ocean has presented a trend of increasing storminess and mean significant wave height (Kushnir et al. 1997; Wang and Swail 2000; Swail et al. 2000; Wang et al. 2003; Dodet et al. 2010; Mentaschi et al. 2017). Further north, in the Arctic Ocean, Waseda et al. (2018) also found a

Submitted: 17-Sept-2021
Approved: 12-July-2022

Associate Editor: Piero Mazzini

© 2022 The authors. This is an open access article distributed under the terms of the Creative Commons license.

trend of increasing wave heights over the past four decades. Recent studies based on global climate change projections indicate that in the mid-latitude oceans, the wave height and period will increase and the mean wave direction will shift from 5–15° to the north due to changing patterns of storm wind speeds (Hemer et al. 2006; Mori et al. 2010; Semedo et al. 2011; Morim et al. 2019).

Wave measurements in the South Atlantic Ocean are very scarce and, in most cases, consist of occasional short-term observations. For this reason, most previous studies that have investigated trends in the wave climate in the South Atlantic were performed based on hindcast or forecast datasets. According to Reguero et al. (2013) and Oliveira et al. (2019a), increasing trends in significant wave heights were identified in the western South Atlantic over the past 60 and 32 years, respectively. By investigating wave energy flux (WEF) projections using global-scale modeling, the study performed by Mentaschi et al. (2017) found that by the end of this century, there will be a significant increase (up to 30%) in the 100-year return level of the WEF in the majority of coastal areas in the southern temperate zone, including the Southwest Atlantic Ocean. Using in-situ buoy data and model data Pegorelli et al. (2018) identified that the Atlantic coast of Brazil has a moderate wave power, once during all the months of the year, the WEF was consistently estimated within the 10 to 30 kW/m range, with the majors WEF values under influence of the passage of cold front systems, with strong winds from the SSW (Rodrigues et al., 2004; Dominguez, 2006).

According to Silva et al. 2020, wave direction oscillations coexist with long-term variations in interhemispheric surface temperature anomalies, which indicates the influence of temperature-driven atmospheric teleconnections on wave generation cycles. For instance, Reguero et al. (2019) found inter-regional correlation of 0.54 between sea surface temperature (SST) variations in North and tropical Atlantic and WEF variations in extratropical South Atlantic. The global climate has preferred patterns of variability, called climate modes. Climate modes, such as the Southern Annular Mode (SAM), El Niño–Southern Oscillation (ENSO) and the Atlantic Multidecadal Oscillation (AMO), are widely considered to be associated with typical natural climate variability at interannual to multidecadal scales, which is mainly reflected in variations in the patterns and distributions of the sea level pressure (SLP), wind and SST (Thompson and Wallace 1998; Kerr 2000; Trenberth et al. 2002; Hurrell et al. 2003; Hemer et al. 2010; Silva et al. 2020). The wave climate variability in different parts of the globe is modulated by one or a combination of several climate modes; thus, reliable projections of wave characteristics require an in-depth understanding of the relationships between climate modes and the wave climate.

Described by Kerr (2000), the AMO is seen as an indicator of global overturning circulation changes (Biastoch et al. 2015), particularly those related to thermohaline circulation variations. The AMO has been identified as a coherent mode of natural variability occurring in the Atlantic Ocean based upon the average anomalies of SST in the North Atlantic basin, typically over 0-70N and is dominated by multidecadal variations with lest than 0.4 °C of magnitude range alternating between warm (positive) and cold (negative) phases with a periodicity of approximately 70 years and and 0.4 °C of anomaly to global SST (Wang et al. 2009; Frajka-Williams et al. 2017; Kayano et al. 2019; Trenberth & Shea 2006; Trenberth et al. 2021). Warm AMO phases occurred during 1870–1900 and 1925–1963, and cold phases occurred during 1900–1925 and 1963–1995. Since 1995, the AMO has been positive in a new warm phase (Ortega et al. 2013; Alexander et al. 2014).

The imprints of the AMO on the SST and SLP fields, although centered in the North Atlantic, extend well beyond this area and have pronounced influences on weather and climates throughout the world. The AMO largely affects global climate change (Yang et al. 2020), and different effects observed across the globe, such as temperature and pressure variations in the South Atlantic and Pacific, which is a zonally elongated band in the Southern Ocean and in the tropical Pacific, as well as warming in the north and southwest Pacific (Lyu and Yu 2017; Odériz et al. 2020), could be pacemakers of the global air temperature (Kravtsov and Spannagle, 2008). As one of the most important

climate modes, the AMO has been widely linked to prominent regional climate anomalies that can have tremendous worldwide socioeconomic consequences, as in the Asian, Indian and South American monsoons (Zhang and Delworth, 2005; Chiessi et al. 2009), summer drought pattern in China (Qian et al. 2014), Siberian rainfall (Sun et al. 2015), low-frequency El Niño–Southern Oscillation modulations (Timmermann et al. 2007), and changes in rainfall and temperatures over the United States, Australia, Europe and northeast Brazil (Knight et al. 2006; O'Reilly et al. 2017), in addition to modulating Atlantic hurricane and tropical cyclone activity (Goldenberg et al., 2001; McCabe et al., 2004; Wang et al. 2008), wave power in the Southern Ocean (Reguero et al. 2019) and affecting the abundance of fish populations in the Mediterranean and North Atlantic (Alheit et al. 2014).

By concentrating the analyses on the Atlantic, we observe that the AMO effects are felt throughout the ocean, imparting dipole behavior, wherein the warm AMO phase features anomalously warm the North Atlantic and anomalously cool the South Atlantic and Southern Oceans, with strong meridional gradients in the 40°-70°S band, while the cold AMO phase shows an almost reversed-sign SST anomaly pattern (Timmermann et al. 2007; Wang et al. 2008; Latif 2013; Lyu and Yu 2017; Kayano et al. 2019; Reguero et al. 2019). This behavior supports the hypothesis that the driving mechanism of the AMO involves fluctuations of the Atlantic meridional overturning circulation (AMOC) (Delworth and Mann, 2000; Knight et al., 2005; Dijkstra et al., 2006). As the AMOC is enhanced, warming and cooling occur in the North and South Atlantic, respectively, and the opposite is observed with a reduction in the AMOC. According to Crowley and Kim (1993), decadal to multidecadal changes in the thermohaline circulation should primarily affect temperatures in the Atlantic and Southern Ocean, with a clear signature in the SST field in the Weddell Sea and Drake Passage, in addition to changes that are almost out-of-phase between the Northern and Southern Hemispheres.

In the South Atlantic Ocean, previous studies based on wave and SST reanalysis data (Ortega et al. 2013; Alexander et al. 2014; Biastoch et al. 2015; Kayano et al. 2019) have revealed strong relationships between changes in ocean–atmosphere interactions and the AMO index. Studies developed by Biastoch et al. 2015 in the Southeast Atlantic determined that Agulhas leakage and the AMO are correlated and covary on multidecadal timescales. Kayano et al. (2019) demonstrated that in general, the SST anomaly patterns feature nearly zonal structures along the southern midlatitudes, with strong meridional gradients in the South Atlantic. According to these authors, AMO-related large-scale SST anomaly patterns play an important role in cyclone trajectories and the Lorenz energy cycle; thus, low-level cyclones in the South Atlantic are clearly modulated by the AMO, becoming even more energetic in the warm AMO phase than in the cold AMO phase.

Therefore, it is possible to infer that SST meridional gradients alter the longwave baroclinicity, which in turn takes part in the energy cycle in the South Atlantic. During the negative and positive AMO phases, heat flows in ocean–atmosphere interactions induce changes in available potential and kinetic energies, low-level extratropical cyclones, wind patterns and, consequently, the wave climate in the western South Atlantic (Escobar et al. 2004; Ortega et al. 2013; Kayano et al. 2019).

Although general linear trends are known, little is known about the temporal variability in the WEF and its relationship with the AMO in the Southwest Atlantic. As previously demonstrated, the wave climate in this region is under the strong influence of teleconnection patterns. Therefore, WEF trend analyses associated with climate indices, not only linear analyses but also analyses considering breakpoints, provide relevant to contributions to the understanding of WEF behavior in the Southwest Atlantic Ocean, including possible oscillatory behavior. Based on the aforementioned theoretical background, the present study aims to investigate the long-term trends and breakpoints of the WEF in the western South Atlantic using 41 years (from 1979 to 2019) of reanalysis data (ERA-5). The work was divided into two sections: 1) validation of the ERA-5 dataset, wherein wave parameters from ERA-5 reanalysis were compared with those of waverider observations, and 2) historical WEF analysis considering trends and

breakpoints, with an investigation of the relationship between WEF temporal variability and the AMO index. To the best of our knowledge, the Southwest Atlantic WEF variability and its relationship with the AMO documented herein have not been described previously.

METHODS

Study area

The present study focuses on the wave climate in the southwestern Atlantic Ocean, specifically on the extreme southern coast of Brazil (Rio Grande do Sul). Southern Brazil is under the influence of two main systems: the South Atlantic Semifixed Tropical Anticyclone (ATAS) and the Migratory Polar Anticyclone (APM). The swell generally comes from the S/SW (longer waves) and wind-sea varies from NE (shorter waves) under the influence of extratropical cyclones ATAS and from S/SE to S/SW in the presence of extratropical cyclones (Pereira et al. 2017). The seasonaly alternation between these two systems favors the predominance of winds from the northeast (NE) during September through March (ATAS) and the southwest (SW) during April through August (APM) (Godolphin 1976). In addition, it is important to note that the region between the Antarctic Peninsula and southern Brazil has the highest rate of cyclone formation in the Southern Hemisphere (Hoskins and Hodges 2005; Pezzi et al. 2016).

According to the global dynamic classification of coasts proposed by Davies (1964) and King (1972), the Rio Grande do Sul coast is characterized as exhibiting "east coast swell" (Calliari and Klein 1993). Long-period waves with high sediment transport capacity, which are usually formed in the subpolar stormy belt and over the Drake Passage, occur predominantly from the southeast (SE) and less frequently from the south (S) due to the more frequent and strong cyclones in the former direction (Tomazelli and Villwock 1992; Gonzales et al. 2016). Sea waves, which are generated by local winds, come mainly from the east (E) and northeast (NE) and are related to the prevailing winds in the region. Storm waves have a lower frequency of occurrence and are formed by strong winds from southern quadrants during extreme meteo-oceanographic events (Motta 1969; Maia et al. 2016).

On the Rio Grande do Sul coast, waves exhibit a directional bimodality distribution (Pereira et al. 2017).. According to Pianca et al. (2010), during the summer, the predominant wave directions are from the NE (28.4%) and S (26.7%), with NE waves presenting heights between 1 and 2 m, with periods between 6 and 8 s, and S waves presenting heights between 1 and 3 m, with periods from 8 to 12 s. In autumn and winter, the dominant wave direction is from the S (36.7%), with heights between 2 and 3 m and periods between 10 and 12 s. In the spring, NE waves are dominant, with heights between 1 and 3 m and periods from 6 to 8 s, although an important contribution from S waves with heights between 1 and 3 m and periods from 8 to 10 s still occurs.

ERA-5 wave data

Wave data were obtained from the ERA-5 reanalysis dataset (Hersbach et al. 2020; Copernicus Climate Change Service (C3S) 2017) covering 41 years (from 1979 to 2019) and we used a 3-h temporal resolution to calculate annual averages for an Eulerian analysis from a single point located at the coordinates 32°30'S/50°W at a 1000 m depth (deep waters) (Figure 1).

The ERA-5 reanalysis is a global atmospheric, wave and ice data assimilation system that provides free products ranging from 1979 to the present in a near real-time scheme and is maintained by the European Centre for Medium-Range Weather Forecasts – ECMWF. ERA-5 wave data are generated by the WAM, which is a 3rd-generation model that integrates the basic transport equation describing the evolution of a two-dimensional ocean wave spectrum without additional unplanned assumptions regarding the spectral shape. The WAM uses altimeter wave height and advanced SAR observations as the source in the model assimilation and ETOPO2 as a bathymetry database from the National Geophysical Data Center (NGDC/NOAA).

There are three explicit source functions that describe the wind input, nonlinear transfer and whitecapping dissipation. There is an additional bottom dissipation source function, and refraction

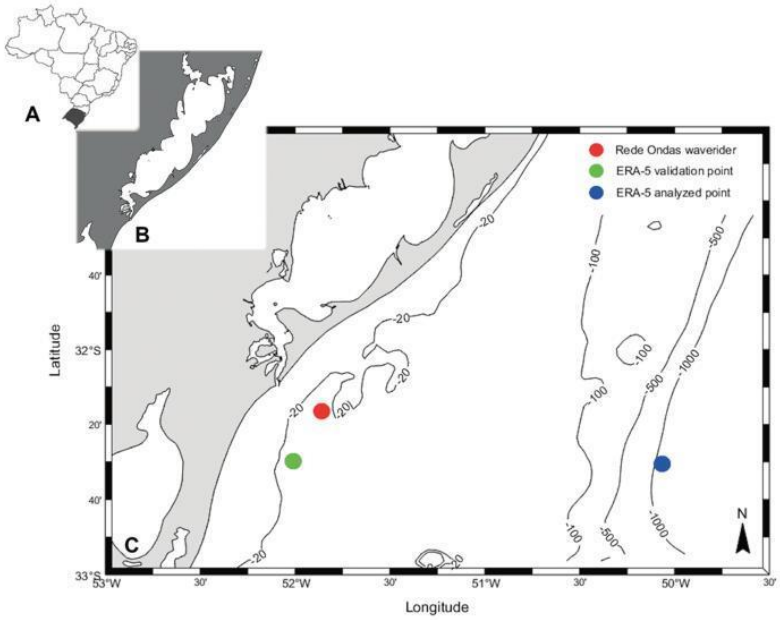


Figure 1. Locations of the Rede Ondas waverider, ERA-5 validation point and ERA-5 analyzed point.

terms are included in the finite-depth version of the model, so it takes in account for basic shallow water physics, namely the maximum wave energy and the frequency down shifting are controlled by the water depth. The model runs on a spherical latitude-longitude grid and can be used in any ocean region. The WAM predicts directional spectra along with wave properties such as the significant wave height, mean wave direction and frequency, swell wave height and mean direction, and wind stress fields corrected by including the wave-induced stress and the drag coefficient at each grid point at chosen output times (The Wamdi Group 1988; Dee et al. 2011). The slow attenuation of long-period swells and the impact of shallow water on the wind input are introduced with the overall return of the level of dissipation due to white capping. Taking into account that the model uses data assimilation in intermediate waters, its products consider the wave transformations induced by the variation of depth and interaction with the bottom. However, it is worth mentioning that due to the 0.5° grid resolution of the model, bathymetric variations smaller than this scale may not be well represented and cause uncertainties in some results, such as the wave direction. A detailed description of ERA-5 may be found in Hersbach et al. (2020). ERA-ECMWF reanalysis data have been extensively used in other studies to provide relevant results (Hoskins and Hodges 2005; Harley et al. 2010; Semedo et al. 2011; Vousdoukas et al. 2018; Waseda et al. 2018; Wan et al. 2018).

Comparison between ERA-5 and in situ observations from a waverider

To validate the ERA-5 data base for our region of interest, wave observations from a local waverider (model Mark III -Datawell) from the Rede Ondas Project (www.redeondas.furg.br), which is part of the Global Ocean Observation Program (GOOS-UNESCO), were used. The waverider is located at coordinates 32°20'23''S/51°53'53''W and we compared it with another ERA-5 point at coordinates 32°30'S/52°W. These points are 20 km apart and are 25 m of deep (Figure 1). Both ERA-5 and waverider data comprise measurements of significant wave height (Hs), mean period (T), and mean wave direction (θ). After validation of the ERA-5 the WEF was computed for our point of interest at 1000m depth following Equation 1:

$$\mathrm{WEF} = \frac{\rho g^2 Hs^2 T}{64\pi} \quad \text{Equation 1}$$

where ρ is the water density (kg/m³), g is the gravitational acceleration (m/s²), Hs is the significant wave height (m), and T*e* is the energy period (s). The energy period (T*e* or T*–10*) can be estimated from the spectral shape and other parameters. The mean period (T or T*01*) and the energy period can be related through the Equation 2:

$$Te = \frac{m_{-1}}{m_0} = \alpha T \quad \text{Equation 2}$$

where α depends on the spectral shape. Here, α is assumed to be 0.538 (Reguero et al. 2015; Antolínez et al. 2016; Reguero et al. 2019). The WEF provides an indication of the potential wave energy (combining both the wave period and height) that can reach the coast and has been widely used in wave climate studies (Antolínez et al. 2016, Mentaschi et al. 2017, Marshall et al. 2018, Reguero et al. 2019, Odériz et al. 2020). To compare both datasets, continuous hourly records covering nine months of 2016 (excluding March, November and December) were used. To evaluate the quality of the comparisons, three statistical parameters were calculated: Pearson's correlation coefficient (R; at a 95% confidence interval), the root mean square error (RMSE) and the bias of the fit. The "R" parameter measures the possible degree of relation between two variables, the RMSE determines the average magnitude of the difference between an estimated and true value, and bias evaluates the differences between measured and simulated data (zero bias means that the predictor parameter is unbiased).

Wave climate trends

For the analysis of 41 years of ERA-5 wave climate data (from 1979 to 2019), the data were separated into four directional sectors containing only the waves that affect the coastal zone, considering the distinct wave climate forcing sources that affect this region and the coastline orientation (NE-SW) (Tomazelli and Villwock 1992; Gonzales et al. 2016; Motta 1969; Maia et al. 2016; Pianca et al., 2010). The annual mean and 98th percentile of the WEF were computed for the 41-year ERA-5 data, and long-term linear trends were calculated using a linear regression model at a 95% confidence level. The statistical significance of long-term trends was verified through an analysis of variance (ANOVA) at a 95% confidence level. ANOVA is a statistical tool that defines whether the mean values of any variable are significantly different from each other (critical F < F; P < 0.05).

Segmented linear regression and breakpoint detection

In this paper, to identify changing trends in WEF time series, we used a method proposed by Muggeo (2003) to fit segmented relationships in regression models. Thus, it was possible to identify breakpoints indicating that there were statistically significant changes in the behavioral trends of the WEF time series analyzed. Segmented linear regression represents a dependent variable Y as a piecewise linear function of an independent variable X. The values of X that determine changes in the linear models are called breakpoints, which can be determined by the iterative Muggeo method. For each breakpoint BPk detected, two linear models consistent with the input data are inferred (Eq. 3 and Eq. 4):

$$\mathbf{Yr = \beta 1.X + c1} \text{ for } \mathrm{X < BPk} \quad \text{Equation 3}$$

$$\mathbf{Yr = \beta 2.X + C2} \text{ for } \mathrm{X > BPk} \quad \text{Equation 4}$$

where Yr is the piecewise linear estimation of variable Y, β1 and β2 are the slopes of the linear models, and c1 and c2 are the constant coefficients of the linear models.

The detection of breakpoints occurs as follows. For a single variable, the residuals resulting from the linear model are normalized by dividing them by their corresponding standard deviation. The normalized residuals are represented by a segmented linear model, giving rise to subperiods, wherein breakpoints are detected using the Muggeo (2003) method. Each segmented linear model is submitted to a F-Test to compare variances, and its p-value at a 95% confidence level indicates whether there is any significant trend in each analyzed

subperiod. The number of breakpoints is increased iteratively while the method converges, and the final number of breakpoints is reported as the result. For a pair of variables or even a larger group, the procedure is the same, except that the normalized residuals from all variables considered are aggregated under the same series.

AMO INDEX

Based on its influence across the Atlantic Ocean, the AMO index was used to represent large-scale processes that may influence climatic conditions in the South Atlantic and was obtained from the National Oceanic and Atmospheric Administration (NOAA). The AMO dataset consists of gridded average anomalies of the Kaplan SST in the North Atlantic basin over 0–70N from 1856 to the present derived from UK Met Office SST data subjected to sophisticated statistical techniques to fill gaps (NOAA; Enfield et al. 2001). To investigate the relationship between the WEF temporal variability and the AMO, a time-window filter of 10 years (Enfield et al. 2001; Lyu and Yu 2017) was applied to both the WEF and AMO datasets. Following this filter, the linear correlation between the WEF annual mean (WEFm), 98th percentile (WEF98) and the AMO index were calculated according to Oderiz et al. (2020), where the range of values for the correlation coefficient was denoted as follows: 0 indicates no relationship between the variables; values between 0 and 0.25 (– 0.25 and 0) indicate a weak positive (negative) correlation; values between 0.25 and 0.5 (– 0.5 and – 0.25) have a moderate positive (negative) correlation; values between 0.5 and 0.75 (– 0.75 and – 0.5) show a strong positive (negative) correlation; and values be- tween 0.75 and 1.0 (– 1.0 and – 0.75) indicate a very strong positive (negative) correlation.

RESULTS

ERA-5 WAVE DATA VALIDATION

The correlation between ERA-5 wave data and waverider measurements indicates good agreement between the majority of compared data (Table 1). Of all compared wave parameters, Hs showed the highest correlation (R = 0.82) and lower RMSE value (0.41), with ERA-5 showing a great ability to capture extreme events (as observed in October 2016) and mean wave heights with similar quality (Table 1 and Figure 2). The bias value indicated that ERA-5 tends to overestimate Hs values by 0.22 m.

The T results showed a value of RMSE=2.79 and a correlation value of R = 0.55, which was considered statistically moderate. The T bias value showed that, on average, ERA-5 underestimated the waverider observations by 0.71 s. The θ showed a slightly higher R value of 0.6, also indicating a moderate agreement between both datasets (Table 1) and the highest value of RMSE, 39.49.

A statistical comparison between the mean and standard deviation (stdv) values computed for the entire validation dataset showed that ERA-5 presented an average Hs value of 1.44 m (stdv=0.54) and T of 8.79 s (stdv=2.34), which were close to the mean values computed based on waverider observations, at 1.22 m (stdv=0.57) and 9.5 s (stdv=3.16), respectively. For the wave direction, the mean values were similar under the predominant wave direction as the SE quadrant (147.2° for the waverider (stdv=23.49) and 137.6° for ERA-5 (stdv=47.44)), which was an expected result, considering that the time series used for this comparison does not include summer months (March, November and December), when

Table 1. Statistical results of the comparison between ERA-5 reanalysis data and Rede Ondas waverider data using nine months of records from 2016 (n=5575 for each parameter). Hs= significant wave height; Tp= peak period; θ= mean wave direction; R= Pearson's correlation coefficient; RMSE= root mean square error.

Parameter	R	RMSE	BIAS
Hs (m)	0.82	0.41	+0.22
Tp (s)	0.55	2.79	-0.71
θ (°)	0.6	39.49	-

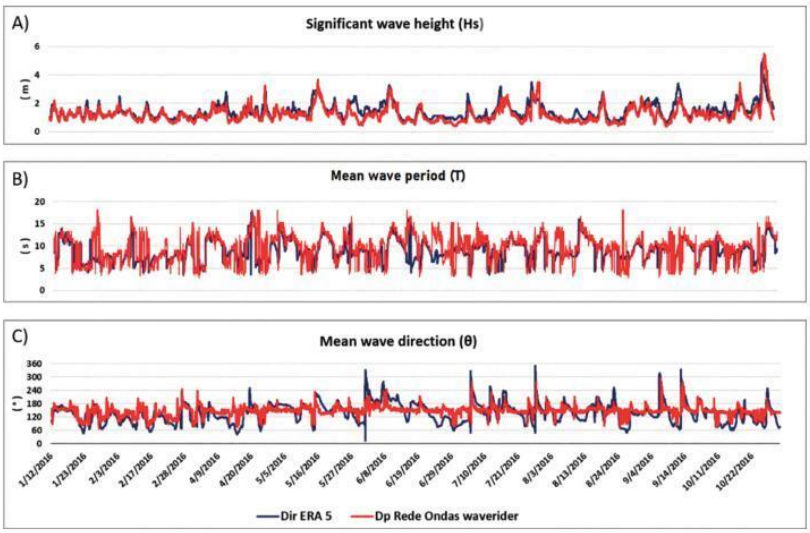


Figure 2. Time series of overlapping Hs (A), T (B) and θ (C) from ERA-5 and Rede Ondas waverider data during 2016.

waves from northern directions are more frequent (Pianca et al. 2010). In addition to this fact and as already pointed out, it is important to consider that some bathymetric features and consequently the refraction processes may not be well represented by the model and thus, the validation process between waverider and ERA-5 may contain inaccuracies. Since refraction reduces the variability of direction towards the coast and tends to keep them in an alignment perpendicular to it, waves registered by waverider seems to be more affected by refraction than waves in the ERA-5 node. This fact can be observed in the higher values of stdv associated with the model data than those associated with that observed by the buoy (47.44 x 23.49) and may also explain the lower correlation value associated with the two databases (R=0.6) as well as its highest RMSE value (39.49).

Despite these potential inaccuracies, in general, the ERA-5 data well represented the values of Hs, T and θ recorded by the Rede Ondas waverider. The high resolution of the hindcast, as well as its validation against in-situ measurements, brings confidence to the data base, particularly for its use in long term and average conditions analysis, as is the case here.

ERA 5 comparisons for Southern Brazil

The ERA-5 wave data effectively represented the Hs, T and θ values recorded by the Rede Ondas waverider. The comparison with other studies that performed validation tests between reanalysis data and in situ measurements is shown in Table 2. As already pointed out by Almeida et al. (2011), these results sometimes differ from other previous studies, probably due to factors such as the different modeling strategies used (e.g., the resolutions of wind fields and model grids) and varying dataset lengths, areas and time periods but, in general, they present similarities between the correlation values of the analyzed variables. The results presented herein, as quantified by the different statistical analyses performed, are similar to comparisons performed in previous studies in different oceans around the globe (Table 2). The statistical evaluation of ERA-5 wave reanalysis performed in the present work provides a high level of confidence that this dataset can be used in this region of the South Atlantic to analyze wave climate variability and trends.

According to Waseda et al. 2018 and Oliveira et al. 2019a, the validation analysis showed that the model skill in hindcasting Hs is higher

Table 2. Statistical validation parameters found in the current work and by other authors, including the database and locations of each study. Hs= significant wave height; T= mean period; θ= mean wave direction; R= Pearson's correlation coefficient; RMSE= root mean square error.

	Present work, ERA-5, Southern Brazilian coast		Almeida et al. (2011) Wave Watch III, Portuguese coast		Wan et al. (2018) ERA-Interim, China sea		Waseda et al. (2018) ERA-Interim, Artic sea		Oliveira et al. (2019a) Wave Watch III, Southern Brazilian coast		Odériz et al. (2020) ERA-5, Pacific Ocean	
Parameter	**R**	**RMSE**	**R**	**RMSE**	**R**	**RMSE**	**R**	**RMSE**	**R**	**RMSE**	**R**	**RMSE**
Hs (m)	0.82	0.41	0.86	0.36	0.95	0.36	0.91	0.78	0.86	0.34	0.8	0.5
T (s)	0.55	2.79	-	-	0.78	0.76	-	-	0.69	1.4	-	-
θ (°)	0.6	39.49	-	-	-	-	-	-	0.69	38	-	-

than its ability to reproduce T and θ, as noted in the "R values" in Table 2. According to these authors, this result may be related to the fact that the wind resolution used to force the model might not have accurately represented the bimodal condition of the sea in the region since it is influenced by local winds.

In this validation process, it is worth mentioning that in both the ERA-5 and Rede Ondas waverider data recorded on October 28 and 29, 2016, the Hs was larger than 5 m, which was the result of the strongest coastal storm in the last 40 years in the region, and the waves were responsible for a large amount of beach erosion (Oliveira et al. 2019b).

Wave climate trends

To analyze the WEF behavior between 1979 and 2019, we calculated the long-term linear trends using linear regression models. In an analysis considering all incident wave directions (ENE-SSW), the results from the regression analysis using 41 years of wave data indicated that the linear trends observed in WEFm and WEF98 records were statistically significant (p-value < 0.05) (Table 3). Over the analyzed periods, the general WEFm and WEF98 presented an ascending trends (Figure 3), with an increment rate of 0.063 and 0.17 kW/m/year respectively.

Table 3. P-values from regression analyses of WEFm and WEF98 from the ERA-5 database tendency analysis. WEFm=mean wave energy flux; WEF98= extreme wave energy flux (98th percentile).

Parameter	p-value	Linear Trend
WEFm	$1.2x10^{-7}$	+0.063 kW/m/year (0.63% /year)
WEF98	$1.24x10^{-2}$	+0.17 kW/m/year (0.29% /year)

In addition to the analysis covering all quadrants in the same series, the WEFm and WEF98 were calculated separately for each quadrant. As shown in Table 4, the SSW quadrant presented the most energetic waves under both mean and extreme conditions (17.21 and 83.53 kW/m, respectively), in contrast to ENE waves, which were less energetic (7.37 and 40.33 kW/m, respectively). As waves begin to come more from the south, the WEFm and WEF98 associated with the waves become greater.

We also performed an ANOVA for WEFm and WEF98, referring to all directional occurrences of incident waves: the ENE, ESE, SSE and SSW quadrants. According to Table 5, we observed that there were relevant variations in the WEFm associated with waves coming all quadrants (F>critical F and p-value <0.05) and that they presented increase rates close to those of the general WEFm, at 0.054, 0.059, 0.073 and 0,094 kW/m/year, respectively. As the waves come more from the south, the greater is the annual WEFm increment associated with them. When isolated, all quadrants under extreme conditions (WEF98) showed no significant linear trend (F<critical F and p-value> 0.05).

Linear trends and breakpoints

Based on variations over the 41 analyzed years, we applied the Muggeo (2003) method for the normalized residual from the linear WEFm and WEF98 models. The breakpoints indicated that the surrounding subperiods presented different trends. Subperiods with continuous lines showed significant variations within the subperiod itself (with trend; p-value<0.05), and subperiods

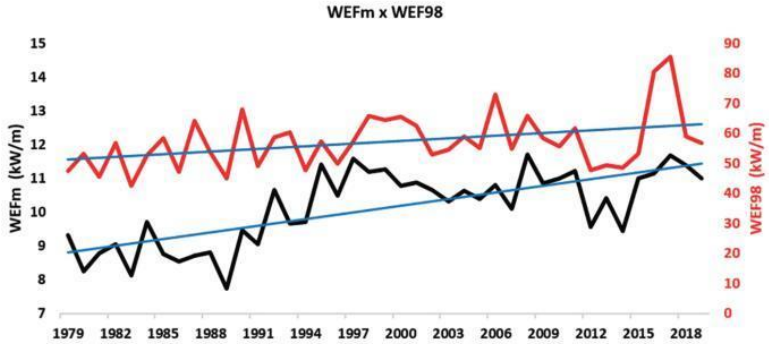


Figure 3. WEF variation between 1979–2019. The black and red lines indicate WEFm and WEF98 variations during all analyzed periods, respectively. The blue continuous lines indicates the significant growth trend of the WEFm and WEF98. WEFm=mean wave energy flux; WEF98= extreme wave energy flux (98th percentile).

Table 4. WEFm and WEF98 associated with each quadrant. WEFm=mean wave energy flux; WEF98= extreme wave energy flux (98th percentile).

	ENE (45–90°)	ESE (90–135°)	SSE (135–180°)	SSW (180–225°)
WEFm (kW/m)	7.37	8.51	10.6	17.21
WEF98 (kW/m)	40.33	44.15	47.31	83.53

Table 5. ANOVA for the WEFm and WEF98 of all wave incidence quadrants. WEFm=mean wave energy flux; WEF98= extreme wave energy flux (98th percentile); F= F-statistics.

Parameter	F	critical F	p-value	Linear Trend
WEFmENE	13.07	2.84	$4.3x10^{-6}$	+0.054 kW/m/year
WEFmESE	9.42	2.83	$7.76x10^{-5}$	+0.059 kW/m/year
WEFmSSE	18.44	3.23	$2.11x10^{-6}$	+0.073 kW/m/year
WEFmSSW	11.33	2.84	$1,63x10^{-5}$	+0.094 kW/m/year
WEF98ENE	2.63	4.08	$1.1x10^{-1}$	-
WEF98ESE	2.34	4.08	$1.34x10^{-1}$	-
WEF98SSE	0.38	4.08	$5.44x10^{-1}$	-
WEF98SSW	$7.89x10^{-3}$	2.84	$9.99x10^{-1}$	-

with segmented lines did not present significant variations within the subperiod (without trend; p-value>0.05) (Figures 4 and 5). We identified three and two breakpoints for the WEFm and WEF98, respectively, which indicated that there were significant changes in the behavioral trends of both parameters. Figure 4 indicates the WEFm breakpoints in 1989, 1997 and 2014 which are the boundaries of the 1979–1989 (I), 1989–1997 (II), 1997–2014 (III) and 2014-2019 (IV) subperiods that presented alternating behaviors regarding the decreasing and increasing trends of the WEFm. Subperiod (I) was characterized by a decreasing trend, followed by subperiod (II) with an increasing trend lasting 10 years. The following subperiod (III) of 18 years showed a downward trend between 1997 and 2014 and the last subperiod (IV) showed upward trend for the last 5 years of the time serie. The first three subperiods showed statistically significant variations in their trends with (continuous line), with p-values=0.04, 0.01 and 0.0001 while the last subperiod didn't show statistically significant trend (segmented line; p-value=0.26) Regarding the WEF98 trends, we identified two inflection points, 2008 and 2012, which delimit the following subperiods: 1979–2008 (I), 2008–2012

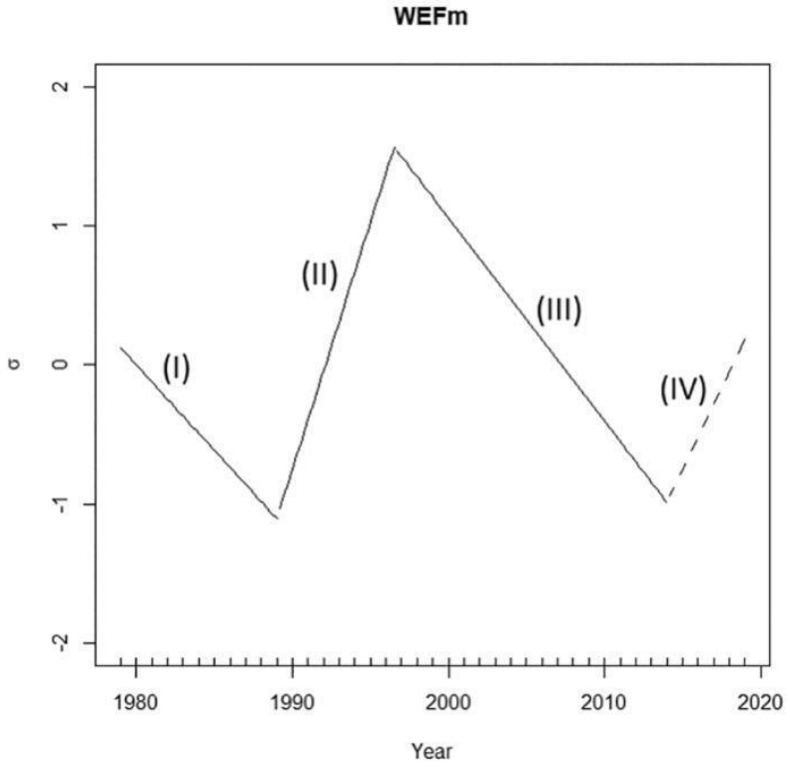


Figure 4. Segmented linear model of the normalized residuals from WEFm linear models. Continuous lines indicate subperiods with significant variations and segmented lines indicate subperiod without significant variations. WEFm=mean wave energy flux.

(II), and 2012–2019 (III) (Figure 5). Similar to the WEFm, the WEF98 presented alternating oscillations between positive and negative trends,but all subperiods, (I), (II) and (III), did not present statistically significant trends (segmented line; p-values=0.32, 0.11 and 0.26, respectively).

Although the WEFm presents oscillatory behavior (Figure 4), there was a statistically significant and generally positive trend between 1979 and 2019 (Table 3, Figure 3), and Table 6 indicates that the mean WEFm in each subperiod identified by the Muggeo method increased over the 41 years. Subperiod (I) presented 8.71 kW/m as the mean WEFm, subperiod (II) presented a value of 9.98 kW/m, while subperiod (III) presented a higher value at 10.71 kW/m and subperiod (IV) had the largest WEFm overall, at 10.95 kW/m. Thus, by presenting the 4 subperiods with mean values of WEFm in a gradually increasing way, Muggeo analysis reinforces the result found of the increasing tendency of general WEFm indicated in Figure 3. The mean values of each WEF98 subperiod identified by the Muggeo method (Figure 5) are adjusted in Table 7 and also present average values in an increasing manner for each sub-period, then 56.3 (I), 57. 86 (II) and 60.1 (III), reinforcing the positive trend found in the general behavior of WEF98 over the 41 analyzed years (Figure 3). We decomposed WEFm and WEF98 into four different quadrants, and through Figs. 6 and 7, it is possible to observe that all quadrants presented breakpoints throughout their time evolution, indicating that there were subperiods with different behavioral tendencies regarding variations in wave energy. For the WEFm (Figure 6), only the ENE quadrant didn't show at least one subperiod with a significant negative or

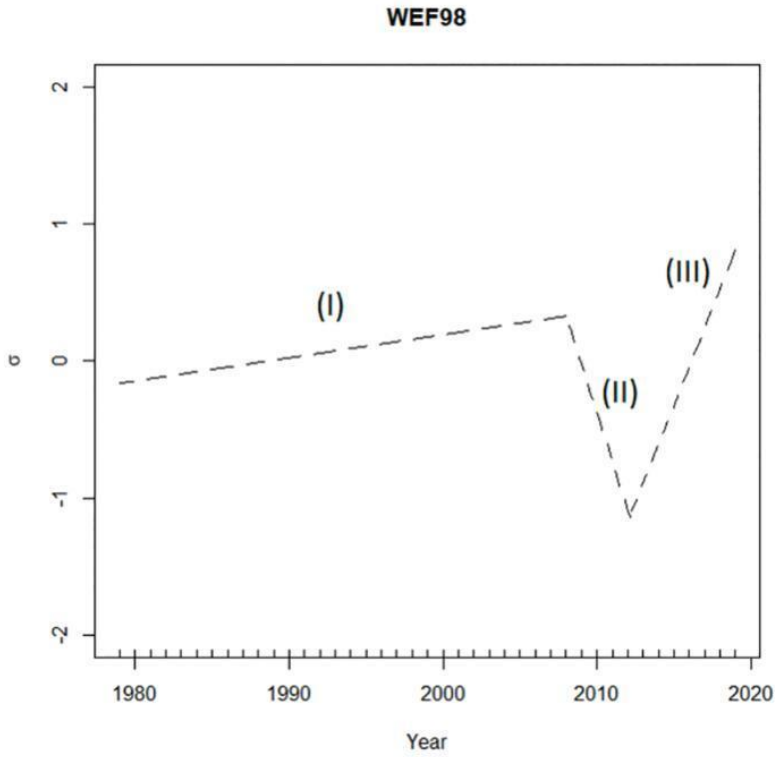


Figure 5. Segmented linear model of the normalized residuals from WEF98 linear models. The segmented lines indicate subperiods without significant variations. WEF98= extreme wave energy flux (98th percentile).

Table 6. WEFm values for the subperiods defined by the breakpoints identified using the Muggeo method. WEFm=mean wave energy flux.

Period	1979–1989 (I)	1989–1997 (II)	1997–2014 (III)	2014-2019 (IV)
WEFm (kW/m)	8.71	9.98	10.71	10.95

Table 7. WEF98 means for the subperiods defined by the breakpoints identified using the Muggeo method. WEF98= extreme wave energy flux (98th percentile).

Period	1979–2008 (I)	2008-2012 (II)	2012–2019 (III)
WEF98 (kW/m)	56.3	57.86	60.1

positive trend (continuous line). Negative subperiods were associated with the ESE quadrant between 1997–2013,SSE quadrant between 1999–2019 and SSW quadrant between 1992-2013 Positive trends were associated with the ESE quadrant between 2013–2019, SSE quadrant between 1989-1999 and the SSW quadrant between 1986–1992.

Regarding WEF98 (Figure 7), all subperiods of all quadrants showed growth and decreasing trends without statistical significance (segmented line).

WEF VARIABILITY AND THE AMO INDEX

In Figure 8, it is possible to observe that since the 1970s, the AMO index has been increasing,

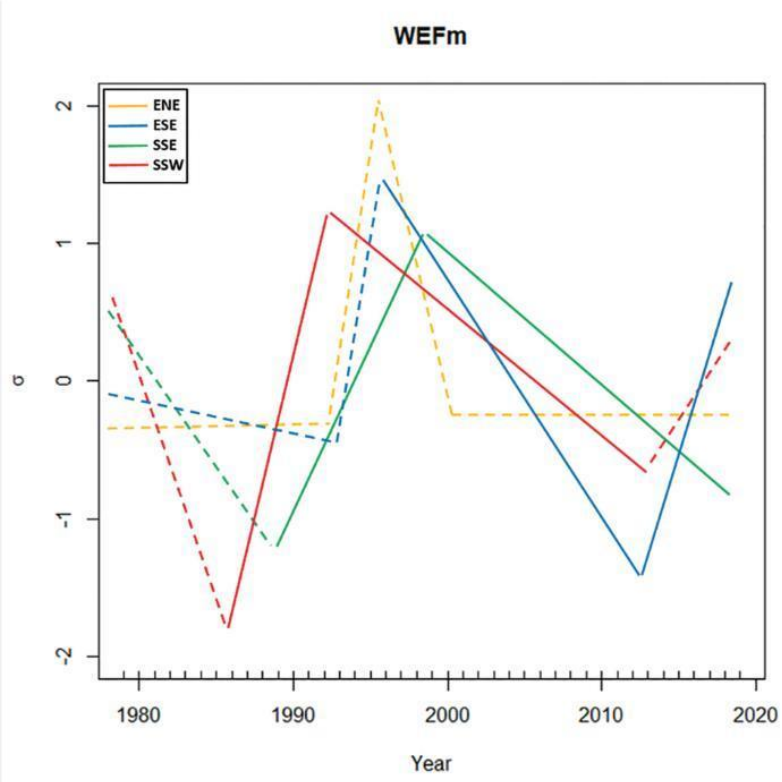


Figure 6. WEFm variation per quadrant. Continuous lines indicate subperiods with significant variations, and segmented lines indicate subperiods without significant variations. WEFm=mean wave energy flux.

shifting to a warm phase in the late 1990s. For the WEFm (Figure 8A), the results show that the 10-year running mean was very well synchronized with this AMO transition, as expressed by the very strong correlation coefficient obtained between the variables (R = 0.92, 95% significance level). For extreme energy conditions, the correlation between the 10-year running mean WEF98 and AMO was also very strong, at R= 0.89. As demonstrated by Odériz et al. (2020), R values between 0.75 and 1 indicate a very strong positive correlation between the WEF and AMO. Both curves have good synchrony with the AMO curve, showing similar behavioral trends, but in 2002, while the AMO stabilized with a small increasing trend, the WEF98 showed a decreasing trend, returning to follow the AMO trend in 2011 (Figure 8B).

We decomposed the average incident energy flux on the coast into the four main quadrants and related them to the AMO index variation from 1979 to 2019 (Figure 9). All quadrants followed the general trend of AMO variation, with a correlation coefficient (95% significance level) for the ENE of R = 0.89; for the ESE of R = 0.91; for the SSE of R = 0.97; and for the SSW of R = 0.86. According to Odériz et al. (2020), the correlation values between the WEF and AMO are considered very strong (R> 0.75). The largest range of WEFm variation was associated with the SSW quadrant, as shown in Figure 9D.

DISCUSSION

WEF TRENDS AND BREAKPOINTS

As shown in Table 3 and Figure 3, the general WEFm presented a significantly positive linear trend over the entire analyzed period (between

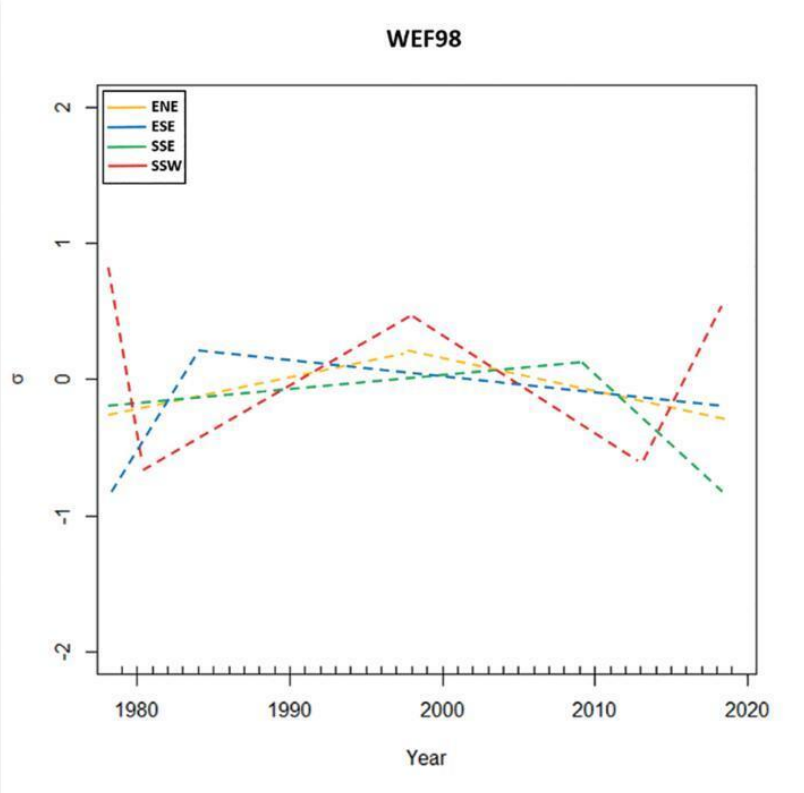


Figure 7. WEF98 variation per quadrant. Segmented lines indicate subperiods without significant variations. WEF98= extreme wave energy flux (98th percentile).

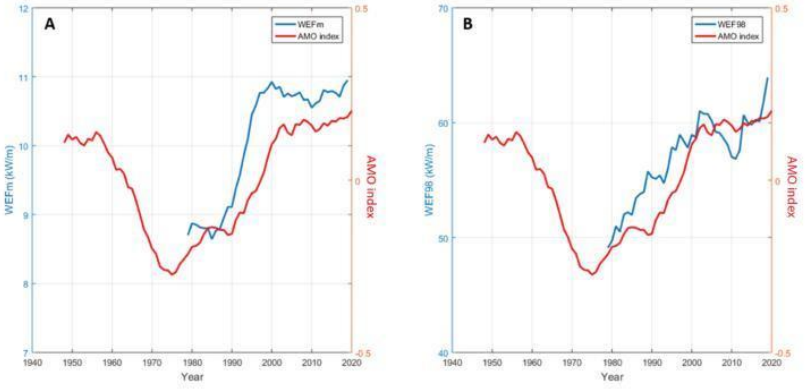


Figure 8. Comparison between the AMO index (red line), 10-year running mean WEFm (blue line, A) and 10-year running mean WEF98 (blue line, B). AMO= Atlantic Multidecadal Oscillation; WEFm = mean wave energy flux; WEF98= extreme wave energy flux (98th percentile).

1979 and 2019) at an increase rate of 0.063 kW/m/year, which was equivalent to an annual increase of 0.63% and indicates more energy transference from the atmosphere to the ocean surface motion. This value is similar to the 0.58% found by Reguero et al. (2019) as a mean of annual increase rate

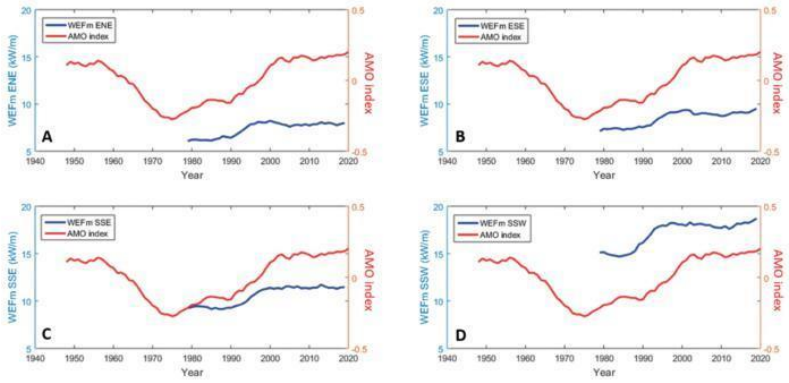


Figure 9. Comparison between the AMO index (red line) and 10-year running mean WEFm values per quadrant (blue lines). AMO= Atlantic Multidecadal Oscillation; WEF = mean wave energy flux.

between 1948 and 2008 to the Southern Ocean (between 40 and 80°S), which besides being that is the most energetic oceanic basin and dominates the other oceans in terms of wave power has a great influence as a generation area on the wave characteristics of our analyzed region. To the same period, according to these authors the global mean WEFm has increased 0,47% per year. The general extreme condition (WEF98) also presented a significantly positive linear trend over the entire analyzed period, with an increase rate of 0.17 kW/m/year, that corresponds to an annual increase of 0.29%. (Table 3 and Figure 3). The results found related with WEFm and WEF98 are in line with global tendencies. According to Mentaschi et al. (2017), the WEF along coasts worldwide is projected to increase significantly by the end of the century, mainly in the Southern Hemisphere. Semedo et al. (2013) found that changes in the wave climate toward the end of the twenty-first century are small to moderate, with the largest signals being a poleward shift in the annual mean significant wave heights in the midlatitudes of both hemispheres, which is more pronounced in the Southern Hemisphere and most likely associated with a corresponding shift in midlatitude storm tracks.

The studies by Reguero et al. (2013) and Alonso and Solari (2021) indicated that the WEF on the West Atlantic coast is undergoing a clockwise rotational trend. These changes are probably related to the trend of rotating toward the poles detected in extratropical storm activity (Meehl et al., 2007), which indicates more storm activity at high latitudes that is more pronounced in the Southern Hemisphere (Bengtsson et al., 2006). In fact, by applying the Muggeo method, we observed in Figure. 6 that the swell coming from the southernmost quadrants (SSW and SSE) were the first to show a significant upward trend in WEFm between 1986-1992 and 1989-1999 respectively, while the ESE swell showed between 1997-2013 the longest range of a subperiod with a significant negative trend.

Rotating southward in the clockwise direction, we observed that waves coming from the ESE (2013-2019), SSE (1989-1999) and SSW (1986-1992) quadrants showed an increasing range scale in significant positive trends associated with general WEFm (Fig. 6) and that only the southern quadrants (SSE and SSW) were responsible for inducing significant positive trends in WEFm (Fig. 4, subperiod II). A relevant factor is associated with the fact that, by decomposing Figure 4 into 4 quadrants of wave incidence we observed that the segmented WEFm trends (Fig. 4) are primarily driven by the swell coming from SSW and secondarily by waves from SSE (Fig. 6).This trends coupled with the fact that the swell from southern quadrants are the most energetic (Table 4) suggests that these waves are probably mainly responsible for the increasing trend of thegeneral WEFm (Figure 3), since as can be seen in Table 5 the SSE and SSW quadrants have the highest annual increment rates associated with WEFm, 0.073 kW/m/year and 0.094 kW/m/year respectively. This scenario is of considerable relevance since swells

generated in the Southern Ocean are projected to be more energetic in the coming years (Young et al. 2011; Babanin et al. 2019) and, in the western South Atlantic Ocean, SW swells are strongly influenced by winds from low latitudes generated by the Migratory Polar Anticyclone (APM), which is responsible for the generation of storms that can suddenly impact the coastline when they reach the continent (Calliari et al. 1998; Parise et al. 2009; Machado et al. 2010).

Although the subperiods associated with WEF98 show no significant trend (Fig. 5), their inflection points and subperiods also resemble the behavior of the WEF98 subperiods associated with the SSE and SSW quadrants. However, it is worth noting that in a linear analysis as evidenced in Figure 3, WEF98 shows a significant growth trend at a rate of 0.17 kW/m/year equaling 0.29% per year (Table 3). These results are relevant since, according to some authors, this trend in extreme wave conditions may intensify in the coming years. Mentaschi et al. (2017) conducted a comprehensive modeling analysis to identify future global trends in extreme wave energy flux along coastlines in the 21st century under a high emission pathway (RCP 8.5 - IPCC) and identified that the WEF increment translates into considerable changes in the recurrence frequency of extreme events, which is projected double in many areas, especially in the Southern Hemisphere where an increase in the extreme WEF is projected until 2100 implying an intensification of coastal erosion and wave-induced impacts. Corroborating these results and also under the RCP 8.5 scenario, Meucci et al. (2020) project an increase by up to 20% in the 100-year significant wave height of the Southern and South Atlantic Oceans by 2100, which would have the potential to increase the extreme conditions of WEF of these regions.

WEF variations and the AMO index

Wave conditions are expected to respond to climatic variations. In recent decades, for example, positive correlations were obtained between sea surface temperatures in the Tropical and North Atlantic and wave power in the southern extratropics, suggesting an intensification of energy transfer from wind fields into wave generation in these regions as a result of warming trends (Reguero et al. 2019; Silva et al. 2020). Consequently, the WEF variability reflects changes in the predominant wave-generating atmospheric systems, which are normally caused by large-scale climatic drivers (Hemer et al. 2010, Reguero et al. 2019, Silva et al. 2020). Globally, Mentaschi et al. (2017) and Odériz et al. (2020) showed that the most significant long-term WEF trends can be explained by the intensification of teleconnection patterns such as the Antarctic Oscillation, El Niño–Southern Oscillation, North Atlantic Oscillation and Atlantic Multidecadal Oscillation.

As demonstrated by Young et al. (2011) and Yang et al. (2020), it is highly likely that long-term oscillations, such as the AMO, significantly influence the global ocean wind and wave climate since global-scale multidecadal SST variability could be driven by the AMO through atmospheric teleconnections and atmosphere–ocean coupling processes. According to Alexander et al. (2014) and Odériz et al. (2020), the Atlantic Ocean exhibits variability over a wide range of temporal and spatial scales but has pronounced variability at decadal and multidecadal timescales, playing a key role in the multidecadal oscillation of global SST (Yang et al. 2020).

Through calculation of correlation between WEF and climate indices Odériz et al. (2020) indicated that the WEF that reaches both Mexican coasts is influenced by the AMO on multidecadal timescales, once the AMO shows a regionally consistent wave climate response of moderate positive correlation on the Yucatan Peninsula and entire Pacific coast for WEF. Thus, according with these authors not only the Atlantic but also the Pacific Ocean may have the long-term variability of WEF driven by AMO, wich positive (negative) phases drives an increase (decrease) in wave power. Kayano et al. (2019) show that low-level extratropical cyclones in the South Atlantic are modulated by AMO-related SST anomalies, with positive anomalies affecting the cyclone trajectories and meridional SST gradients that influence the baroclinicity of long waves, which in turn enters the energy Lorenz cycle. This fact is of great importance for the region, once extratropical cyclones are known to generate extreme significant wave height values and consequentely improving

WEF at the ocean surface in the western South Atlantic (Sasaki et al. 2021). At atmospheric levels in both AMO phases, the highest baroclinic and barotropic energy conversion values occur along the 30°–50° and 20°–50°S bands, with the largest cyclone local counts in the southwestern Atlantic, specifically on the Argentina, Uruguay and southern Brazil coasts (Sinclair 1995, 1997; Kayano et al. 2019). According to Kayano et al. (op. cit.), the kinetic energy in warm AMO phases surpasses that in cold AMO phases; thus, the considerably more energetic low-level cyclones lead to higher energy conversion terms in warm phases than in cold phases, inducing more energetic cyclones with high potential to transfer energy from the atmosphere to the ocean and increase the WEF during warm phases.

As documented by Escobar et al. (2004), Bischoff (2005) and Ortega et al. (2013), SE storms were at a minimum during the downward phase of the AMO curve and increased thereafter, especially at the beginning of the warm AMO phase. Corroborating these results, we observed that the WEFm curves associated with SE quadrants present, in addition to the larger ones, a very strong correlation with the AMO curve (SSE, R = 0.97, Figure 9C and ESE, R = 0.91, Figure 9B), where such curves develop covariant behavior from the cold until warm phases of AMO.. In this sense, in the western South Atlantic Ocean and along the rising phase of the AMO curve, D'Onofrio et al. (2008) showed that the decadal average frequency and duration of positive surges have increased, and Codignotto et al. (2012) described an increment in the frequency and height of wind waves propagating from the south. Additionally, related to variations in AMO phases, Wang et al. (2008) described that between 1854–2006, Atlantic hurricanes presented major and minor activities during the warm and cold AMO phases, respectively, suggesting that multidecadal variability in oceanic temperatures may be responsible for multidecadal variation in Atlantic hurricane activity. These authors also showed that Atlantic tropical cyclone activities have largely increased in frequency and intensity since the late 1980s. Reinforcing these results, we observed that during the transition period from the cold to warm AMO phase between the late 1980s and 1990s, the WEF98 and mainly the WEFm curve covary with the AMO curve (Figure 8A and B), exhibiting a growing trend. In the same period, the WEFm associated with the SSE and SSW quadrants also showed a significant growth trends (Figure 6) and similar behavior to that of the AMO curve (Figure 9C and D). Since that the driving mechanism of the AMO is related to variability in the oceanic thermohaline circulation (Knight et al., 2005) involving fluctuations of the Atlantic meridional overturning circulation (AMOC) (Delworth and Mann, 2000; Knight et al., 2005; Dijkstra et al., 2006) and on a multidecadal scale the Southern Ocean is first to show changes in this circulation patters (Crowley and Kim 1993), Kayano et al. 2019 demonstrated that during the AMO warm phase the region between 40°-70°S latitudes, which is exactly where the most energetic waves (SSE and SSW) come from, presented strong SST anomalies and inverse temperature patterns in relation to the cold phase. On the whole, spatiotemporal SST gradients are known to be a critical driver in ocean-atmosphere teleconnections and influence wind patterns and consequently WEF along the oceans (Reguero et al. 2019). Thus, it is to be expected that eventual changes in SST patterns in the Southern Ocean eventually induced by AMO influence the variability of the WEF in our study area. As can be seen in Figure 6 the SSW quadrant swell was the first to show a significant trend of increasing WEFm (late 1980s) and subsequently the SSE swell also started a significant growth phase. Such swells have their origin related to the higher latitudes, reflecting primarily the changes in the Southern Ocean eventually induced by the AMO during its transition from the cold phase to the warm phase (Fig. 8, late 1980s and 1990s; Fig.4, subperiod II). This kind of behavior is in agreement with other studies in the western South Atlantic Ocean, which also found a link between the recent warm phase of the AMO and physical environmental changes (Bischoff 2005 and Ortega et al. 2013), reinforcing the evidence of a correlation between the warm AMO phases and the energy intensification associated with meteo-oceanographic elements.

Increases in wave height primarily occur from increased surface wind energy, but the global wind

patterns change in response to spatiotemporal SST variations (Inatsu et al. 2002; Bengtsson et al. 2006). For this reason, to understand WEF trend changes in the southern Brazil we studied their correlations with the long-term tendencies of the AMO index, a SST-based climate index Although we focused on this singular mode (AMO), wave generation and the wave climate in the South Atlantic Ocean results from variability in a number of atmospheric patterns, large-scale drivers and teleconnections, many of which remain understudied compared with those in other global regions (Reguero et al. 2013; Reguero et al. 2019; Silva et al. 2020). Although the relationship between the AMO and WEF does not explain the interannual variability, it seems to have a profound effect on long-term WEF variations and trends. As evidence for this statement, the long-term trend computed with the 10-year filtered WEFm and WEF98 resulted in very strong correlations with the AMO curve. These results suggest that the trends observed in WEFm and WEF98 curves presented in this study likely represent the result of a long-term transition from a cold (negative) to warm (positive) AMO phase, which could modulate the long-term component of the interannual WEF98 and mainly the WEFm in the western South Atlantic. This relationship between the AMO and the western South Atlantic Ocean WEF has not been previously described. Since the AMO is still in its warm phase, it is expected that the WEF in coastal regions adjacent to the western South Atlantic Ocean will remain high in the next few years. This requires planning regarding the coastal management of these areas to avoid and mitigate potential wave-induced impacts attributed to the high flux of energy from the adjacent ocean. Further research should be performed, preferably using longer wave time series to identify WEF breakpoints and to investigate the effect of a full cycle of the AMO index on the wave characteristics.

CONCLUSION

This study investigated historical breakpoints and trends in wave energy flux (WEF) over 41 years in southern Brazil. The comparison between ERA-5 data and measurements from a waverider showed overall high agreement for wave parameters, proving ERA-5 to be a very useful database for long-term analyses. The WEFm and WEF98 presented a significantly positive linear trends between 1979 and 2019, with an increasing rates of 0.063 and 0.17 kW/m/year corresponding to 0.63 and 0.29% per year respectively.. Among all quadrants, the incident waves of the SSE and SSW quadrants presented the highest values of both the WEFm and WEF98, and by the Muggeo method, it was possible to identify that the WEFm associated with these quadrants seems to be related to subperiods that present positive advancing trends in the incremental general WEFm. The present results highlight that the general long-term WEFm and WEF98 signals are very strongly correlated with the AMO index (correlation coefficient = 0.92 and 0.89, respectively) and, consequently, suggest that the identified positive trends in the WEFm and WEF98 are likely related to the transition of cold to warm AMO phase in the western South Atlantic Ocean. We also determined that the WEFm curves of all quadrants follow the general trend of the AMO curve variation; however, the WEFm curve from the SSE quadrant has a greater correlation. Given that the AMO is still in its warm phase and that we have observed a very strong correlation between it and the WEF behavior, high WEF values are still expected in the western South Atlantic Ocean in the coming years. These incremental trends reinforce the need to develop efficient coastal management policies to adapt mainly regions with low declivity and chiefly mitigate potential impacts related to erosion and flooding processes. Along with coastal planning, further investigation should be performed to explore the relationship between WEF characteristics and full cycles of the AMO, as well as other climatic indices with different periodicities.

ACKNOWLEDGMENTS

We thank CAPES for providing resources to support the Graduate Program in Oceanology.

AUTHOR CONTRIBUTIONS

N.Z.M.: Conceptualization, Methodology, Formal analysis, Investigation, Writing - original draft, Writing - review & editing

L.P.A.: Conceptualization, Methodology, Formal analysis, Investigation, Writing - review & editing

L.E.: Methodology, Formal analysis, Investigation, Writing - review & editing

J.L.N.: Formal analysis, Investigation, Writing - review & editing

L.C.: Formal analysis, Investigation, Writing - review & editing

REFERENCES

ALEXANDER, M. A., KILBOURNE, K. H. & NYE, J. A. 2014. Climate variability during warm and cold phases of the Atlantic Multidecadal Oscillation (AMO) 1871-2008. *Journal of Marine Systems*, 133, 14-26, DOI: https://doi.org/10.1016/j.jmarsys.2013.07.017

ALHEIT, J., LICANDRO, P., COOMBS, S., GARCIA, A., GIRÁLDEZ, A., SANTAMARÍA, M. T. G., SLOTTE, A. & TSIKLIRAS, A. C. 2014. Atlantic Multidecadal Oscillation (AMO) modulates dynamics of small pelagic fishes and ecosystem regime shifts in the eastern North and Central Atlantic. *Journal of Marine Systems*, 133, 88-102, DOI: https://doi.org/10.1016/j.jmarsys.2014.02.005

ALMEIDA, L. P., FERREIRA, Ó., VOUSDOUKAS, M. I. & DODET, G. 2011. Historical variation and trends in storminess along the Portuguese South Coast. *Natural Hazards and Earth System Science*, 11(9), 2407-2417, DOI: https://doi.org/10.5194/nhess-11-2407-2011

ANTOLÍNEZ, J. A. A., MENDEZ, F. J., CAMUS, P., VITOUSEK, S., GONZÁLEZ, E. M., RUGGIERO, P. & BARNARD, P. 2016. A multiscale climate emulator for long-term morphodynamics (MUSCLE- morpho). *Journal of Geophysical Research-Oceans*, 121(1), 775-791, DOI: https://doi.org/10.1002/2015JC011107

BABANIN, A. V., ROGERS, W. E., CAMARGO, R., DOBLE, M., DURRANT, T., FILCHUCK, K., EWANS, K., HEMER, M., JANSSEN, T., KELLY-GERREYN, B., MACHUTCHON, K., MCCOMB, P., QIAO, F., SCHULZ, E., SKVORTSOV, A., VICHI, M., VIOLANTE-CARVALHO, N., WANG, D., WASEDA, T., WILLIAMNS, G. & YOUNG, I. R. 2019. Waves and swells in high wind and extreme fetches, measurements in the southern ocean. *Frontiers in Marine Science*, 6, 361, DOI: https://doi.org/10.3389/fmars.2019.00361

BENGTSSON, L., HODGES, K. & ROECKNER, E. 2006. Storm tracks and climate change. *Journal of Climate,* 19, 3518-3543.

BIASTOCH, A., DURGADOO, J. V., MORRISON, A. K., VAN SEBILLE, E., WEIJER, W. & GRIFFIES, S. M. 2015. Atlantic multi-decadal oscillation covaries with Agulhas leakage. *Nature Communications*, 6, 10082, DOI: https://doi.org/10.1038/ncomms10082

BISCHOFF, S. 2005. Sudestadas. *In:* BARROS, V., MENÉNDEZ, A. & NAGY, G. (eds.). *El Cambio Climatico en el Rio de la Plata*. Buenos Aires: Universidad de Buenos Aires, pp. 53-67.

CALLIARI, L. J. & KLEIN, A. H. F. 1993. Características morfodinâmicas e sedimentológicas das praias oceânicas entre Rio Grande e Chuí, RS. *Pesquisas em Geociências,* 20(1), 48-56.

CALLIARI, L. J., TOZZI, H. A. M. & KLEIN, A. H. F. 1998. Beach morphology and coastline erosion associated with storm surges in Southern Brazil - Rio Grande to Chuí, RS. *Anais da Academia Brasileira de Ciência*, 70(2), 175-188.

CHIESSI, C. M., MULITZA, S., PÄTZOLD, J., WEFER, G. & MARENGO, J. A. 2009. Possible impact of the Atlantic Multidecadal Oscillation on the South American summer monsoon. *Geophysical Research Letters*, 36(21), 1-5, DOI: https://doi.org/10.1029/2009GL039914

CODIGNOTTO, J. O., DRAGANI, W. C., MARTIN, P. B., SIMIONATO, C. G., MEDINA, R. A. & ALONSO, G. 2012. Wind-wave climate change and increasing erosion in the outer Río de la Plata, Argentina. *Continental Shelf Research*, 38, 110-116, DOI: https://doi.org/10.1016/j.csr.2012.03.013

COPERNICUS CLIMATE CHANGE SERVICE (CCCS). 2017. *ERA5: Fifth generation of ECMWF atmospheric reanalyses of the global climate*. Brussels: Copernicus Climate Change Service Climate Data Store (CDS).

CROWLEY, T. J. & KIM, K. Y. 1993. Towards development of a strategy for determining the origin of decadal-centennial scale climate variability. *Quaternary Science Reviews*, 12(6), 375-385, DOI: https://doi.org/10.1016/S0277-3791(05)80003-4

DAVIES, J. L. 1964. A morphogenic approach to world shorelines. *Geomorphology*, 8(5), 27-142.

DEE, D. P., UPPALA, S. M., SIMMONS, A. J., BERRISFORD, P., POLI, P., KOBAYASHI, S., ANDRAE, U., BALMASEDA, M. A., BALSAMO, G., BAUER, P., BECHTOLD, P., BELJAARS, A. C. M., VAN DE BERG, L., BIDLOT, J., BORMANN, N., DELSOL, C., DRAGANI, R., FUENTES, M., GEER, A. J., HAIMBERGER, L., HEALY, S. B., HERSBACH, H., HOLM, E. V., ISAKSEN, L., K´ALLBERG, P., KOHLER, M., MATRICARDI, M., MCNALLY, A. P., MONGE-SANZ, B. M., MORCRETTE, J. J., PARK, B. K., PEUBEY, C., ROSNAY, P., TAVOLATO, C., THEPAUT, J. N. & VITART, F. 2011. The ERA-Interim reanalysis: configuration and performance of the data assimilation system. *Quaternary Journal of the Royal Meteorological Society*, 137(656), 553-597, DOI: https://doi.org/10.1002/qj.828

DE LEO, F., BESIO, G. & MENTASCHI, L. 2021. Trends and variability of ocean waves under RCP8.5 emission scenario in the Mediterranean Sea. *Ocean Dynamics*, 71, 97-117, DOI: https://doi.org/10.1007/s10236-020-01419-8

DELWORTH, T. L. & MANN, M. E. 2000. Observed and simulated multidecadal variability in the Northern Hemisphere. *Climate Dynamics*, 16, 661-676, DOI: https://doi.org/10.1007/s003820000075

DIJKSTRA, H. A., TE RAA, L., SCHMEITS, M. & GERRITS, J. 2006. On the physics of the Atlantic Multidecadal Oscillation. *Ocean Dynamics*, 56, 36-50, DOI: https://doi.org/10.1007/s10236-005-0043-0

DODET, G., BERTIN, X. & TABORDA, R. 2010. Wave climate variability in the North-East Atlantic Ocean over the last six decades. *Ocean Modelling*, 31(3), 120-131.

D'ONOFRIO, E. E., FIORE, M. E. & POUSA, J. L. 2008. Changes in the regime of storm surges at Buenos Aires, Argentina. *Journal of Coastal Research*, 24(1A), 260-265.

ENFIELD, D. B., MESTAS-NUÑEZ, A. M. & TRIMBLE, P. J. 2001. The Atlantic Multidecadal Oscillation and its relationship to rainfall and river flows in the continental U.S. *Geophysical Research Letters*, 28(10), 2077-2080, DOI: https://doi.org/10.1029/2000GL012745

ESCOBAR, G., VARGAS, W. & BISCHOFF, S. 2004. Wind tides in the Rio de la Plata estuary: meteorological conditions. *International Journal of Climatology*, 24(9), 1159-1169.

FRAJKA-WILLIAMS, E., BEAULIEU, C. & DUCHEZ, A. 2017. Emerging negative Atlantic Multidecadal Oscillation index in spite of warm subtropics. *Scientific Reports*, 7(1), 11224, DOI: https://doi.org/10.1038/s41598-017-11046-x

FURG (Universidade Federal do Rio Grande). *Rede Ondas* [online]. Porto Alegre: FURG (Universidade Federal do Rio Grande). Avaliable at: www.redeondas.furg.br [Accessed: YEAR Mo DAY].

GARNER, A. J., MANN, M. E., EMANUEL, K. A., KOPP, R. E., LIN, N., ALLEY, R. B. & POLLARD, D. 2017. Impact of climate change on New York City's coastal flood hazard: Increasing flood heights from the preindustrial to 2300 CE. *Proceedings of the National Academy of Sciences of the United States of America,* 114(45), 11861-11866, DOI: https://doi.org/10.1073/pnas.1703568114

GODOLPHIM, M. F. 1976. *Geologia do Holoceno Costeiro do Município do Rio Grande, RS*. MSc. Porto Alegre: UFRGS (Universidade Federal do Rio Grande do Sul) - Instituto de Geociências.

GOLDENBERG, S. B., LANDSEA, C. W., MESTAS-NUNEZ, A. M. & GRAY, W. M. 2001. The recent increase in Atlantic hurricane activity: causes and implications. *Science*, 293(5529), 474-479, DOI: https://doi.org/10.1126/science.1060040

GONZALES, M., NICOLODI, J. L., GUTIÉRREZ, O. Q., LOSADA, V. C. & HERMOSA, A. E. 2016. Brazilian coastal processes: wind, wave climate and sea level. *In:* SHORT, A. D. & KLEIN, A. H. F. (orgs.). *Brazilian beach systems.* Switzerland: Springer International Publishing, v. 17, pp. 37-66.

HARLEY, M. D., TURNER, I. L., SHORT, A. D. & RANASINGHE, R. 2010. Interannual variability and controls of the Sydney wave climate. *International Journal of Climatology*, 30(9), 1322-1335.

HEMER, M. A., CHURCH, J. A. & HUNTER, J. R. 2010. Variability and trends in the directional wave climate of the Southern Hemisphere. *International Journal of Climatology*, 30(4), 475-491, DOI: https://doi.org/10.1002/joc.1900

HEMER, M. A., CHURCH, J. A., SWAIL, V. & WANG, X. 2006. Coordinated global wave climate projections. *Atmosphere-Ocean Interactions,* 2, 185-218.

HERSBACH, H., BELL, B., BERRISFORD, P., HIRAHARA, S., HORÁNYI, A., MUÑOZ-SABATER, J. & THÉPAUT, J. N. 2020. The ERA5 global reanalysis. *Quarterly Journal of the Royal Meteorological Society*, 146(730), 1999-2049, DOI: https://doi.org/10.1002/qj.3803

HOSKINS, B. J. & HODGES, K. I. A. 2005. New Perspective on Sourthern Hemisphere Storm Tracks. *Journal of Climate*, 18, 4108-4129.

HURREL, H., KUSHNIR, Y., OTTERSEN, G. & VISBECK, M. 2003. An overview of the North Atlantic oscillation. The North Atlantic Oscillation: climatic significance and environmental impact. *Geophysical Monograph Series*, 134, 1-35.

KAYANO, M. T., ROSA, M. B., RAO, V. B., ANDREOLI, R. V. & SOUZA, R. A. F. 2019. Relations of the low-level extratropical cyclones in the southeast Pacific and South Atlantic to the Atlantic multidecadal oscillation. *Journal of Climate*, 32(14), 4167-4178, DOI: https://doi.org/10.1175/JCLI-D-18-0564.1

KERR, R. A. 2000. A North Atlantic climate pacemaker for the centuries. *Science*, 288(5473), 1984-1986, DOI: https://doi.org/10.1126/science.288.5473.1984

KING, C. A. M. 1972. *Beaches and coasts*. London: Edward Arnold.

KNIGHT, J. R., ALLAN, R. J., FOLLAND, C. K., VELLINGA, M. & MANN, M. E. 2005. A signature of persistent natural thermohaline circulation cycles in observed climate. *Geophysical Research Letters*, 32, L20708, DOI: https://doi.org/10.1029/2005GL024233

KNIGHT, J. R., FOLLAND, C. K. & SCAIFE, A. A. 2006. Climate impacts of the Atlantic Multidecadal Oscillation. *Geophysical Research Letters,* 33(17), L17706, DOI: https://doi.org/10.1029/2006GL026242

KRAVTSOV, S. V. & SPANNAGLE, C. 2008. Multi-decadal climate variability in observed and modeled surface temperature. *Journal of Climate*, 21(5), 1104-1121, DOI: https://doi.org/10.1175/2007JCLI1874.1

KUSHNIR, Y., CARDONE, V. J., GREENWOOD, J. G. & CANE, M. A. 1997. The recent increase in North Atlantic wave heights. *Journal of Climate*, 10, 2107-2113.

LATIF, M. 2013. The Ocean's role in modeling and predicting decadal climate variations. *In:* SIEDLER, G., GRIFFIES, S. M., GOULD, J. & CHURCH, J. A. (eds.). *International geophysics*. London: Academic Press, v. 103, pp. 645-665.

LYU, K. & YU, J. Y. 2017. Climate impacts of the Atlantic Multidecadal Oscillation simulated in the CMIP5 models: a re-evaluation based on a revised index. *Geophysical Research Letters*, 44(8), 3867-3876, DOI: https://doi.org/10.1002/2017GL072681

MACHADO, A. A., CALLIARI, L. J., MELO, E. & KLEIN, A. H. F. 2010. Historical assessment of extreme coastal sea state conditions in southern Brazil and their relation to erosion episodes [online]. *Pan American Journal of Aquatic Sciences*, 5(2), 277-286. Available at: http://www.panamjas.org/pdf_artigos/PANAMJAS_5(2)_277-286.pdf [Accessed: YEAR Mo DAY].

MAIA, N. Z., CALLIARI, L. J. & NICOLODI, J. L. 2016. Analytical model of sea level elevation during a storm: Support for coastal flood risk assessment associated with cyclone passage. *Continental Shelf Research*, 124, 23-34, DOI: https://doi.org/10.1016/j.csr.2016.04.012

MARSHALL, A. G., HEMER, M. A., HENDON, H. H. & MCINNES, K. L. 2018. Southern annular mode impacts on global ocean surface waves. *Ocean Modelling*, 129, 58-74, DOI: https://doi.org/10.1016/j.ocemod.2018.07.007

MCCABE, G. J., PALECKI, M. A. & BETANCOURT, J. L. 2004. Pacific and Atlantic Ocean influences on multidecadal drought frequency in the United States. *Proceedings of the National Academy of Sciences of the United States of America*, 101(12), 4136-4141, DOI: https://doi.org/10.1073/pnas.0306738101

MEEHL, G., STOCKER, T., COLLINS, W., FIEDLINGSTEIN, P., GAYE, A., GREGORY, KITOH, A., KNUTTI, R., MURPHY, J., NODA, A., RPER, S., WATTERSON, I., WEAVER, A. & ZHAO, Z. 2007. *Climate change 2007: the physical science basis. Contribution of Working Group I to the Fourth Assessment Report of the Intergovernmental Panel on Climate Change, Chapter Global Climate Projections*. Cambridge: Cambridge University Press.

MENTASCHI, L., VOUSDOUKAS, M. I., VOUKOUVALAS, E., DOSIO, A. & FEYEN, L. 2017. Global changes of extreme coastal wave energy fluxes triggered by intensified teleconnection patterns. *Geophysical Research Letters,* 44(5), 2416-2426.

MORI, N., YASUDA, T., MASE, H., TOM, T. & OKU, Y. 2010. Projection of extreme wave climate under global warming. *Hydrological Research Letters,* 4, 14-19.

MORIM, J., HEMER, M., WANG, X. L., CARTWRIGHT, N., TRENHAM, C., SEMEDO, A., YOUNG, I., BRICHENO, L., CAMUS, P., CASAS-PRAT, M., ERIKSON, L., MENTASCHI, L., MORI, N., SHIMURA, T., TIMMERMANS, B., AARNES, O., BREIVIK, O., BEHRENS, A., DOBRYIN, M., MENENDEZ, M., STANEVA, J., WEHNER, M., WOLF, J., KAMRANZAD, B., WEBB, A., STOPA, J. & ANDUTTA, F. 2019. Robustness and uncertainties in global multivariate wind-wave climate projections. *Nature Climate Change*, 9(9), 711-718, DOI: https://doi.org/10.1038/s41558-019-0542-5

MOTTA, V. F. 1969. Relatório-diagnóstico sobre a melhoria e o aprofundamento do acesso pela barra de Rio Grande. MSc. Porto Alegre: UFRGS (Universidade Federal do Rio Grande do Sul) - Instituto de Pesquisas Hidráulicas.

MUGGEO, V. M. 2003. Estimating regression models with unknown break-points. *Statistics in Medicine*, 22(19), 3055-3071.

NOAA (National Oceanic and Atmospheric Administration). 2001. *Climate Timeseries – AMO (Atlantic Multidecadal Oscillation) index* [online]. Boulder: NOOA. Available at: https://psl.noaa.gov/data/timeseries/AMO/ [Accessed: 2020 Apr 04].

ODÉRIZ, I., SILVA, R., MORTLOCK, T. R. & MENDOZA, E. 2020. Climate drivers of directional wave power on the Mexican coast. *Ocean Dynamics*, 70(9), 1253-1265, DOI: https://doi.org/10.1007/s10236-020-01387-z

OLIVEIRA, B. A., SOBRAL, F., FETTER, A. & MENDEZ, F. J. 2019. A high-resolution wave hindcast off Santa Catarina (Brazil) for identifying wave climate variability. *Regional Studies in Marine Science*, 32, 100834.

OLIVEIRA, U. R., SIMÕES, R. S., CALLIARI, L. J. & GAUTÉRIO, B. C. 2019. Erosão de dunas sob ação de um evento extremo de alta energia de ondas na costa central e sul do Rio Grande do Sul, Brasil. *Revista Brasileira de Geomorfologia*, 20(1), 1-22, DOI: http://dx.doi.org/10.20502/rbg.v20i1.1352

O'REILLY, C. H., WOOLLINGS, T. & ZANNA, L. 2017. The dynamical influence of the Atlantic multidecadal oscillation on continental climate. *Journal of Climate*, 30(18), 7213-7230, DOI: https://doi.org/10.1175/JCLI-D-16-0345.1

ORTEGA, L., CELENTANO, E., FINKL, C. & DEFEO, O. 2013. Effects of climate variability on the morphodynamics of Uruguayan sandy beaches. *Journal of Coastal Research*, 29(4), 747-755.

PARISE, C. K., CALLIARI, L. J. & KRUSCHE, N. 2009. Extreme storm surges in the south of Brazil: atmospheric conditions and shore erosion. *Brazilian Journal of Oceanography*, 57(3), 175-188.

PEZZI, L. P., SOUZA, R. B. & QUADRO, M. F. L. 2016. Uma revisão dos processos de interação oceano-atmosfera em regiões de intenso gradiente termal do oceano Atlântico Sul baseada em dados observacionais. *Revista Brasileira de Meteorologia*, 31(4), 428-453, DOI: https://doi.org/10.1590/0102-778631231420150032

PIANCA, C., MAZZINI, P. L. & SIEGLE, E. 2010. Brazilian offshore wave climate based on NWW3 reanalysis. *Brazilian Journal of Oceanography*, 58(1), 53-70.

QIAN, C., YU, J. Y. & CHEN, G. 2014. Decadal summer drought frequency in China: the increasing influence of the Atlantic multi-decadal oscillation. *Environmental Research Letters*, 9(12), 124004, DOI: https://doi.org/10.1088/1748-9326/9/12/124004

RASMUSSEN, D. J., BITTERMANN, K., BUCHANAN, M. K., KULP, S., STRAUSS, B. H., KOPP, R. E. & OPPENHEIMER, M. 2018. Extreme sea level implications of 1.5 °C, 2.0 °C, and 2.5 °C temperature stabilization targets in the 21st and 22nd century. *Environmental Research Letters*, 13, 034040.

REGUERO, B. G., LOSADA, I. J. & MENDEZ, F. J. 2019. A recent increase in global wave power as a consequence of oceanic warming. *Nature Communications*, 205, 1-14.

REGUERO, B. G., MÉNDEZ, F. J. & LOSADA, I. J. 2013. Variability of multivariate wave climate in Latin America and the Caribbean. *Global and Planetary Change,* 100, 70-84.

SEMEDO, A., SUSELIJ, K., RUTGERSSON, A. & STERL, A. 2011. A global view on the wind sea and swell climate and variability from ERA-40. *Journal of Climate,* 24(5), 1461-1479.

SEMEDO, A., WEISSE, R., BEHRENS, A., STERL, A., BENGTSSON, L. & GÜNTHER, H. 2013. Projection of global wave climate change toward the end of the twenty-first century. *Journal of Climate*, 26(21), 8269-8288, DOI: https://doi.org/10.1175/JCLI-D-12-00658.1

SILVA, A. P., KLEIN, A. H. F., FETTER-FILHO, A. F. H., HEIN, C. J., MÉNDEZ, F. J., BROGGIO, M. F. & DALINGHAUS, C. 2020. Climate-induced variability in South Atlantic wave direction over the past three millennia. *Scientific Reports*, 10, 18553, DOI: https://doi.org/10.1038/s41598-020-75265-5

SINCLAIR, M. R. 1995. A climatology of cyclogenesis for the Southern Hemisphere. *Monthly Weather Review*, 123, 1601-1619.

SINCLAIR, M. R. 1997. Objective identification of cyclones and their circulation intensity, and climatology. *Weather and Forecasting*, 12(3), 595-612.

SUN, C., LI, J. & ZHAO, S. 2015. Remote influence of Atlantic multidecadal variability on Siberian warm season precipitation. *Scientific Reports*, DOI: https://doi.org/10.1038/srep16853

SWAIL, V. R., CECCACCI, E. A. & COX, A. T. 2000. The AES40 north Atlantic wave reanalysis validation and climate assessment. *In: 6th International Workshop on Wave Hindcasting and Forecasting (WWHF)*. Monterey, California, USA, 2000 Nov 6-10. Monterey: WWHF, pp. 1-17.

THE WAMDI GROUP. 1988. The WAM Model - A Third Generation Ocean Wave Prediction Model. *Journal of Physical Oceanography*, 18(12), 1775-1810.

THOMPSON, D. & WALLACE, J. M. 1998. The Arctic Oscillation signature in the wintertime geopotential height and temperature fields. *Geophysical Research Letters*, 25(9), 1297-1300.

TIMMERMANN, A., OKUMURA, Y., AN, S. I., CLEMENT, A., DONG, B., GUILYARDI, E., HU, A., JUNCLAUS, J. H., RENOLD, M., STOCKER, T. F., STOUFFER, R. J., SUTTON, R., XIE, S. P. & YIN, J. 2007. The influence of a weakening of the Atlantic meridional overturning circulation on ENSO. *Journal of Climate*, 20(19), 4899-4919, DOI: https://doi.org/10.1175/JCLI4283.1

TOMAZELLI, L. J. & VILLWOCK, J. A. 1992. Algumas Considerações sobre o Ambiente Praial e a Deriva Litorânea de Sedimentos ao Longo do Litoral Norte do Rio Grande do Sul, Brasil. *Pesquisas em Geociências*, 19(1), 1-26.

TRENBERTH, K., CARON, J., STEPANIAK, D. & WORLEY, S. 2002. Evolution of El Nino-Southern Oscillation and global atmospheric surface temperatures. *Journal of Geophysical Research*, 107, 4065, DOI: https://doi.org/10.1029/2000JD000298

TRENBERTH, K., ZHANG, R. & NCAR (National Center for Atmospheric Research Staff) (eds.). 2021. *The Climate Data Guide: Atlantic Multi-decadal Oscillation (AMO)* [online]. Boulder: NCAR. Available at: https://climatedataguide.ucar.edu/climate-data/atlantic-multi-decadal-oscillation-amo [Accessed: YEAR Mo DAY].

VOUSDOUKAS, M. I., MENTASCHI, L., VOUKOUVALAS, E., BIANCHI, A., DOTTORI, F. & FEYEN, L. 2018. Climatic and socioeconomic controls of future coastal flood risk in Europe. *Nature Climate Change*, 8(9), 776-780, DOI: https://doi.org/10.1038/s41558-018-0260-4

WAN, W., Y., FAN, C., DAI, Y., LI, L., SUN, W. & ZHOU, P. 2018. Assessment of the joint development potential of wave and wind energy in the South China Sea. *Energies*, 11(2), 1-26, DOI: https://doi.org/10.3390/en11020398

WANG, C., LEE, S. K. & ENFIELD, D. B. 2008. Atlantic warm pool acting as a link between Atlantic Multidecadal Oscillation and Atlantic tropical cyclone activity. *Geochemistry, Geophysics, Geosystems*, 9(5), DOI: https://doi.org/10.1029/2007GC001809

WANG, X. L. & SWAIL, V. R. 2000. Changes of extreme wave heights in Northern hemisphere oceans and related atmospheric circulation regimes. *Journal of Climate*, 14(10), 2204-2221.

WANG, X. L., ZWIERS, F. W. & SWAIL, V. R. 2003. North Atlantic Ocean wave climate change scenarios for the twenty-first century. *Journal of Climate*, 17, 2368-2383.

WANG, Y., LI, S. & LUO, D. 2009. Seasonal response of Asian monsoonal climate to the Atlantic Multidecadal Oscillation. *Journal of Geophysical Research*, 114(D2), DOI: https://doi.org/10.1029/2008JD010929

WASEDA, T., WEBB, A., SATO, K., INOUE, J., KOHOUT, A., PENROSE, B. & PENROSE, S. 2018. Correlated increase of high ocean waves and winds in the ice-free waters of the Arctic Ocean. *Scientific Reports*, 8, 4489, DOI: https://doi.org/10.1038/s41598-018-22500-9

YANG, Y. M., AN, S. I., WANG, B. & PARK, J. H. 2020. A global-scale multidecadal variability driven by Atlantic multidecadal oscillation. *National Science Review*, 7(7), 1190-1197, DOI: https://doi.org/10.1093/nsr/nwz216

YOUNG, I. R., ZIEGER, S. & BABANIN, A. V. 2011. Global trends in wind speed and wave height. *Science*, 332(6028), 451-455.

ZHANG, R. & DELWORTH, T. L. 2005. Simulated tropical response to a substantial weakening of the Atlantic thermohaline circulation. *Journal of Climate*, 18(12), 1853-1860, DOI: https://doi.org/10.1175/JCLI3460.1

Capítulo VI: Artigo 2

“Long-term trends and wave climate variability in the South Atlantic Ocean: the influence of climate indices”

6.2 Artigo 2

O segundo manuscrito originado desta Tese é de autoria de Natan Zambroni Maia, Luis Pedro Almeida, João Luiz Nicolodi, Lauro Calliari e Bruno Castelle, intitulado ***“Long-term trends and wave climate variability in the South Atlantic Ocean: the influence of climate indices”***, submetido em 2023 para o periódico *“**Regional Studies in Marine Science**”* e até o momento da elaboração da versão final desta tese se encontra com status ”em revisão”.

Long-term trends and wave climate variability in the South Atlantic Ocean: the influence of climate indices

Natan Z. Maia [a,b,*], Luis Pedro Almeida [c], João Luiz Nicolodi [a], Lauro Calliari [a], Bruno Castelle [b]

[a] *Universidade Federal do Rio Grande "FURG" - Instituto de Oceanografia - Laboratório de Oceanografia Geológica.* Av. Itália, CP 474, Rio Grande, RS, 96201-900, Brazil. natanzambroni@gmail.com; joaoluiznicolodi@gmail.com; calliarilauro@gmail.com

[b] *Univ. Bordeaux, CNRS, Bordeaux INP, EPOC, UMR 5805, F-33600 Pessac, France. bruno.castelle@u-bordeaux.fr*

[c] *CoLAB +Atlantic – Edifício Diogo Cão, Doca de Alcântara Norte, 1350-352. Lisbon, Portugal. melolp@gmail.com*

*Corresponding author: natanzambroni@gmail.com

Universidade Federal do Rio Grande "FURG" - Instituto de Oceanografia - Laboratório de Oceanografia Geológica. Av. Itália, CP 474, Rio Grande, RS, 96201-900, Brazil.

ABSTRACT

Linking wave climate variability and trends with climate indices is important to better understand and predict large-scale patterns of wave variability down to wave conditions at the coast. This study investigates such links in the South Atlantic Ocean using 72 years of ERA5 wave hindcast. Different wave parameters are computed, including storm wave statistics, and are further analyzed in terms of long-term trends and interannual changes. Our results indicate that, over the last decades, wave height has been significantly increasing across the entire domain, while extreme events statistics are also increasing, although with more complex spatial variability. The variations of these wave properties are primarily correlated, from low to high latitudes, with the Atlantic Multidecadal Oscillation (AMO), Tropical Southern Atlantic Index (TSA) and Southern Annular Mode (SAM), with different preferred timescales. We think that better understanding and predicting the evolution of these climate indices, including under climate change, will be critical to anticipate coastal hazards in this region.

Keywords: South Atlantic Ocean; Wave climate; Storm waves; long-term trends; interannual variability; Climate indices.

1. Introduction

The generation and propagation of ocean waves is of great practical significance presenting far-reaching implications for coastal areas (Babanin et al., 2019; Reguero et al., 2019). The wave climate on the world's coasts is highly variable in both time and space. At the coast, ocean waves drive nearshore currents and sea water level variations through depth-induced breaking, with wave-driven processes control sediment transport as well as shoreline shape and changes (Castelle and Masselink, 2023). Extreme wave events can also cause coastal flooding and threaten coastal installations and protection structures (Van der Meer et al., 2016; Mentaschi et al., 2017). The wave climate therefore deeply affects where and how coastal and offshore infrastructures such as harbors and wave power generation plants can be built (Reguero et al., 2013, 2019). It is thus critical to understand the ocean wave climate variability and trends (Barnard et al., 2015; Mentaschi et al., 2017; Marshall et al., 2018; Reguero et al., 2019; De Leo et al., 2021; Maia et al., 2022). In addition, according to Morim et al. (2019), approximately 50% of the world's coastline is at risk from wave climate change, with ~40% revealing robust changes in wave properties.

Ocean surface gravity waves are generated by winds flowing across ocean basins and are thus intrinsically linked to atmospheric variability (Hemer et al., 2010; Reguero et al., 2012). It has long been known that atmospheric and oceanic circulation shows large-scale patterns of variability on interannual and longer timescales, which is reflected in wave climate variability (Garner et al., 2017; Castelle et al., 2017; Rasmussen et al., 2018; Vousdoukas et al., 2018; Oliveira et al., 2019). Large-scale patterns of atmospheric and/or oceanic variability are often addressed though climate indices such as the Southern Annular Mode (SAM) (also referred to as the high-latitude mode and the Antarctic Oscillation (AAO)), Tropical Southern Atlantic Index (TSA), Tropical Northern Atlantic Index (TNA), Western Hemisphere Warm Pool (WHWP) and the Atlantic Multidecadal Oscillation (AMO) (Thompson and Wallace, 2000; Kerr, 2000; Trenberth et al., 2002; Hemer et al., 2010; Reguero et al., 2013). Given that these patterns mostly superimpose and that waves are generated from different locations, the wave climate variability at a given location is modulated by the combination of several climate indices and teleconnections patterns (Castelle et al., 2017; Reguero et al., 2019; Silva et al., 2020; Maia et al., 2022), and a given mode of variability can affect multiple ocean basins and hemispheres (Oliveira et al., 2019). According to Silva et al. (2020), in the recent decades the predominant wind-wave climate has been shifting in both direction and magnitude in both the Northern and Southern Hemispheres (Reguero et al., 2019), a phenomenon likely in response to altered atmospheric dynamics and interhemispheric teleconnections in association with increasing global temperature (Morim et al., 2019; Meucci et al., 2020; O'Grady et al., 2021).

The Southern Hemisphere (SH) has the most energetic ocean, Southern Ocean (Reguero et al., 2019), with waves generated by eastwards tracking, intense, extra-tropical cyclones impacting on almost all of the coasts globally (Hemer et al., 2010). According to Sterl and Caires (2005), 15% of the global wave variability is due to the swell propagating from the SH storm track region, and it governs the variability of the global mean. On SH, the Atlantic Ocean

exhibits variability over a wide range of temporal and spatial scales but has pronounced variability at decadal and multidecadal timescales (Alexander et al., 2014). The SAM is the primary mode of variability in the atmospheric circulation of the SH extratropics and high latitudes (Marshall, 2003) and also, the primary mode influencing both wave height and directional variability beyond its energy flux both in medium and extreme conditions (Hemer et al., 2010; Mentaschi et al., 2017; Marshall et al., 2018).

There are some studies documenting the global warming trend associated with an increasing SAM trend over the past decades (Cai et al., 2003; Wang and Cai, 2013; Mentaschi et al., 2017), involving more frequent storms (Grassi et al., 2005) with potential implications for coastal sediment budgets and shoreline stability (Marshall et al., 2018). In addition to SAM, in the South Atlantic Ocean previous studies have also revealed strong relationships between changes in ocean–atmosphere interactions and the AMO index. According to Wang et al. (2008) and Kayano et al. (2019), the hurricanes and cyclones behaviors in the Atlantic Ocean are modulated by AMO oscillations, respectivly. Reguero et al. (2019) and Maia et al. (2022) identified strong correlations between the wave energy flux (*WEF*) and AMO behavior in the Southern Ocean and western South Atlantic Ocean, respectively. Another relevant climate index with important influence in the Atlantic Ocean is the TSA pattern which is associated with wave height increase in the northern equatorial Atlantic border of the continent and in the Rio dela Plata area, whereas the *WEF* affects wave directionality (Reguero et al., 2013).

This paper investigates the wave climate variability (means and extreme events) and trend in the South Atlantic Ocean, and systematically addresses the links with the dominant regional modes of climate variability. This work is based on a 1950-2021 wave hindcast and a statistical analysis on wave and climate parameters. It will be shown that along the South Atlantic Ocean, wave climate variability is linked with, from low to high latitudes, AMO, TSA and SAM, together with increased duration, frequency and intensity of extreme events. Our results present new insights into the South Atlantic long-term wave climate variability and their drivers, including extreme conditions.

2. Data and Method

2.1 Wave hindcast

In situ offshore wave data in the SH are scarce, with very few waverider buoy records compared to the NH. Global wave models thus provide a useful alternative to address the space and time variability and trends of wave conditions in the SH (Hemer et al., 2010). We used the 3-hourly 72-years global wave hindcast produced by the European Centre for Medium-Range Weather Forecasts (ECMWF) – ERA 5 (see Hersbach et al., 2020) from 1950 to 2021, from which significant wave height (*Hs*), peak wave period (*Tp*) and direction (θ) were extracted, from which the wave energy flux *WEF* was also computed (Antolínez et al., 2016; Mentaschi et al., 2017; Marshall et al., 2018; Reguero et al., 2019; Odériz et al., 2020a; Odériz et al., 2020b; Maia et al., 2022):

$$WEF = \frac{\rho\, g^2\, Hs^2\, T}{64\,\pi} \qquad (1)$$

Where ρ is the water density, g the gravitational acceleration, Hs significant wave height and T the peak period. Outputs were extracted on a regular grid with 0.5° resolution covering the southern Atlantic Ocean between 5°N-60°S and 69.5°W-20°E, thus a total of 23,580 individual grid points. ERA5 validation for the South Atlantic Ocean is given in Odériz et al. (2020a), Odériz et al. (2020b), Maia et al. (2022) and Cotrim et al. (2022), with ERA5 showing a generally good performance in replicating wave high inter-annual variability compared to altimetry and buoy measurements. Three virtual wave buoys were used to address the spatial distribution of wave heights in deep waters along the South Atlantic Ocean: Nt: North; Ct: Central; St: South (Figure 1).

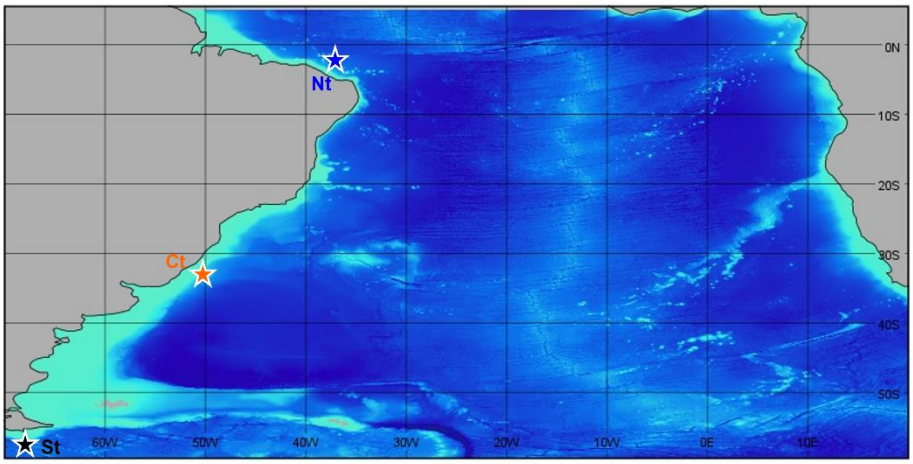


Figure 1. Spatial domain for wave field. The locations of the North (Nt), Central (Ct) and South (St) virtual buoys are indicated by the colored stars.

2.2 Climate Indices

Monthly teleconnection indices available since January 1950 were downloaded from the National Oceanic and Atmospheric Administration (NOAA) Physical Sciences Laboratory (www.psl.noaa.gov), nominally AMO (Enfield et al., 2001), WHWP (Wang et al., 2001), TSA (Einfield et al., 1999), TNA (Einfield et al., 1999). SAM (Marshall, 2003) was obtained from British Antarctic Survey (www.bas.ac.uk/), available since 1957.

2.3 Analyzes

2.3.1 Extreme events definitions

The peak over threshold method was applied on *Hs* to address extreme events (Dorsch et al., 2008). Following the definition by Masselink et al. (2014) and subsequently used in other studies, for each grid point an extreme event was defined as an event where *Hs* exceeded the 0.95 quantile (*Hs95*). A single extreme event was defined as a continuous period of *Hs* exceeding this threshold over at least 12 hours (Sénéchal et al., 2015; Angnuureng et al., 2017). Additionally,

the individualization of extreme events was made through an independence criterion defined as when 30 hours elapsed between consecutive *Hs* records based on Almeida et al. (2011).

2.3.2 Extreme events statistics

We defined three parameters to study the extreme events behavior: duration (*D)*, frequency (F) and intensity (*I)*. For the duration, each year we calculated the number of hours under extreme conditions. The number of extreme events for each year was used to compute the storm frequency. Intensity (Karunarathna et al., 2014; Sénéchal et al., 2015; Angnuureng et al., 2017) was computed following Mendoza et al. (2011):

$$I = \int_{t1}^{t2} Hs(t)^2 dt \qquad \text{Eq.2}$$

where the extreme event duration starting and ending at *t1* and *t2*, respectively.

2.3.3 Correlation and trends

The yearly time series of all wave parameters described above were used to address the variability and trends of the wave climate. At each grid point, each climate index was used to compute correlations with the wave parameters, which were also linearly regressed to compute long-term trends. The statistical significance of correlations and trends for all variables was checked through a Student's t-test at a 95% level.

3. Results

3.1 Annual averages and trends of wave and extreme events

Figure 2 shows the time-average (a-d) and long-term trend (e-h) of *Hs* and extreme events parameters for the entire South Atlantic Ocean between 1950 and 2021. The average *Hs* (Figure 2a) shows values between 0.5 and 4 m, with lower values close to coastal regions and gradually increasing towards higher latitudes to the south, especially to the southeast from latitude 36°S and to the southwest from latitude 55°S. The largest waves (*Hs* between 2.5 and 4 m) are predominantly incident from west quadrant. In contrast, the intertropical region shows smaller *Hs* between 0.5 and 1.5 m with a dominant southeast to northeast incidence as latitude decreases. The spatial distributions of time-averaged extreme event parameters show similar patterns, as the highest values of Intensity, Duration and Frequency of extreme events are observed in the temperate zone between latitudes 24 and 48°S, and below 48°S north of the Antarctic Peninsula and south of the African continent. For these regions, the highest values of cumulative Intensity are of the order of 1.5×10^4 m^2hr/year (Figure 2b), followed by an average accumulation of 250 hours of Duration in extreme conditions per year (Figure 2c) with records of up to 13 annual extreme events (Figure 2d). Figures 2b-d also reveals a localized area of large extreme event

parameters with up to 16 events per year, for a total average yearly duration of up to 800 hours and up to 0.7x10^4 m^{2}hr in Intensity in the region near the north coast of Brazil, in the Equatorial Atlantic.

The right-hand panels of Figure 2 highlight that all the wave parameters show an increasing trend, with areas where trends are not statistically significant essentially limited to a few points close to coordinates 5°N-36°W. Overall, the entire South Atlantic Ocean shows increasing yearly-average *Hs* (Figure 2e), at rates increasing southwards. The largest increasing *Hs* rates are located in the northern part of the Southern Ocean, ranging 1-1.2 cm/year. Intensity trends are mostly similar in patterns to that of *Hs*, peaking at 350 m^{2}hr/year between the American continent and Antarctica. In contrast, both Duration and Frequency trends show the highest increasing rates in the subtropical and tropical zones, with the exception of the northwest equatorial region. In addition to these areas, large Duration and Frequency increasing rates are observed in the southwestern region of the Atlantic Ocean, north of the Southern Ocean, up to 10 hours/year and 0.25 extreme events per year.

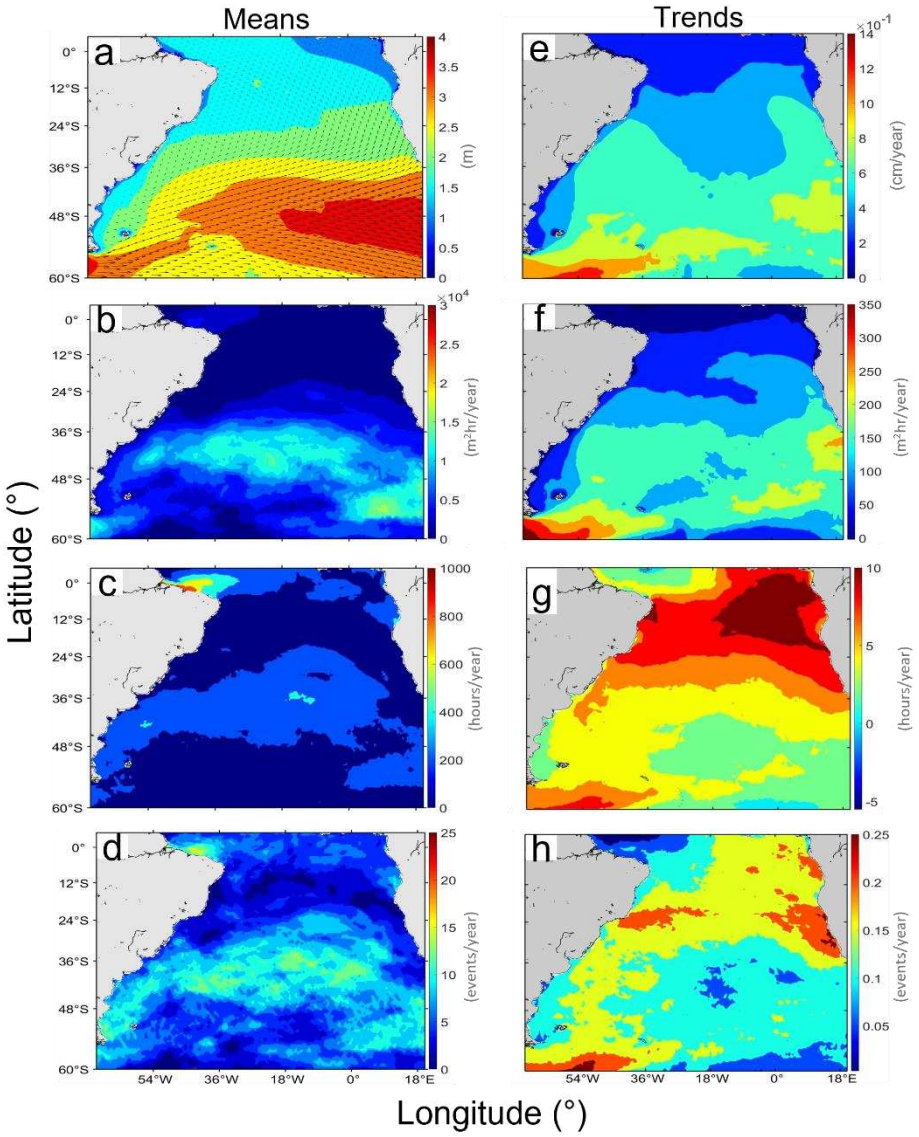


Figure 2. Time-average (left-hand panels) and trend (right-hand panels) of *Hs* and extreme event parameters between 1950 and 2021: (a,e) *Hs*; (b,f) cumulative Intensity; (c,g) cumulative Duration; (d,h) Frequency.

3.2 Correlation with climate indices

Table 1 shows the correlation between the main climate indices that influence the South Atlantic Ocean wave climate. TNA and WHWP indices show a high correlation with AMO (r = 0.82 and 0.7, respectively) and were thus discarded in the analysis below. In contrast, AMO, SAM and TSA systematically show low correlation between each other (r < 0.5) and are therefore assumed to result in contrasting correlation map with the computed wave parameters and are thus all kept for analysis.

Table 1. Correlation coefficients (r) between climate indices

	AMO	**SAM**	**TNA**	**TSA**	**WHWP**
AMO	1	0.46	0.82	0.26	0.7
SAM	0.46	1	0.36	0.39	0.47
TNA	0.82	0.36	1	0.32	0.75
TSA	0.26	0.39	0.32	1	0.41
WHWP	0.7	0.47	0.75	0.41	1

AMO: Atlantic Multidecadal Oscillation; SAM: Southern Annular Mode; TNA: Tropical North Atlantic Index; TSA: Tropical South Atlantic Index; WHWP: Western Hemisphere Warm Pool

The left-hand panels of Figure 3 show the spatial distribution of the correlations between *Hs* and AMO, TSA and SAM indices. Interestingly enough, all climate indices mostly show a positive correlation, although with contrasting patterns. The highest correlations with the AMO (SAM) index are found in northern (southern) part of the domain, while TSA is dominant between latitudes 12 and 50°S. The right-hand panels of Figure 3 show the corresponding time series of *Hs* and dominant climate at three representative virtual buoys located in the three areas described above (North Nt, Central Ct and South St). The *Hs* anomalies identified at the Nt point have r = 0.65 with AMO, while the Ct point has r = 0.61 with TSA and to the south, St and SAM present r = 0.65. Interestingly, AMO shows a strong correlation with a clear multi-decadal variability, while

TSA and SAM show a positive trend with superimposed interannual variability, which is reflected in the *Hs* variability at the selected virtual buoys.

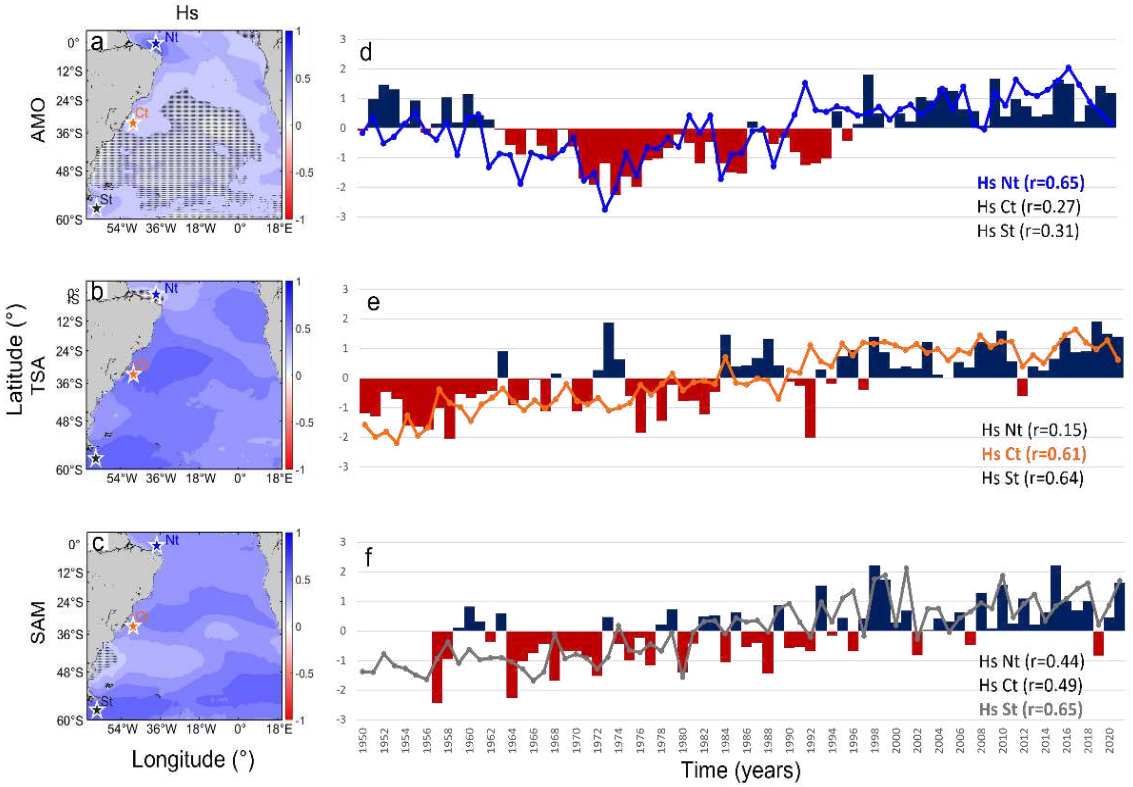


Figure 3. Left-hand panels: spatial distribution of correlations between *Hs* and (a) AMO, (b) TSA and (c) SAM, respectively. The hatched areas show locations where correlation is not statistically significant. The locations of the North (Nt), Central (Ct) and South (St) virtual buoys are indicated by the colored stars. Right-hand panel: corresponding time series of *Hs* anomaly (solid line) and (d) AMO (Nt), (e) TSA (Ct) and (f) SAM (St) (colored bars) with indication of computed correlations.

Figure 4 shows the spatial distribution of correlations between the climate indices and the extreme events parameters, which, overall, are similar in patterns with those computed for *Hs*. At the Nt, Ct and St points, the indices that best correlate with variations in *Hs*, Duration, Frequency and Intensity are respectively AMO, TSA and SAM (Table 2).

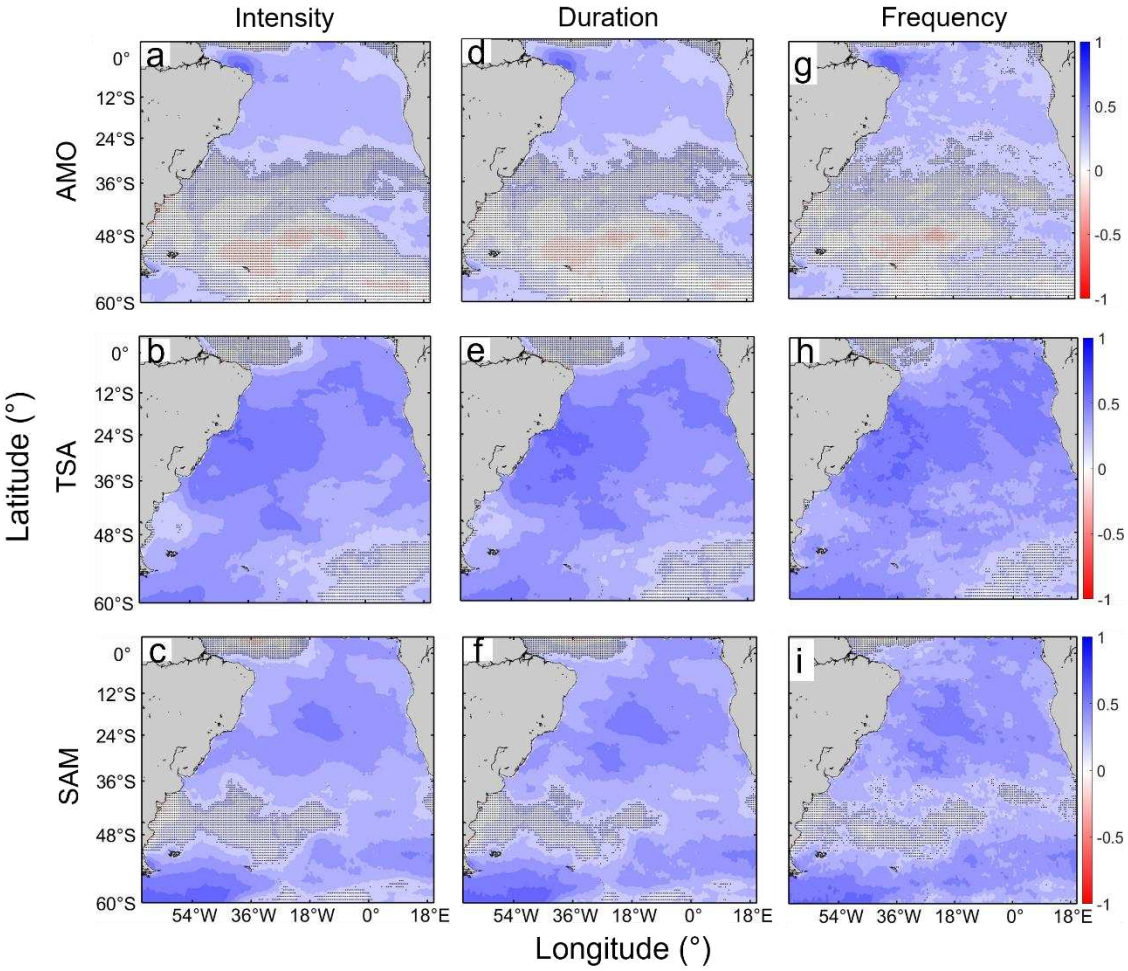


Figure 4. Spatial distribution of correlations between extreme events parameters and climate indices considering the entire analyzed period. (a-c) Intensity; (d-f) Duration; (g-i) Frequency. The hatched areas show locations where correlation is not statistically significant.

Table 2. Correlation coefficients r between climate indices, *Hs* and extreme event parameters at North (Nt), Central (Ct) and South (St) points. The values in parentheses indicate the percentage of parameter variance explained by the climate index.

	Hs			**Duration**			**Frequency**			**Intensity**		
	Nt	**Ct**	**St**	**Nt**	**Ct**	**St**	**Nt**	**Ct**	**St**	**Nt**	**Ct**	**St**
AMO	0.65 (42%)	0.27 (7%)	0.31 (10%)	0.60 (36%)	0.20 (4%)	0.30 (10%)	0.64 (41%)	0.19 (4%)	0.30 (9%)	0.59 (35%)	0.21 (4%)	0.30 (9%)
TSA	0.15 (2%)	0.61 (37%)	0.64 (41%)	0.13 (2%)	0.55 (30%)	0.52 (27%)	0.14 (2%)	0.52 (27%)	0.53 (28%)	0.14 (2%)	0.55 (30%)	0.50 (25%)
SAM	0.44 (19%)	0.49 (24%)	0.65 (42%)	0.27 (7%)	0.43 (19%)	0.57 (33%)	0.32 (10%)	0.34 (12%)	0.54 (29%)	0.26 (7%)	0.46 (21%)	0.58 (34%)

In order to provide insight into the wave field anomaly during the positive and negative phases of the dominant climate indices, Figure 5 shows the *Hs* and *WEF* fields averaged over the 5 years with the strongest/positive and weakest/negative records of each climate index. The systematically positive (negative) anomaly observed for positive (negative) phases is in line with the positive correlations found in Figure 3. A notable exception is the positive anomaly in the northwest and southeast South Atlantic during the positive phase of TSA (Figure 5e). *WEF* anomalies provides new insight into the origin of the largest or smallest wave conditions during the positive and negative phases. In particular, during the positive phases of AMO and SAM, the large *Hs* positive anomaly at the largest latitude is clearly due to intensified wave energy flux travelling eastwards.

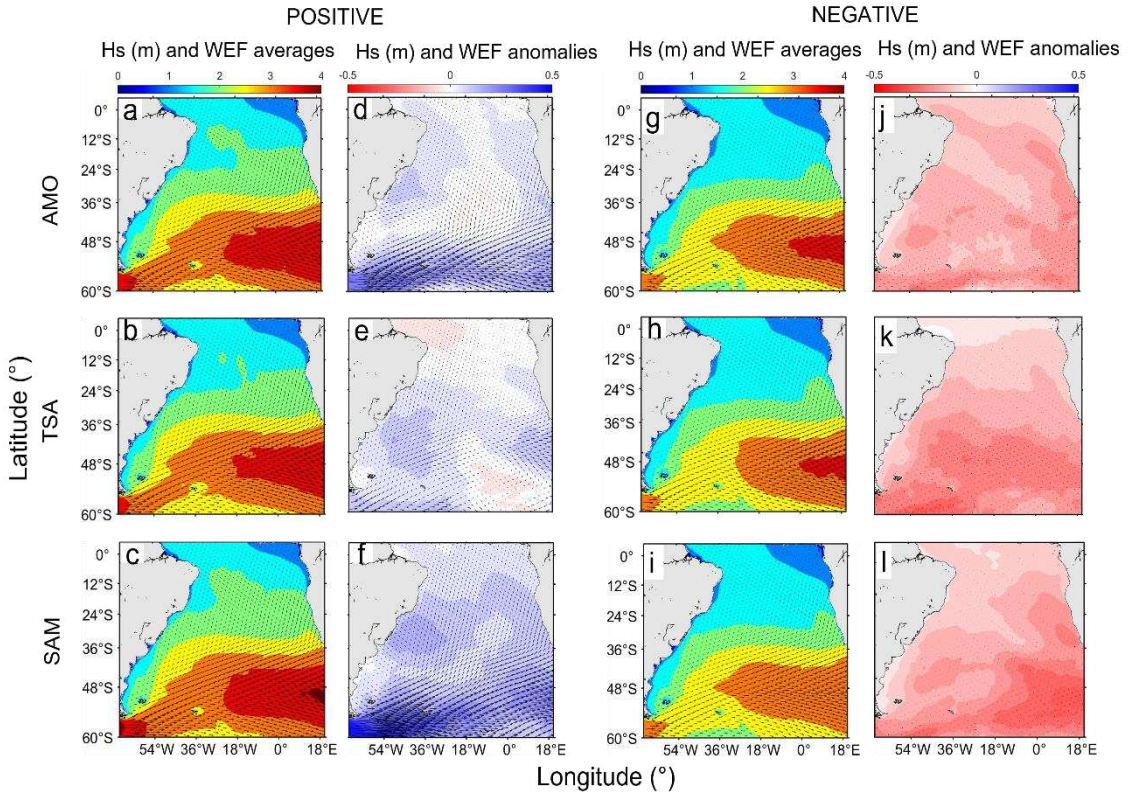


Figure 5. Mean *Hs* and *WEF* and corresponding anomalies over the 5 most (left-hand panels, positive phase) and less (right-hand panels, negative phase) intense years of each climate index.

4. Discussion

From 1950 to 2021, overall the entire South Atlantic Ocean shows trends of waves and extreme events parameters increasing yearly-average. The positive *Hs* trend is in line with previous studies (Young et al., 2011; Reguero et al., 2013; Reguero et al., 2019; Oliveira et al., 2019; Odériz et al., 2020b; Maia et al., 2022; Cotrim et al., 2022). The largest increasing rates of *Hs* are located at higher latitudes, which is in line with Young et al. (2011) and Reguero et al. (2019). This increasing trend is largely explained by the greater occurrence of extreme conditions which is reflected in the increasing trend in Intensity. According to Young et al. (2011) and

Reguero et al. (2019), at these high latitudes the Atlantic Ocean has some of the most extreme wave heights on the planet, and the Southern Ocean is the most energetic basin and dominates the other oceans in values and increasing rates of *WEF*.

Reguero et al. (2019) suggest that long-term changes in wave behavior need to be studied considering ocean atmosphere teleconnections and interannual variability. Although all climate indices have significant correlation values in virtually all points of the South Atlantic Ocean (Figure 3) there are areas of greater correlation for each index. The variations of *Hs* and extreme events parameters at the Nt point present higher correlation values with the AMO index (Table 2), which explains more than 42% of *Hs* variability, whereas the variability explanation of the extreme events parameters is between 35-41% (Table 2). As for the point Ct the TSA index explains 37% of *Hs* variance and that of the other parameters between 27-30%. Finally, the St point shows the largest correlation with the SAM index for all parameters, explaining 42% of *Hs* variance and between 29-34% of the extremes. Climate indices are also strongly linked with the magnitude and direction of the *WEF* (Figure 5).

Figure 3d shows the co-variation between *Hs* at the Nt point and AMO phase alternation, especially on a multidecadal scale. The relationship between AMO and wave behavior in the Atlantic Ocean is in line with previous studies (Wang et al., 2008; Kayano et al., 2019; Reguero et al., 2019; Maia et al., 2022), showing that the positive and negative phases of AMO have a great influence on cyclone activities and on the *WEF* in the South Atlantic Ocean, especially on long-term time scales. Our findings (Fig. 5d) corroborate Reguero et al. (2019) who identified significant positive correlations between wave behavior and AMO on the coasts of Africa and Brazil. Maia et al. (2022) also suggested that the identified positive trends in the *WEF* are related to the transition of negative to positive AMO phase. During this transition phase, since the late 1980s, Atlantic tropical cyclone activity has been shown to have largely increased in frequency and intensity (e.g., Elsner et al., 2000; Goldenberg et al., 2001; Emanuel, 2005; Webster et al., 2005). Reinforcing this, according to Wang et al. (2008) and Kayano et al. (2019) the low-level cyclones multidecadal variability in the South Atlantic are modulated by the AMO, and are more energetic during the positive phases. Thus, AMO patterns play an important role in the cyclone trajectories and consequently in the generation and propagation of waves along the South Atlantic.

For the Ct point, the highest correlations associated with the TSA index are also shown by Reguero et al. (2013), where the TSA pattern is associated with increase in the wave height and change in the *WEF* on the eastern edge of the American continent, especially in tropical and subtropical regions. According to the authors, this is mainly caused by Atlantic warming and the reinforcement of the south–east trade winds and the easterly winds in the western equatorial Atlantic because of a northward migration of the intertropical convergence zone.

In general, the highest positive correlation with wave climate in mid- to high-latitudes and in the Southern Ocean have been associated with SAM (Meehl et al., 2007; Hemer et al., 2010; Reguero et al., 2013; Wang and Cai 2013; Mentaschi et al., 2017; Marshall et al., 2018; Oliveira et al., 2019; Silva et al., 2020). The positive trend observed in SAM in recent decades (Figure 3f)

is consistent with earlier studies (Thompson and Wallace, 2000; Thompson and Solomon, 2002; Marshall, 2003; Cai et al., 2005; Cai and Cowan, 2007; Hemer et al., 2010; Marshall et al., 2018; Cotrim et al., 2022), showing that part of the trends obtained in *Hs* and in the extreme events parameters might be explained by an increase in the SAM index, evidenced by the relative contribution of the high-energy southerly swells in *WEF* (Figures 5c, f). Figures 2e-h indicate trends of significant increase in all analyzed properties in the region of point St and, according to Sterl and Caires (2005), the increasing *Hs* trend in the Southern Ocean is due to the increased number of storms in this region. Corroborating these results, Hemer et al. (2008), Reboita et al. (2009), Hemer et al. (2010), Maia et al. (2016) and Cotrim et al. (2022) suggest that the increased *Hs*, storminess and cyclogenetic activity near the South American coast are related to the positive SAM phases that intensifies the extratropical storm belt generating extreme winds related to extreme waves. As evidenced in Figure 3f, the SAM shows a strong correlation with an interannual *Hs* variability. According to Marshall et al. (2018) the SAM is a probable candidate for driving significant surface wave variations due to its large spatial scale (hemispheric) and temporal scale (up to season) and thus, may be a valuable source of wave variability predictability in the SH.

Long-term variations in SST anomalies coexist with oscillations in *Hs* and *WEF* which indicates the influence of temperature-driven atmospheric teleconnections on wave-generation cycles (Silva et al., 2020; Maia et al., 2022) and characterizing the climate indices as proxies for wave behavior (Mentaschi et al., 2017; Reguero et al., 2019). Especially, over the past several decades Antarctic ozone depletion and emissions of greenhouse gases have been forcing a positive trend of the SAM (Thompson and Wallace, 2000; Gillett and Thompson, 2003; Marshall, 2003; Hemer et al., 2010; Mentaschi et al., 2017). These scenarios can consequently be expected to result in continuing observed trends in the Southern Ocean wave climate including wave height increases, poleward shift of the storm tracks (Arblaster et al., 2011; Wang and Cai, 2013; Zheng et al., 2013) beyond considerable changes in the recurrence frequency of extreme events by the end of the 21st century, which are projected to occur twice as frequently along many areas, especially in the SH (Mentaschi eta al., 2017).

5. Conclusions

We investigated wave climate variations and trends in the South Atlantic Ocean between 1950 and 2021 and identified that *Hs* is increasing across this region. We also observed that the extreme events are stronger, longer and more frequent. The variation of these properties presents correlations with the AMO, TSA and SAM climate indices, mainly from low to high latitudes respectively. During the positive (negative) phases of each index, higher (lower) *Hs* and *WEF* are observed, as well as predominantly west (east) swell. We consider that, given these indices show strong correlation with wave climate variation and trends, they are critical to understanding and predicting coastal hazards such as flooding and erosion in the South Atlantic Ocean to support the development of coastal management plans. Better understanding the influence of climate

change on these climate indices should also improve our understanding of the impact of climate change on coastal response in the future.

Acknowledgments

We would like to thank “CAPES PRINT - Programa Institucional de Internacionalização” for the financial support.

CRediT authorship contribution statement

Natan Z. Maia: Conceptualization; Data curation; Formal analysis; Investigation; Methodology; Supervision; Validation; Visualization; Roles/Writing - original draft; Writing - review & editing. **Luis Pedro Almeida**: Conceptualization; Investigation; Methodology; Supervision; Writing - review & editing. **João Nicolodi**: Supervision; Writing - review & editing. **Lauro Calliari**: Conceptualization; Supervision. **Bruno Castelle**: Conceptualization; Formal analysis; Investigation; Methodology; Supervision; Visualization; Writing - review &editing.

6. References

Alexander, M. A., Kilbourne, K. H. & Nye, J. A., 2014. Climate variability during warm and cold phases of the Atlantic Multidecadal Oscillation (AMO) 1871-2008. Journal of Marine Systems, 133, 14-26, DOI: https://doi.org/10.1016/j.jmarsys.2013.07.017

Almeida, L. P., Ferreira, Ó., Vousdoukas, M. I., & Dodet, G., 2011. Historical variation and trends in storminess along the Portuguese South Coast. Natural Hazards and Earth System Science, 11(9), 2407–2417. https://doi.org/10.5194/nhess-11-2407-2011

Angnuureng, D. B., Almar, R., Senechal, N., Castelle, B., Addo, K. A., Marieu, V., & Ranasinghe, R., 2017. Shoreline resilience to individual storms and storm clusters on a meso-macrotidal barred beach. Geomorphology, 290(August 2015), 265–276. https://doi.org/10.1016/j.geomorph.2017.04.007

Antolínez, J. A. A., Mendez, F.J., Camus, P., Vitousek, S., González, E.M., Ruggiero, P. & Barnard, P., 2016. A multiscale climate emulator for long- term morphodynamics (MUSCLE- morpho), Journal of Geophysical. Research-Oceans, 121, 775–791, doi:10.1002/2015JC011107.

Arblaster, J. M., G. A. Meehl, and D. J. Karoly., 2011. Future climate change in the Southern Hemisphere: Competing effects of ozone and greenhouse gases, Geophys. Res. Lett.,38, L02701, doi:10.1029/2010GL045384.

Babanin, A. v., Rogers, W. E., de Camargo, R., Doble, M., Durrant, T., Filchuk, K., Ewans, K., Hemer, M., Janssen, T., Kelly-Gerreyn, B., Machutchon, K., McComb, P., Qiao, F., Schulz, E., Skvortsov, A., Thomson, J., Vichi, M., Violante-Carvalho, N., Wang, D., … Young, I. R., 2019. Waves and swells in high wind and extreme fetches, measurements in the Southern Ocean. Frontiers in Marine Science, 6(JUL), 1–12. https://doi.org/10.3389/fmars.2019.00361

Barnard, P. L. et al., 2015. Coastal vulnerability across the Pacific dominated by El Niño/Southern Oscillation. Nature Geosci.8, 801–807

British Antarctic Survey. www.bas.ac.uk/. Access in 06/13/2022

Cai, W. & Cowan, T., 2007. Trends in Southern Hemisphere Circulation in IPCC AR4Models over 1950–99: Ozone Depletion versus Greenhouse Forcing. J. Clim.20,681–693.

Cai, W., Shi, G., Cowan, T., Bi, D. & Ribbe, J., 2005. The response of the southern annular mode, the east Australian Current, and the southern midlatitude ocean circulation to global warming. Geophys. Res. Lett.32, L23706.

Cai WJ, Whetton PH, Karoly DJ., 2003. The response of the Antarctic Oscillation to increasing and stabilized CO2.Journal of Climate16:1525 – 1538

Castelle, B., Dodet, G., Masselink, G., & Scott, T., 2017. A new climate index controlling winter wave activity along the Atlantic coast of Europe: The West Europe Pressure Anomaly. Geophysical Research Letters, 44(3), 1384–1392. https://doi.org/10.1002/2016GL072379

Castelle, B., Masselink, G., 2023. Morphodynamics of wave-dominated beaches. Cambridge Prisms: Coastal Futures, 1, e1, 1–13, https://doi.org/10.1017/cft.2022.2

Cotrim, C.S.; Semedo, A.; Lemos, G. Brazil Wave Climate from a High-Resolution Wave Hindcast.Climate., 2022. 10, 53. https://doi.org/10.3390/cli10040053

De Leo, F., Besio, G., & Mentaschi, L., 2021. Trends and variability of ocean waves under RCP8.5 emission scenario in the Mediterranean Sea. Ocean Dynamics, 71(1), 97–117. https://doi.org/10.1007/s10236-020-01419-8

Dorsch, W., Newland, T., Tassone, D., Tymons, S., Walker, D., 2008. A statistical approach to modeling the temporal patterns of ocean storms. J. Coast. Res. 24 (6), 1430–1438

Elsner, J. B., T. Jagger, and X.-F. Liu., 2000. Changes in the rates of North Atlantic major hurricane activity during the 20th century, Geophys. Res. Lett.,27, 1743–1746, DOI:10.1029/2000GL011453

Emanuel, K., 2005. Increasing destructiveness of tropical cyclones over the past 30 years, Nature,436, 686–688, PubMed, doi:10.1038/nature03906

Enfield, D.B., A.M. Mestas, D.A. Mayer, and L. Cid-Serrano., 1999: How ubiquitous is the dipole relationship in tropical Atlantic sea surface temperatures? JGR-O, 104, 7841-7848

Enfield, D.B., A. M. Mestas-Nunez and P.J. Trimble., 2001: The Atlantic multidecadal oscillation and it's relation to rainfall and river flows in the continental U.S.. Geophysical Research Letters, Vol. 28, 2077-2080.

Garner, A. J., Mann, M. E., Emanuel, K. A., Kopp, R. E., Lin, N., Alley, R. B., Horton, B. P., DeConto, R. M., Donnelly, J. P., & Pollard, D., 2017. Impact of climate change on New York City's coastal flood hazard: Increasing flood heights from the preindustrial to 2300 CE. Proceedings of the National Academy of Sciences of the United States of America, 114(45), 11861–11866. https://doi.org/10.1073/pnas.1703568114

Gillett, N.P. & Thompson, D.W.J., 2003. Simulation of recent Southern Hemisphere climate change. Science302: 273 – 275.

Goldenberg, S. B., C. W. Landsea, A. M. Maestas-Nunez, and W. M. Gray., 2001. The recent increase in Atlantic hurricane activity: Causes and implications, Science,293, 474–479, PubMed, doi:10.1126/science.1060040.

Grassi, B., G. Redaelli, and G. Visconti., 2005. Simulation of Polar Antarctic trends: Influence of tropical SST,Geophys. Res. Lett.,32, L23806. Doi:10.1029/2005GL023804.

Hemer, M. A., Church, J. A., & Hunter, J. R., 2010. Variability and trends in the directional wave climate of the Southern Hemisphere. International Journal of Climatology, 30(4), 475–491. https://doi.org/10.1002/joc.1900

Hemer, M.A., Simmonds I, Keay K., 2008. A classification of wave generation characteristics during large wave events on the Southern Australian margin. Continental Shelf Research28: 634 – 652

Hersbach, H., Bell, B., Berrisford, P., Hirahara, S., Horányi, A., Muñoz-Sabater, J., Nicolas, J., Peubey, C., Radu, R., Schepers, D., Simmons, A., Soci, C., Abdalla, S., Abellan, X., Balsamo, G., Bechtold, P., Biavati, G., Bidlot, J., Bonavita, M., … Thépaut, J. N., 2020. The ERA5 global reanalysis. Quarterly Journal of the Royal Meteorological Society, 146(730), 1999–2049. https://doi.org/10.1002/qj.3803

Kayano, M. T., Rosa, M. B., Rao, V. B., Andreoli, R. V., & de Souza, R. A. F., 2019. Relations of the low-level extratropical cyclones in the southeast Pacific and South Atlantic to the Atlantic multidecadal oscillation. Journal of Climate, 32(14), 4167–4178. https://doi.org/10.1175/JCLI-D-18-0564.1

Karunarathna, H., Pender, D., Ranasinghe, R., Short, A.D., Reeve, D.E., 2014. The effects of storm clustering on beach profile variability. Mar. Geol. 348, 103–112

Kerr, R. A., 2000. A North Atlantic climate pacemaker for the centuries. *Science*, *288* (5473), 1984–1986. https://doi.org/10.1126/science.288.5473.1984

Maia, N. Z., Calliari, L. J. & Nicolodi, J. L., 2016. Analytical model of sea level elevation during a storm: Support for coastal flood risk assessment associated with cyclone passage. Continental Shelf Research, 124, 23–34. https://doi.org/10.1016/j.csr.2016.04.012

Maia, N. Z., Almeida, L. P., Emmendorfer, L., Nicolodi, J. L., & Calliari, L., 2022. Wave climate trends and breakpoints during the Atlantic Multidecadal Oscillation (AMO) in southern Brazil. *Ocean and Coastal Research*, *2022*, 22027. https://doi.org/10.1590/2675-2824070.21086nzm

Marshall, G. J., 2003. Trends in the Southern Annular Mode from observations and reanalyses .J. Clim.16, 4134–4143.

Marshall, A. G., Hemer, M. A., Hendon, H. H. & Mcinnes, K. L., 2018. Southern annular mode impacts on global ocean surface waves. Ocean Modelling, 129, 58–74. https://doi.org/10.1016/j.ocemod.2018.07.007

Masselink, G., Austin, M., Scott, T., Poate, T., & Russell, P., 2014. Role of wave forcing, storms and NAO in outer bar dynamics on a high-energy, macro-tidal beach. Geomorphology, 226, 76–93. https://doi.org/10.1016/j.geomorph.2014.07.025

Meehl, G., Stocker, T., Collins, W., Fiedlingstein, P., Gaye, A., Gregory, Kitoh, A., Knutti, R.,Murphy, J., Noda, A., Rper, S., Watterson, I., Weaver, A., Zhao, Z., 2007. Climate change2007: the physical science basis. Contribution of Working Group I to the Fourth Assessment Report of the Intergovernmental Panel on Climate Change, Chapter Global Climate Projections. Cambridge University Press, Cambridge, United Kingdom and New York, NY, USA. ISBN: 978-0-521-88009-1

Mendoza, E.T., Jimenez, J.A., Mateo, J., 2011. A coastal storms intensity scale for the Catalan sea (NW Mediterranean). Nat. Hazards Earth Syst. Sci. 11, 2453–2462

Mentaschi, L., Vousdouskas, M. I., Voukuvalas, E., Dosio, A. & Feyen, L., 2017. Global changes of extreme coastal wave energy fluxes triggered by intensified teleconnection patterns. Geophysical Research Letters. 44, 2416–2426.

Meucci, A., Young, I. R., Hemer, M., Kirezci, E., & Ranasinghe, R., 2020. Projected 21st century changes in extreme wind-wave events. Science Advances, 6(24), 1–10. https://doi.org/10.1126/sciadv.aaz7295

Morim, J., Hemer, M., Wang, X. L., Cartwright, N., Trenham, C., Semedo, A., Young, I., Bricheno, L., Camus, P., Casas-Prat, M., Erikson, L., Mentaschi, L., Mori, N., Shimura, T., Timmermans, B., Aarnes, O., Breivik, Ø., Behrens, A., Dobrynin, M., Andutta, F., 2019. Robustness and uncertainties in global multivariate wind-wave climate projections. Nature Climate Change, 9(9), 711–718. https://doi.org/10.1038/s41558-019-0542-5

National Oceanic and Atmospheric Administration (NOAA) Physical Sciences Laboratory (www.psl.noaa.gov, Access in 06/06/2022)

Odériz, I., Silva, R., Mortlock, T. R. & Mendoza, E., 2020a. Climate drivers of directional wave power on the Mexican coast. Ocean Dynamics, 70(9), 1253–1265. https://doi.org/10.1007/s10236-020-01387-z

Odériz, I., Silva, R., Mortlock, T. R., & Mori, N., 2020b. El niño-southern oscillation impacts on global wave climate and potential coastal hazards. Journal of Geophysical Research: Oceans, 125, e2020JC016464. https://doi.org/10.1029/2020JC016464

O'Grady, J. G., Hemer, M. A., McInnes, K. L., Trenham, C. E., & Stephenson, A. G., 2021. Projected incremental changes to extreme wind-driven wave heights for the twenty-first century. Scientific Reports, 11(1), 1–8. https://doi.org/10.1038/s41598-021-87358-w

Oliveira, B. A., Sobral, F., Fetter, A., & Mendez, F. J., 2019. A high-resolution wave hindcast off Santa Catarina (Brazil) for identifying wave climate variability. Regional Studies in Marine Science, 32, 100834. https://doi.org/10.1016/j.rsma.201. Regional Studies in Marine Science, 32, 100834. https://doi.org/10.1016/j.rsma.2019.100834

Rasmussen, D. J., Bittermann, K., Buchanan, M. K., Kulp, S., Strauss, B. H., Kopp, R. E., & Oppenheimer, M., 2018. Extreme sea level implications of 1.5 °c, 2.0 °c, and 2.5 °c temperature stabilization targets in the 21st and 22nd centuries. Environmental Research Letters, 13(3). https://doi.org/10.1088/1748-9326/aaac87

Reboita, M. S., Ambrizzi, T. & Rocha, R. P., 2009. Relationship between the Southern Annular Mode and southern hemisphere atmospheric systems. Rev. Bras. Meteorol.24, 48–55.

Reguero, B. G., Losada, I. J. & Mendéz, F. J., 2019. A recent increase in global wave power as a consequence of oceanic warming. Nature Communications. 205, 1–14

Reguero, B. G., Méndez, F. J., & Losada, I. J., 2013. Variability of multivariate wave climate in Latin America and the Caribbean. Global and Planetary Change, 100, 70–84. https://doi.org/10.1016/j.gloplacha.2012.09.005

Reguero, B. G., Menéndez, M., Méndez, F. J., Mínguez, R., & Losada, I. J., 2012. A Global Ocean Wave (GOW) calibrated reanalysis from 1948 onwards. Coastal Engineering, 65, 38–55. https://doi.org/10.1016/j.coastaleng.2012.03.003

Sénéchal, N., Coco, G., Castelle, B., & Marieu, V., 2015. Storm impact on the seasonal shoreline dynamics of a meso- to macrotidal open sandy beach (Biscarrosse, France). Geomorphology, 228, 448–461. https://doi.org/10.1016/j.geomorph.2014.09.025

Silva, A. P., Klein, A. H. F., Fetter-Filho, A. F. H., Hein, C. J., Méndez, F. J., Broggio, M. F., & Dalinghaus, C., 2020. Climate-induced variability in South Atlantic wave direction over the

past three millennia. Scientific Reports, 10(1), 1–12. https://doi.org/10.1038/s41598-020-75265-5

Sterl A. & Caires S., 2005. Climatology, variability and extrema of ocean waves: the web-based KNMI/ERA-40 wave atlas. International Journal of Climatology25(7): 963 – 977

Thompson, D. W. J. & Wallace, J. M., 2000. Annular modes in the extratropical circulation. Part I: Month-to-month variability. J. Clim.13, 1000–1016.

Thompson, D. W. J. & Solomon, S., 2002. Interpretation of recent Southern Hemisphere climate change. Science296, 895–899.

Trenberth, K. E., J. M. Caron, D. P. Stepaniak, and S. Worley., 2002. Evolution of El Nin˜o Southern Oscillation and global atmospheric sur-face temperatures. J. Geophys. Res.,107(D8), 4065, doi:10.1029/2000JD000298

Van der Meer, J.W., Allsop, N.W.H., Bruce, T., De Rouck, J., Kortenhaus, A., Pullen, T., Schüttrumpf, H., Troch, P. and Zanuttigh, B., 2016. EurOtop, Manual on wave overtopping of sea defences and related structures. An overtopping manual largely based on European research, but for worldwide application www.overtopping-manual.com.

Vousdoukas, M. I., Mentaschi, L., Voukouvalas, E., Bianchi, A., Dottori, F., & Feyen, L., 2018. Climatic and socioeconomic controls of future coastal flood risk in Europe. Nature Climate Change, 8(9), 776–780. https://doi.org/10.1038/s41558-018-0260-4

Wang, G., & Cai, W., 2013. Climate-change impact on the 20th-century relationship between the Southern Annular Mode and global mean temperature. Scientific Reports, 3, 1–6. https://doi.org/10.1038/srep02039

Wang, C., and D.B. Enfield., 2001: The tropical Western Hemisphere warm pool, Geophys. Res. Lett., 28, 1635-1638.

Wang, C., Lee, S. K., & Enfield, D. B., 2008. Atlantic warm pool acting as a link between atlantic multidecadal oscillation and atlantic tropical cyclone activity. Geochemistry, Geophysics, Geosystems, 9(5). https://doi.org/10.1029/2007GC001809

Webster, P. J., G. J. Holland, J. A. Curry, and H.-R. Chang., 2005. Changes in tropical cyclone number, duration, and intensity in a warming environment. Science,309, 1844–1846 PubMed, doi:10.1126/science.1116448

Young, I. R., Zieger, S., and Babanin, A. V., 2011. Global trends in wind speed and wave height. Science332, 451–455. DOI: 10.1126/science.1197219

Zheng, F., J. Li, R. T. Clark, and H. C. Nnamchi., 2013. Simulation and projection of the Southern Hemisphere annular mode in CMIP5 models. J. Clim.,26(24), 9860–9879, doi:10.1175/JCLI-D-13-00204.1.

Capítulo VII: Síntese da Discussão e Conclusões

Neste capítulo são apresentados os principais pontos das discussões destacados nos artigos científicos 1 e 2 e, após a discussão, é apresentada a conclusão geral da Tese. Por fim, são apresentadas as considerações finais e perspectivas para trabalhos futuros.

7.1 Artigo 1: "*Wave climate trends and breakpoints during the Atlantic Multidecadal Oscillation (AMO) in southern Brazil" [Maia et al., 2022]*

Este artigo é referente à primeira fase da Tese e foi desenvolvido no Laboratório de Oceanografia Geológica da Universidade Federal do Rio Grande (LOG-FURG, Brasil) sob a supervisão do Dr. Lauro Calliari e contribuições dos demais autores.

7.1.1 Variações e tendências do *WEF*

Através de uma abordagem Euleriana analisamos a variação do clima de ondas entre 1979 e 2019 em um ponto em águas profundas em frente ao estado do Rio Grande do Sul (Brasil), especificamente nas coordenadas 32°30'S e 50°W. Encontramos que o *WEFm* e o *WEF98* que se propagaram em direção ao sul do Brasil aumentaram com uma tendência linear significativa nas últimas quatro décadas, com um incremento de 0,063 e 0,17 kW/m/ano, respectivamente 0,63 e 0,29% ao ano. Tais taxas indicam que em condições médias o *WEF* em 2019 foi 29,4% maior que em 1979, ao passo que em condições extremas o *WEF98* aumentou 12,6% ao longo dos 41 anos,

evidenciando assim maior transferência de energia da atmosfera para o movimento da superfície oceânica nas últimas décadas.

Os estudos de Reguero et al. [2013] e Alonso e Solari [2021] indicaram que o *WEF* no Atlântico Oeste está passando por uma tendência de rotação no sentido horário. Essas mudanças provavelmente estão relacionadas à tendência de rotação em direção aos polos detectada em atividades de tempestades extratropicais [Meehl et al., 2007], o que indica maior atividade de tempestades em altas latitudes sobretudo no *HS* [Bengtsson et al., 2006]. O fato de o swell dos quadrantes sul ser o mais energético sugere que estas ondas são provavelmente as principais responsáveis pelo impulsionamento e tendências de aumento do *WEFm* geral, pois os quadrantes SSE e SSW têm as maiores taxas de incremento anual associadas ao *WEFm* com valores de 0,073 e 0,094 kW/m/ano, respectivamente.

Este cenário é de considerável relevância uma vez que os swells gerados no Oceano Antártico são projetados para serem mais energéticos nos próximos anos [Young et al., 2011; Babanin et al., 2019] e, no Oceano Atlântico Sul ocidental, o swell de SW é fortemente influenciado por ventos de baixas latitudes gerados pelo Anticiclone Polar Migratório (APM), responsável pela geração de tempestades que podem impactar repentinamente o litoral quando atingem o continente [Calliari et al., 1998; Parise et al., 2009; Machado et al., 2010].

Os resultados encontrados em relação ao *WEFm* e *WEF98* estão em linha com as tendências mundiais. Segundo Mentaschi et al. [2017], o *WEF* ao longo das costas em todo o mundo deverá aumentar significativamente até o final deste século, principalmente no *HS*. Semedo et al. [2013] evidenciam que as mudanças no clima de onda no final do século XXI serão de pequenas a moderadas, com os maiores sinais sendo uma mudança em direção aos polos na média anual de alturas significativas das ondas nas latitudes médias de ambos os hemisférios, porém sendo mais pronunciado no *HS* e provavelmente associado a uma mudança correspondente nas trilhas de tempestades de latitudes médias. Neste sentido, Mentaschi et al. [2017] conduziram uma análise de modelagem abrangente para identificar futuras tendências globais no *WEF* extremo ao longo do século XXI sob um cenário de alta emissão de gases estufa

(RCP 8.5 - IPCC) e identificaram que o incremento do *WEF* se traduz em mudanças consideráveis na frequência de recorrência de eventos extremos, que se projeta duplicar em muitas áreas, especialmente no *HS*, implicando uma intensificação da erosão costeira e outros impactos induzidos pelas ondas.

7.1.2 Relações entre o *WEF* e o AMO

De uma forma geral, as variações espaço-temporais na temperatura da superfície do mar são conhecidas por serem um fator crítico nas teleconexões na interface oceano-atmosfera e influenciam os padrões de vento que, por consequência, definem as propriedades do *WEF* ao longo dos oceanos [Reguero et al. 2019]. Assim, dado o comportamento dipolo no Oceano Atlântico entre os Hemisférios Norte e Sul durante o AMO e a relevância do Oceano Austral para os oceanos extratropicais como fonte geradora de ondas, eventuais mudanças nos padrões de SST em altas latitudes eventualmente induzidas pelo AMO podem influenciar a variabilidade do *WEF* no sul do Brasil. Observamos que o swell do quadrante SSW foi o primeiro a mostrar uma tendência significativa de aumento do *WEFm* no final dos anos 1980 e posteriormente o swell SSE também iniciou uma fase significativa de crescimento. Tais ondulações têm suas origens relacionadas às latitudes mais altas e nossos resultados sugerem que as tendências positivas observadas nos valores interanuais do *WEF* provavelmente estão relacionadas à transição de longo prazo da fase fria para quente do AMO no oeste do Oceano Atlântico Sul.

Os resultados deste artigo corroboram outros trabalhos que investigaram processos ocorrentes na interface oceano-atmosfera no Oceano Atlântico. Wang et al. [2008] descreveram que, entre 1854-2006, os furacões no Oceano Atlântico apresentaram atividades maiores e menores durante as fases quentes e frias do AMO, respectivamente, sugerindo que a variabilidade nas temperaturas oceânicas pode ser responsável pela variação multidecadal na atividade dos furacões no Oceano Atlântico. Esses autores também mostraram que as atividades de ciclones tropicais no Atlântico aumentaram amplamente em frequência e intensidade desde o final da década de 1980. Reforçando esses resultados, observamos que durante o período de transição da fase fria para a

fase quente do AMO entre o final da década de 1980 e a década de 1990, as curvas do *WEFm* e *WEF98* co-variaram com a curva do AMO, exibindo tendências crescentes. No mesmo período, o *WEFm* associado aos quadrantes mais energéticos de SSE e SSW também apresentou tendências de crescimento significativo e co-variações com o comportamento do AMO.

Kayano et al. [2019] mostram que ciclones extratropicais no Atlântico Sul são modulados por anomalias de SST relacionadas ao AMO, com anomalias positivas afetando os gradientes meridionais de temperatura do mar e as trajetórias dos ciclones. Segundo estes autores, a energia cinética nas fases quentes do AMO supera a das fases frias, induzindo a formação de ciclones mais energéticos com alto potencial para transferir energia da atmosfera para o oceano e aumentar o *WEF* durante as fases quentes. Este fato é de grande importância para a região, uma vez que os ciclones extratropicais são conhecidos por gerarem valores extremos de altura de onda e consequentemente aumentam os valores de *WEF* no oeste do Atlântico Sul [Sasaki et al. 2021].

Os resultados deste artigo sugerem que as tendências observadas nas curvas do *WEFm* e *WEF98* provavelmente representam o efeito de uma transição de longo prazo de uma fase fria (negativa) para quente (positiva) do AMO ao longo do período analisado. Embora a relação entre o *WEF* e o AMO não explique a variabilidade interanual do comportamento das ondas, ela parece ter um efeito profundo nas variações e tendências da componente de longo prazo do *WEF* no oeste do Atlântico Sul.

7.2 Artigo 2: “*Long-term trends and wave climate variability in the South Atlantic Ocean: the influence of climate indices*”

Este artigo é referente à segunda fase da Tese e foi desenvolvido no Environnements et Paléoenvironnements Océaniques et Continentaux da Université de Bordeaux (EPOC-UB, França) sob a supervisão do Dr. Bruno Castelle e contribuições dos demais autores. Este período compreende a fase *sanduíche* do doutorado financiado pelo Programa Institucional de Internacionalização CAPES – PrInt. Durante a estadia no EPOC-UB foi possível utilizar recursos computacionais altamente capazes de processar centenas de Gigabytes de dados em curto intervalo de tempo. Assim, atrelada à atualização da base de dados do ERA5, entre o Artigo 1 e o Artigo 2 as séries temporais e coberturas espaciais foram expandidas de 41 para 72 anos e de 1 para 23.580 pontos respectivamente, contemplando assim 7 décadas do comportamento de ondas ao longo de todo o Oceano Atlântico Sul. Desta forma, foi possível observar e compreender melhor processos que até então estavam ocultos, fragmentados e desconhecidos.

7.2.1 Tendências do clima de ondas e Eventos Extremos

As menores alturas de onda são encontradas em regiões próximas à costa e gradualmente aumentam em direção às maiores latitudes ao sul, ao passo que os maiores valores associados aos parâmetros de eventos extremos são observados nas zonas temperadas e também em altas latitudes. De uma forma geral todo o Oceano Atlântico Sul mostra tendências de aumento nas médias anuais de altura de onda e de duração, frequência e intensidade de eventos extremos entre 1950 e 2021. As maiores taxas de incremento de *Hs* estão localizadas em latitudes mais altas, abaixo de 48°S, e é explicada pela maior ocorrência de condições extremas o que se reflete na tendência crescente da Intensidade. Estes resultados corroboram Young et al. [2011] e Reguero et al. [2019] que, de acordo com os autores, o Oceano Austral é a bacia mais energética e domina os demais oceanos em valores e taxas crescentes de *WEF*. A ondulação gerada nesta região se propaga para a costa sul americana e,

conforme observado por Maia et al. [2022] (Artigo 1), é responsável pelo incremento de *WEF* médio e extremo em latitudes subtropicais.

7.2.2 Correlações entre clima de ondas e Índices Climáticos

Conforme apontado por Reguero et al. [2019], é necessário considerar as teleconexões que ocorrem na interface oceano-atmosfera e sua variabilidade para estudar e compreender o comportamento de longo termo das ondas. De uma forma geral as correlações entre as propriedades das ondas e os Índices Climáticos apresentam comportamento meridional, sendo as maiores correlações na área norte do domínio com o índice AMO, na área central com o TSA e na região sul do domínio com o índice SAM. Porém, vale ressaltar que a influência dos Índices Climáticos não se limita a estas áreas e sim, influencia em diferentes graus o comportamento do clima de ondas ao longo de quase todo o Oceano Atlântico Sul.

Em uma análise da variação anual das alturas de onda na região no norte do domínio, o *Hs* co-varia com o AMO sobretudo em escala multidecadal, acompanhando inclusive as mudanças entre as fases positivas e negativas deste Índice. É importante ressaltar que o AMO possui uma fase de aproximadamente 35 anos (período de 70 anos). Este comportamento corrobora autores como Wang et al. [2008], Kayano et al. [2019], Reguero et al. [2019] e Maia et al. [2022] onde é evidenciado que as fases positivas e negativas do AMO exercem grande influência nas atividades dos ciclones e no *WEF* do Oceano Atlântico Sul, especialmente em escalas de tempo de longo prazo, sendo os ciclones e o *WEF* mais energéticos durantes as fases positivas do AMO com ondulações incidindo principalmente do quadrante oeste.

As maiores correlações de *Hs* com o índice TSA na área central do domínio corrobora Reguero et al. [2013], onde o padrão TSA está associado ao aumento da altura das ondas e alterações do *WEF* na borda leste do continente americano, principalmente nas regiões tropicais e subtropicais.

A região ao sul do domínio apresenta uma dinâmica bastante interessante e, de uma forma geral, também as maiores taxas de incremento de *Hs* e dos

parâmetros de Eventos Extremos. Além disso, há influência de todos os índices climáticos sobretudo a sudoeste do domínio, mas, em geral, as maiores correlações estão associadas ao SAM corroborando assim diversos trabalhos como Meehl et al. [2007], Hemer et al. [2010], Reguero et al. [2013], Wang e Cai [2013], Mentaschi et al. [2017], Marshall et al. [2018], Oliveira et al. [2019] e Silva et al. [2020]. Ao longo das últimas décadas o SAM apresentou tendência positiva e parte das tendências obtidas em *Hs* e nos parâmetros de Eventos Extremos podem ser explicadas por esta intensificação de fase, intensificando o cinturão de ciclones extratropicais gerando ventos extremos e induzindo assim a formação de ondulação de elevado valor de *WEF* provenientes do quadrante oeste principalmente em altas latitudes, corroborando Hemer et al. [2008], Reboita et al. [2009], Hemer et al. [2010] e Cotrim et al. [2022].

De uma forma geral, as fases positivas dos Índices AMO, TSA e SAM possuem significativa influência no incremento de *Hs* e *WEF* ao longo do Oceano Atlântico Sul e, analogamente durante as fases negativas de cada Índice, os valores de *Hs* e *WEF* são anomalamente menores. Este comportamento se faz bastante evidente principalmente durante as fases positivas do AMO e SAM em altas latitudes, onde *Hs* e *WEF* assumem vales muito positivamente anômalos e com incidência de oeste. De forma bastante interessante, o Índice AMO mostra uma forte correlação com a variação da altura de onda com uma clara variabilidade multidecadal, enquanto TSA e SAM mostram uma tendência positiva com variabilidade interanual sobreposta. As escalas temporais destas variabilidades se relacionam com o período de variação de cada Índice, que possuem oscilações multidecadais (AMO) a interanuais/sazonais (TSA e SAM).

7.2.3 Clima de ondas e mudanças climáticas

Variações de longo prazo em anomalias de SST coexistem com oscilações em *Hs* e *WEF*, indicando a influência de teleconexões atmosféricas impulsionadas pela temperatura nos ciclos de geração de ondas. Uma vez havendo significativas correlações, os Índices Climáticos caracterizam-se como proxies para o comportamento de ondas [Mentaschi et al., 2017; Reguero et al., 2019]. De acordo com Thompson e Wallace [2000], Gillett e Thompson [2003],

Marshall [2003], Hemer et al. [2010] e Mentaschi et al. [2017] as emissões de gases de efeito estufa e a destruição do ozônio em altas latitudes está forçando uma tendência positiva do Índice SAM. Por consequência, espera-se que estas alterações induzam o aumento da altura de ondas e influenciem o comportamento e parâmetros dos eventos extremos não somente, mas sobretudo em altas latitudes, área de maior influência do SAM conforme aqui observado e descrito. Segundo Mentaschi et al. [2017], em um cenário de mudanças climáticas a frequência de eventos extremos deve dobrar em muitas áreas especialmente do Hemisfério Sul, potencializando processos erosivos e eventos de inundação além de causar danos às infraestruturas costeiras e prejuízos socioeconômicos.

7.3 Conclusões

Investigamos as variações e tendências do clima de ondas no Oceano Atlântico Sul ao longo das últimas décadas e identificamos que o *Hs* e o *WEF* estão aumentando nessa região. Observamos também que os eventos extremos aumentaram em intensidade, duração e frequência, logo, estão mais fortes, longos e recorrentes. De uma forma geral a variação do clima de ondas incluindo condições extremas está sujeita a algum grau de influência dos três Índices Climáticos analisados ao longo de quase todo o Oceano Atlântico Sul, porém a variação destas propriedades apresenta maiores correlações e co-variações com os índices climáticos AMO, TSA e SAM, principalmente de baixas para altas latitudes, respectivamente. O Índice AMO mostra uma forte correlação com a variação da altura de onda em uma escala multidecadal, ao passo que os Índices TSA e SAM mostram maiores correlações sobretudo com a variabilidade interanual das mesmas. Durante as fases positivas de cada índice, maiores valores de *Hs* e *WEF* são observados, bem como há o predomínio da incidência do swell de quadrante oeste. Nas fases negativas, condições opostas são observadas, com a diminuição de *Hs* e *WEF*.

Por fim, uma vez que estes Índices Climáticos mostram forte correlação com as variações e tendências do clima de ondas, eles são críticos para entender e prever potenciais riscos associados à eventos de inundação e

processos erosivos em regiões costeiras adjacentes ao Oceano Atlântico Sul e, portanto, devem ser considerados como subsídio para o desenvolvimento de planos de gestão e manejo de áreas costeiras e marinhas. Desta forma, uma melhor compreensão e previsão da evolução destes Índices Climáticos considerando padrões de teleconexão em um cenário de mudanças climáticas globais é fundamental para antecipar os perigos e preparar as regiões costeiras para o enfrentamento das ameaças futuras.

7.4 Considerações finais e perspectivas para trabalhos futuros

Sabendo que o comportamento das ondas é influenciado por um ou uma combinação de Índices Climáticos e padrões de teleconexão, faz-se necessária uma profunda compreensão dos processos atuantes na interface oceano-atmosfera em diferentes escalas temporais. Dada a relevância do tema em uma perspectiva de riscos costeiros associada ao cenário de mudanças climáticas, o entendimento da relação entre o comportamento das ondas e a oscilação destes índices é de suma importância para identificar os riscos e minimizar potenciais impactos associados ao processo através do subsídio ao desenvolvimento de políticas e planos de gerenciamento e manejo costeiros. Sobretudo, é importante considerar eventuais impactos em áreas especialmente vulneráveis como costas arenosas e expostas de baixa declividade, setores com cordão dunar não preservado bem como áreas estratégicas a exemplo de terminais portuários e plantas de geração de energia em áreas costeiras e oceânicas. Além disso, com o aumento da intensidade, frequência e duração dos Eventos Extremos, as zonas costeiras devem ser preparadas para minimizar os efeitos socioeconômicos adversos relativos a processos erosivos e eventos de inundação.

Capítulo VIII: Referências Bibliográficas

ALEXANDER, M. A., HALIMEDA KILBOURNE, K. & NYE, J. A. 2014. Climate variability during warm and cold phases of the Atlantic Multidecadal Oscillation (AMO) 1871-2008. *Journal of Marine Systems*, 133(February), 14–26. https://doi.org/10.1016/j.jmarsys.2013.07.017.

ALHEIT, J., LICANDRO, P., COOMBS, S., GARCIA, A., GIRÁLDEZ, A., SANTAMARÍA, M.T.G., SLOTTE, A. & TSIKLIRAS, A.C. 2014. Atlantic Multidecadal Oscillation (AMO) modulates dynamics of small pelagic fishes and ecosystem regime shifts in the eastern North and Central Atlantic. *Journal of Marine Systems*. V.133, 88-102. ISSN 0924-7963. https://doi.org/10.1016/j.jmarsys.2014.02.005.

ALMEIDA, L. P., FERREIRA, Ó., VOUSDOUKAS, M. I. & DODET, G. 2011. Historical variation and trends in storminess along the Portuguese South Coast. *Natural Hazards and Earth System Science*, 11(9), 2407–2417. https://doi.org/10.5194/nhess-11-2407-2011

ALONSO, R., & SOLARI, S. 2021. Comprehensive wave climate analysis of the Uruguayan coast. *Ocean Dynamics*, *71*(8), 823–850. https://doi.org/10.1007/s10236-021-01469-6

ANTOLÍNEZ, J. A. A., MENDEZ, F.J., CAMUS, P., VITOUSEK, S., GONZÁLEZ, E.M., RUGGIERO, P. & BARNARD, P 2016. A multiscale climate emulator for long- term morphodynamics (MUSCLE- morpho), *Journal of Geophysical. Research-Oceans*, 121, 775–791, doi:10.1002/2015JC011107.

ANGNUURENG, D. B., ALMAR, R., SÉNÉSHAL, N., CASTELLE, B., ADDO, K. A., MARIEU, V., & RANASINGHE7, R., 2017. Shoreline resilience to individual storms and storm clusters on a meso-macrotidal barred beach. *Geomorphology*, 290(August 2015), 265–276. https://doi.org/10.1016/j.geomorph.2017.04.007

ARBLASTER, J. M., G. A. MEEHL, and D. J. KAROLY., 2011. Future climate change in the Southern Hemisphere: Competing effects of ozone and greenhouse gases, *Geophys. Res. Lett.*,38, L02701, doi:10.1029/2010GL045384.

BABANIN AV ET AL. 2019. Waves and swells in high wind and extreme fetches, measurements in the southern ocean. *Frontiers in Marine Science*. 6:361. https://doi.org/10.3389/fmars.2019.00361

BARNARD, P. L. et al., 2015. Coastal vulnerability across the Pacific dominated by El Niño/Southern Oscillation. *Nature Geosci*.8, 801–807

BENGTSSON, L., HODGES, K. & ROECKNER, E. 2006. Storm tracks and climate change. *Journal of Climate* 19, 3518–3543.

BIASTOCH, A., DURGADOO, J. V., MORRISON, A. K., VAN SEBILLE, E., WEIJER, W., & GRIFFIES, S. M. 2015. Atlantic multi-decadal oscillation covaries with Agulhas leakage. *Nature Communications*, 6. https://doi.org/10.1038/ncomms10082

BISCHOFF, S., 2005. Sudestadas. In: Barros, V.; Menéndez, A., and Nagy, G. (eds.*), El Cambio Climatico en el Rio de la Plata*. Buenos Aires, Argentina: Universidad de Buenos Aires, pp. 53-67]

BRITISH ANTARTIC SURVEY. www.bas.ac.uk/. Access in 06/13/2022

CAI, W. & COWAN, T., 2007. Trends in Southern Hemisphere Circulation in IPCC AR4Models over 1950–99: Ozone Depletion versus Greenhouse Forcing. J. Clim.20,681–693.

CAI, W., SHI, G., COWAN, T., Bi, D. & RIBBE, J., 2005. The response of the southern annular mode, the east Australian Current, and the southern midlatitude ocean circulation to global warming. Geophys. Res. Lett.32, L23706.

CAI, W., WHETTON, P. H. & KAROLY, D. J. 2003. The response of the Antarctic Oscillation to increasing and stabilized atmospheric CO2.J. Clim.16, 1525–1538

CALLIARI, L.J. & KLEIN, A.H.F. 1993. Características Morfodinâmicas e Sedimentológicas das Praias Oceânicas Entre Rio Grande e Chuí, RS. *Pesquisas em Geociências* 20 (1): 48-56.

CALLIARI, L.J., TOZZI, H.A.M. & KLEIN, A.H.F. 1998. Beach Morphology and Coastline Erosion Associated with Storm Surges in Southern Brazil-Rio Grande to Chuí, RS. *Anais da Academia Brasileira de Ciência*, 70 (2).

CASTELLE, B., DODET, G., MASSELINK, G., & SCOTT, T., 2017. A new climate index controlling winter wave activity along the Atlantic coast of Europe: The West Europe Pressure Anomaly. Geophysical Research Letters, 44(3), 1384–1392. https://doi.org/10.1002/2016GL072379

CHIESSI, C. M., MULITZA, S., PÄTZOLD, J., *WEF*ER, G., & MARENGO, J. A. 2009. Possible impact of the Atlantic Multidecadal Oscillation on the South American summer monsoon. *Geophysical Research Letters*, 36(21), 1–5. https://doi.org/10.1029/2009GL039914

CODIGNOTTO, J. O., DRAGANI, W. C., MARTIN, P. B., SIMIONATO, C. G., MEDINA, R. A. & ALONSO, G. 2012. Wind-wave climate change and increasing erosion in the outer Río de la Plata, Argentina. *Continental Shelf Research*, 38, 110–116. https://doi.org/10.1016/j.csr.2012.03.013

COPERNICUS CLIMATE CHANGE SERVICE (C3S). 2017. ERA5: Fifth generation of ECMWF atmospheric reanalyses of the global climate. *Copernicus Climate Change Service Climate Data Store* (CDS).

COTRIM, C.S.; SEMEDO, A.; LEMOS, G. Brazil Wave Climate from a High-Resolution Wave Hindcast.Climate., 2022. 10, 53. https://doi.org/10.3390/cli10040053

CROWLEY, T. J. &K.-Y. KIM. 1993. Towards development of a strategy for determining the origin of decadal-centennial scale climate variability. *Quaternary Science Reviews*, 12, 375–385, https://doi.org/ 10.1016/S0277-3791(05)80003-4.

DAVIES, J.L. 1964. A morphogenic approach to world shorelines. Zeit. f. *Geomorphology*., 8:27-142.

DEE, D.P., UPPALA SM., SIMMONS, A.J., BERRISFORD, P., POLI P., KOBAYASHI, S., ANDRAE, U., BALMASEDA, M.A., BALSAMO, G., BAUER, P., BECHTOLD, P. BELJAARS, A.C.M., VAN DE BERG, L., BIDLOT, J., BORMANN, N., DELSOL, C., DRAGANI, R., FUENTES, M., GEER, A.J., HAIMBERGER, L., HEALY, S.B., HERSBACH, H., HOLM, E.V., ISAKSEN, L., K´ALLBERG, P., KOHLER, M., MATRICARDI, M., MCNALLY, A.P., MONGE-SANZ, B.M., MORCRETTE, J.J., PARK, B.K., PEUBEY, C., DE ROSNAY, P., TAVOLATO, C., THEPAUT, J.N. & VITART, F. 2011. The ERA-Interim reanalysis: configuration and performance of the data assimilation system. *Quaternary Journal of the Royal Meteorological Society*. 137: 553–597. DOI:10.1002/qj.828.

DE LEO, F., BESIO, G. & MENTASCHI, L. 2021. Trends and variability of ocean waves under RCP8.5 emission scenario in the Mediterranean Sea. *Ocean Dynamics*. 71, 97–117. https://doi.org/10.1007/s10236-020-01419-8

DELWORTH, T. L. & MANN, M.E. 2000. Observed and simulated multidecadal variability in the Northern Hemisphere, *Climate Dynamics*, 16, 661–676, doi:10.1007/s003820000075.

DIJKSTRA, H. A., TE RAA, L., SCHMEITS, M. & GERRITS, J. 2006. On the physics of the Atlantic multidecadal oscillation, *Ocean Dynamics*, 56, 36–50, doi:10.1007/s10236-005-0043-0.

DODET, G., BERTIN, X. & TABORDA, R. 2010 Wave climate variability in the North-East

Atlantic Ocean over the last six decades, *Ocean Modelling*, 31, 120–131.

DOMINGUEZ, J. M. L. 2006. The Coastal Zone of Brazil: An Overview. *Journal of Coastal Research*, 1, 16-20.

D'ONOFRIO, E.E.; FIORE, M.E. & POUSA, J.L. 2008. Changes in the regime of storm surges at Buenos Aires, Argentina. *Journal of Coastal Research*, 24(1A), 260-265.

DORSCH, W., NEWLAND, T., TASSONE, D., TYMONS, S., WALKER, D., 2008. A statistical approach to modeling the temporal patterns of ocean storms. J. Coast. Res. 24 (6), 1430–1438

ELSNER, J. B., T. JAGGER, and X.-F. LIU., 2000. Changes in the rates of North Atlantic major hurricane activity during the 20th century, Geophys. Res. Lett.,27, 1743–1746, DOI:10.1029/2000GL011453

ENFIELD, D.B., A.M. MESTAS, D.A. MAYER, and L. CID-SERRANO., 1999: How ubiquitous is the dipole relationship in tropical Atlantic sea surface temperatures? JGR-O, 104, 7841-7848

ENFIELD, D.B., MESTAS-NUNEZ, A.M. & TRIMBLE, P.J. 2001. The Atlantic Multidecadal Oscillation and its relationship to rainfall and river flows in the continental U.S., *Geophysical Research Letters*, 28: 2077-2080. https://doi.org/10.1029/2000GL012745

EMANUEL, K., 2005. Increasing destructiveness of tropical cyclones over the past 30 years, Nature,436, 686–688, PubMed, doi:10.1038/nature03906

ESCOBAR, G., VARGAS, W. & BISCHOFF, S. 2004. Wind tides in the Rio de la Plata estuary: meteorological conditions. *International Journal of Climatology*, 24(9), 1159-1169.

FOGT, R. L., & MARSHALL, G. J. 2020. The Southern Annular Mode: Variability, trends, and climate impacts across the Southern Hemisphere. WIREs Climate Change, 11(4). doi:10.1002/wcc.652

FRAJKA-WILLIAMS, E., BEAULIEU, C. & DUCHEZ, A. 2017. Emerging negative Atlantic Multidecadal Oscillation index in spite of warm subtropics. *Scientific Reports*, 7(1), 1–8. https://doi.org/10.1038/s41598-017-11046-x

GILLETT, N. P. & THOMPSON, D. W. J. 2003. Simulation of recent Southern Hemisphere climate change. Science 302, 273–275

GARNER, A. J., MANN, M. E., EMANUEL, K. A., KOPP, R. E., LIN, N., ALLEY, R. B. & POLLARD, D. 2017. Impact of climate change on New York City's coastal flood hazard: Increasing flood heights from the preindustrial to 2300 CE. *Proceedings of the National Academy of Sciences of the United States of America,* 114(45), 11861–11866. https://doi.org/10.1073/pnas.1703568114

GODOLPHIM, M.F. 1976. Geologia do Holoceno Costeiro do Município do Rio Grande, RS. *Dissertação de mestrado*, Instituto de Geociências da UFRGS, Porto Alegre, 146 p.

GOLDENBERG, S. B., LANDSEA, C.W., MESTAS-NUNEZ, A. M. & GRAY, W. M. 2001. The recent increase in Atlantic hurricane activity: Causes and implications, *Science*, 293, 474–479, doi:10.1126/science.1060040.

GONZALES, M., NICOLODI, J. L., GUTIÉRREZ, O. Q., LOSADA, V. C. & HERMOSA, A. E. 2016. Brazilian Coastal Processes: Wind, Wave Climate and Sea Level. In: Short, A. D.; Klein, A. H. F. (Org.). *Brazilian Beach Systems.* 1.ed. Switzerland: Springer International Publishingv. 17, p. 37-66

GRASSI, B., G. REDAELLI, and G. VISCONTI., 2005. Simulation of Polar Antarctic trends: Influence of tropical SST,Geophys. Res. Lett.,32, L23806. Doi:10.1029/2005GL023804.

HARLEY, M.D., TURNER, I.L., SHORT, A.D. & RANASINGHE, R. 2010. Interannual variability and controls of the Sydney wave climate. *International Journal of Climatology*. 30 (9), 1322–1335

HEMER, M., CHURCH, J., SWAIL, V. & WANG, X. 2006. Coordinated global wave climate projections. *Atmosphere–Ocean Interactions.* 2, 185–218.

HEMER, M. A., CHURCH, J. A. & HUNTER, J. R. 2010. Variability and trends in the directional wave climate of the Southern Hemisphere. *International Journal of Climatology*, 30(4), 475–491. https://doi.org/10.1002/joc.1900

HEMER, M.A., SIMMONDS, I., KEAY, K., 2008. A classification of wave generation characteristics during large wave events on the Southern Australian margin. Continental Shelf Research28: 634 – 652

HERSBACH, H., BELL, B., BERRISFORD, P., HIRAHARA, S., HORÁNYI, A., MUÑOZ-SABATER, J. &THÉPAUT, J. N. 2020. The ERA5 global reanalysis. *Quarterly Journal of the Royal Meteorological Society*, 146(730), 1999–2049. https://doi.org/10.1002/qj.3803

HOSKINS, B.J. & HODGES, K.I.A. 2005. New Perspective on Sourthern Hemisphere Storm Tracks. *Journal of Climate*, v.18, p. 4108-4129

HURREL, H., KUSHNIR, Y., OTTERSEN, G. & VISBECK, M. 2003. An overview of the North Atlantic oscillation. The North Atlantic Oscillation: Climatic Significance and Environmental Impact, *Geophysical Monograph Series*, Vol. 134, Amer. Geophys. Union, 1–35

INATSU, M., MUKOUGAWA, M. & XIE, S. Tropical and extratropical SST effects on the midlatitude storm track. *J. Meteorol. Soc*. Japan 80, 1069–1076 (2002).

KAYANO, M. T., ROSA, M. B., RAO, V. B., ANDREOLI, R. V. & DE SOUZA, R. A. F. 2019.

Relations of the low-level extratropical cyclones in the southeast Pacific and South Atlantic to the Atlantic multidecadal oscillation. *Journal of Climate*, 32(14), 4167–4178. https://doi.org/10.1175/JCLI-D-18-0564.1

KARUNARATHNA, H., PENDER, D., RANASINGHE, R., SHORT, A.D., REEVE, D.E., 2014. The effects of storm clustering on beach profile variability. Mar. Geol. 348, 103–112

KERR, R. A. 2000: A North Atlantic climate pacemaker for the centuries. *Science*, 288, 1984–1986, https://doi.org/10.1126/ science.288.5473.1984.

KING, C.A.M. 1972. *Beaches and Coasts*. Edward Arnold, London. 573p.

KNIGHT, J. R., ET AL. 2005. A signature of persistent natural thermohaline circulation cycles in observed climate, *Geophysical Research Letters*. 32, L20708, doi:10.1029/2005GL024233.

KNIGHT, J. R., FOLLAND, C. K. & SCAIFE, A. A. 2006. Climate impacts of the Atlantic Multidecadal Oscillation, *Geophysical Research. Letters*. 33, L17706, doi:10.1029/2006GL026242.

KRAVTSOV, S. V. & SPANNAGLE, C. 2008. Multi-decadal climate variability in observed and modeled surface temperatures, *Journal of Climate*. 21, 1104–1121, doi:10.1175/2007JCLI1874.1

KUSHNIR, Y., CARDONE, V. J., GREENWOOD, J. G. & CANE, M. A. 1997. The recent increase in North Atlantic wave heights, *Journal of Climate*, 10, 2107–2113.

LATIF, M. 2013. *The Ocean's Role* in *Modeling and Predicting Decadal Climate Variation*s. Chapter 25. Editor(s): Gerold Siedler, Stephen M. Griffies, John Gould, John A. Church. International Geophysics, Academic Press. Volume 103. Pgs 645-665. ISSN 0074-6142. ISBN 9780123918512.

LYU, K. & YU, J. Y. 2017. Climate impacts of the Atlantic Multidecadal Oscillation simulated in the CMIP5 models: A re-evaluation based on a revised index. *Geophysical Research Letters*, 44(8), 3867–3876. https://doi.org/10.1002/2017GL072681

LORENZ, D.J., HARTMANN, D.L. 2001. Eddy-zonal flow feedback in the Southern Hemisphere. J. Atmosph. Sci. 58, 3312–3327

MACHADO, A. A., CALLIARI, L. J., MELO, E. & KLEIN, A. H. F. 2010. Historical assessment of extreme coastal sea state conditions in southern Brazil and their relation to erosion episodes. *Pan American Journal of Aquatic Sciences*, 5(OCTOBER), 277–286. Retrieved from http://www.panamjas.org/pdf_artigos/PANAMJAS_5(2)_277-286.pdf

MAIA, N. Z., ALMEIDA, L. P., EMMENDORFER, L., NICOLODI, J. L., & CALLIARI, L., 2022. Wave climate trends and breakpoints during the Atlantic Multidecadal Oscillation (AMO) in

southern Brazil. *Ocean and Coastal Research*, *2022*, 22027. https://doi.org/10.1590/2675-2824070.21086nzm

MAIA, N. Z., CALLIARI, L. J. & NICOLODI, J. L. 2016. Analytical model of sea level elevation during a storm: Support for coastal flood risk assessment associated with cyclone passage. *Continental Shelf Research*, 124, 23–34. https://doi.org/10.1016/j.csr.2016.04.012

MARSHALL, G. J., 2003. Trends in the Southern Annular Mode from observations and reanalyses .J. Clim.16, 4134–4143.

MARSHALL, G. J. & CONNOLLEY, W. M. 2006 Effect of changing Southern Hemisphere winter sea surface temperatures on Southern Annular Mode strength. Geophys.Res. Lett.33, L17717

MARSHALL, A. G., HEMER, M. A., HENDON, H. H. & MCINNES, K. L. 2018. Southern annular mode impacts on global ocean surface waves. *Ocean Modelling*, 129, 58–74. https://doi.org/10.1016/j.ocemod.2018.07.007

MASSELINK, G., AUSTIN, M., SCOTT, T., POATE, T., & RUSSELL, P., 2014. Role of wave forcing, storms and NAO in outer bar dynamics on a high-energy, macro-tidal beach. Geomorphology, 226, 76–93. https://doi.org/10.1016/j.geomorph.2014.07.025

MCCABE, G. J., PALECKI, M. A. & BETANCOURT, J. L. 2004. Pacific and Atlantic Ocean influences on multidecadal drought frequency in the United States. *Proceedings of the National Academy of Sciences of the United States of America*. 101, 4136–4141, doi:10.1073/ pnas.0306738101

MEEHL, G., STOCKER, T., COLLINS, W., FIEDLINGSTEIN, P., GAYE, A., GREGORY, KITOH, A., KNUTTI, R., MURPHY, J., NODA, A., RPER, S., WATTERSON, I., WEAVER, A. & ZHAO, Z. 2007. *Climate change 2007: the physical science basis*. Contribution of Working Group I to the Fourth Assessment Report of the Intergovernmental Panel on Climate Change, Chapter Global Climate Projections. Cambridge University Press, Cambridge, United Kingdom and New York, NY, USA. ISBN: 978-0-521-88009-1.

MENDOZA, E.T., JIMENEZ, J.A., MATEO, J., 2011. A coastal storms intensity scale for the Catalan sea (NW Mediterranean). Nat. Hazards Earth Syst. Sci. 11, 2453–2462

MENTASCHI, L., VOUSDOUKAS, M. I., VOUKOUVALAS, E., DOSIO, A. & FEYEN, L. 2017. Global changes of extreme coastal wave energy fluxes triggered by intensified teleconnection patterns. *Geophysical Research Letters*. 44, 2416–2426.

MEUCCI, A., YOUNG, I. R., HEMER, M., KIREZCI, E., & RANASINGHE, R. 2020. Projected 21st century changes in extreme wind-wave events. *Science Advances*, *6*(24), 1–10. https://doi.org/10.1126/sciadv.aaz7295.

MO, K.C., WHITE, G.H. 1985. Teleconnections in the Southern Hemisphere. Mon. Weather Rev. 113, 22–37

MORI, N., YASUDA, T., MASE, H., TOM, T. & OKU, Y. 2010. Projection of extreme wave climate under global warming. *Hydrological Research Letters* 4, 14–19.

MORIM, J., HEMER, M., WANG, X. L., CARTWRIGHT, N., TRENHAM, C., SEMEDO, A., … & ANDUTTA, F. 2019. Robustness and uncertainties in global multivariate wind-wave climate projections. *Nature Climate Change*, 9(9), 711–718. https://doi.org/10.1038/s41558-019-0542-5.

MOTTA, V. F. 1969. *Relatório-diagnóstico sobre a melhoria e o aprofundamento do acesso pela barra de Rio Grande*.

MUGGEO, V. M. 2003. Estimating regression models with unknown break-points. *Statistics in medicine*, 22(19):3055–3071.

NATIONAL OCEANOC AND ATMOSPHERIC ADMINISTRATION (NOAA) Physical Sciences Laboratory (www.psl.noaa.gov, Access in 06/06/2022)

ODÉRIZ, I., SILVA, R., MORTLOCK, T. R. & MENDOZA, E. 2020a. Climate drivers of directional wave power on the Mexican coast. *Ocean Dynamics*, 70(9), 1253–1265. https://doi.org/10.1007/s10236-020-01387-z

ODÉRIZ, I., SILVA, R., MORTLOCK, T. R., & MORI, N., 2020b. El niño-southern oscillation impacts on global wave climate and potential coastal hazards. Journal of Geophysical Research: Oceans, 125, e2020JC016464. https://doi.org/10.1029/2020JC016464

OLIVEIRA, B. A., SOBRAL, F., FETTER, A. & MENDEZ, F. J. 2019a. A high-resolution wave hindcast off Santa Catarina (Brazil) for identifying wave climate variability. *Regional Studies in Marine Science*, 32, 100834. https://doi.org/10.1016/j.rsma.201.

OLIVEIRA, U. R., SIMÕES, R. S., CALLIARI, L. J. & GAUTÉRIO, B. C. 2019b. Erosão de dunas sob ação de um evento extremo de alta energia de ondas na costa central e sul do Rio Grande do Sul, Brasil. *Revista Brasileira de Geomorfologia*. https://doi.org/http://dx.doi.org/10.20502/rbg.v20i1.1352

O'GRADY, J. G., HEMER, M. A., MCINNES, K. L., TRENHAM, C. E., & STEPHENSON, A. G., 2021. Projected incremental changes to extreme wind-driven wave heights for the twenty-first century. Scientific Reports, 11(1), 1–8. https://doi.org/10.1038/s41598-021-87358-w

O'REILLY, C. H., WOOLLINGS, T. & ZANNA, L. 2017. The dynamical influence of the Atlantic multidecadal oscillation on continental climate. *Journal of Climate*, 30(18), 7213–7230. https://doi.org/10.1175/JCLI-D-16-0345.1

ORTEGA, L., CELENTANO, E., FINKL, C. & DEFEO, O. 2013. Effects of climate variability on

the morphodynamics of Uruguayan sandy beaches. *Journal of Coastal Research*, 29, 747-755.

PARISE, C. K., CALLIARI, L. J. & KRUSCHE, N. 2009. Extreme storm surges in the south of Brazil: atmospheric conditions and shore erosion. *Brazilian Journal of Oceanography*, 57(3): 175-188.

PEREIRA, H. R., REBOITA, M. S., & AMBRIZZI, T. 2017. Características da Atmosfera na Primavera Austral Durante o El Niño de 2015/2016. *Revista Brasileira de Meteorologia*, *32*(2), 293–310. https://doi.org/10.1590/0102-77863220011

PEGORELLI, C., DOTTORI, M., & FORTES, J. F. 2018. Evaluating the gravity wave energy potential off the Brazilian coast. *Brazilian Journal of Oceanography*, *66*(2), 220–233. https://doi.org/10.1590/s1679-87592018011706602PEREIRA, H. P. P., VIOLANTE-CARVALHO, N., NOGUEIRA, I. C. M., BABANIN, A., LIU, Q., de PINHO, U. F., … PARENTE, C. E. (2017). Wave observations from an array of directional buoys over the southern Brazilian coast. *Ocean Dynamics*, *67*(12), 1577–1591. https://doi.org/10.1007/s10236-017-1113-9

PIANCA, C., MAZZINI, P. L., & SIEGLE, E. 2010. Brazilian Offshore Wave Climate Based on NWW3 Reanalysis. *Brazilian Journal of Oceanography*, 58(1), 53-70.

PEZZI, L. P., SOUZA, R. B. DE & QUADRO, M. F. L. 2016. Uma Revisão dos Processos de Interação Oceano-Atmosfera em Regiões de Intenso Gradiente Termal do Oceano Atlântico Sul Baseada em Dados Observacionais. *Revista Brasileira de Meteorologia*, 31(4), 428–453. https://doi.org/10.1590/0102-778631231420150032

QIAN, C., J.-Y. YU, & G. CHEN. 2014. Decadal summer drought frequency in China: The increasing influence of the Atlantic Multi-decadal Oscillation, *Environmental Research Letters*. 9 (12), 124004, doi:10.1088/1748-9326/9/12/124004.

RASMUSSEN, D.J., BITTERMANN, K., BUCHANAN, M.K., KULP, S., STRAUSS, B.H., KOPP, R.E. & OPPENHEIMER, M. 2018. Extreme sea level implications of 1.5 °C, 2.0 °C, and 2.5 °C temperature stabilization targets in the 21st and 22nd century. *Environmental Research Letters*. 13, 034040

REBOITA, M. S., AMBRIZZI, T. & ROCHA, R. P., 2009. Relationship between the Southern Annular Mode and southern hemisphere atmospheric systems. Rev. Bras. Meteorol.24, 48–55.

REDE ONDAS. Universidade Federal do Rio Grande, RS. Avaliable on: www.redeondas.furg.br.

REGUERO, B. G., I. J. LOSADA, & F. J. MENDEZ. 2015. A global wave power resource and its seasonal, interannual and long-term variability, Appl. Energy, 148, 366–380, doi:10.1016/j.apenergy.2015.03.114.

REGUERO, B.G., MÉNDEZ, F.J. & LOSADA, I.J. 2013. Variability of multivariate wave climate in latin america and the Caribbean. *Global and Planetary Change.* 100, 70–84.

REGUERO, B. G., MENÉNDEZ, M., MÉNDEZ, F. J., MÍNGUEZ, R., & LOSADA, I. J., 2012. A Global Ocean Wave (GOW) calibrated reanalysis from 1948 onwards. Coastal Engineering, 65, 38–55. https://doi.org/10.1016/j.coastaleng.2012.03.003

REGUERO, B. G., LOSADA, I. J. & MENDEZ, F. J. 2019. A recent increase in global wave power as a consequence of oceanic warming. *Nature Communications*. 205, 1–14

RODRIGUES, M. L. G., FRANCO, D. & SUGAHARA, S. 2004. Climatologia de frentes frias no litoral de Santa Catarina. *Revista Brasileira de Geofísica*, 22, 135-151.

ROGERS, J.C., VAN LOON, H. 1982. Spatial variability of sea level pressure and 500 mb height anomalies over the Southern Hemisphere. Monthly Weather Rev. 110,1375–1392

SASAKI, D. K., GRAMCIANINOV, C. B., CASTRO, B., & DOTTORI, M. (2021). Intraseasonal variability of ocean surface wind waves in the western South Atlantic: the role of cyclones and the Pacific South American pattern. *Weather and Climate Dynamics*, *2*(4), 1149–1166. https://doi.org/10.5194/wcd-2-1149-2021

SEM GUPTA, A; ENGLAND, M.H. 2006. Coupled Ocean–Atmosphere–Ice Response to Variations in the Southern Annular Mode. Journal of Climate. 19, 4457–4486

SEMEDO, A., SUSELIJ, K., RUTGERSSON, A. & STERL, A. 2011. A global view on the wind sea and swell climate and variability from ERA-40. *Journal of Climate* 24 (5), 1461-1479.

SEMEDO, A., WEISSE, R., BEHRENS, A., STERL, A., BENGTSSON, L. & GÜNTHER, H. 2013. Projection of global wave climate change toward the end of the twenty-first century. *Journal of Climate*, 26(21), 8269–8288. https://doi.org/10.1175/JCLI-D-12-00658.1

SÉNÉCHAL, N., COCO, G., CASTELLE, B., & MARIEU, V., 2015. Storm impact on the seasonal shoreline dynamics of a meso- to macrotidal open sandy beach (Biscarrosse, France). Geomorphology, 228, 448–461. https://doi.org/10.1016/j.geomorph.2014.09.025

SILVA, A.P., KLEIN, A.H.F., FETTER-FILHO, A. F. H., HEIN, C.J., MÉNDEZ, F.J., BROGGIO, M,F. & DALINGHAUS, C. 2020. Climate-induced variability in South Atlantic wave direction over the past three millennia. *Scientific Reports*, 10:18553 | https://doi.org/10.1038/s41598-020-75265-5.

SINCLAIR, M.R. 1995. A climatology of cyclogenesis for the Southern Hemisphere. *Monthly Weather Review*. 123, 1601–1619, https://doi.org/ 10.1175/1520-0493(1995)123,1601:ACOCFT.2.0.CO;2.

SINCLAIR,M.R. 1997. Objective identification of cyclones and their circulation intensity, and climatology. *Weather and Forecasting*, 12, 595–612, https://doi.org/10.1175/1520-0434(1997)012,0595: OIOCAT.2.0.CO;2.

STERL A. & CAIRES, S., 2005. Climatology, variability and extrema of ocean waves: the web-based KNMI/ERA-40 wave atlas. International Journal of Climatology25(7): 963 – 977

SUN, C., J. LI. & S. ZHAO. 2015. Remote influence of Atlantic multidecadal variability on Siberian warm season precipitation, *Scientific Reports*. doi:10.1038/srep16853.

SWAIL, V. R., CECCACCI, E. A. & COX, A. T. 2000. The AES40 north Atlantic wave reanalysis validation and climate assessment, *6th International Workshop on wave hindcasting and forecasting*, Monterey, California, USA.

THE WAMDI GROUP. 1988. The WAM Model - A Third Generation Ocean Wave Prediction Model. *Journal of Physical Oceanography*, 18, 1775-1810.

THOMPSON, D. & WALLACE, J. 1998: The Arctic Oscillation signature in the wintertime geopotential height and temperature fields. *Geophysical Research Letters*, 25, 1297–1300

THOMPSON, D.W.J., WALLACE, J.M. 2000. Annular Modes in the Extratropical Circulation. Part I: Month-to-Month Variability. Journal of Climate. 13, 1000–1016

THOMPSON, D. W. J. & SOLOMON, S. 2002. Interpretation of recent Southern Hemisphere climate change. Science 296, 895–899

TIMMERMANN, A. & COAUTHORS. 2007: The influence of a weakening of the Atlantic meridional overturning circulation on ENSO. *Journal of Climate*, 20, 4899–4919, https://doi.org/10.1175/ JCLI4283.1.

TOMAZELLI, L. J. & VILLWOCK, J. A. 1992. Algumas Considerações sobre o Ambiente Praial e a Deriva Litorânea de Sedimentos ao Longo do Litoral Norte do Rio Grande do Sul, Brasil. *Pesquisas em Geociências*, 19, 1-26.

TRENBERTH, K.E. 1979. Interannual variability of the 500 mb zonal-mean flow in the Southern Hemisphere. Monthly Weather Rev. 107, 1515–1524

TRENBERTH, K., CARON, J., STEPANIAK, D. & WORLEY, S. 2002: Evolution of El Nino–Southern Oscillation and global atmospheric surface temperatures. *Journal of Geophysical Research*, 107, 4065, doi:10.1029/ 2000JD000298.

TRENBERTH, K.E, et al. 2007. Observations : Surface and Atmospheric Climate Change. In Climate Change 2007: The Physical Science Basis. Contribution os Work Group I to the Forth Assessment Report of the Intergovernmental Panel on Climate Change.

TRENBERTH, K. E. & SHEA, D. J. 2006. Atlantic hurricanes and natural variability in 2005.

Geophysical Research Letters 33, L12704, doi:10.1029/2006GL026894.

TRENBERTH, KEVIN, ZHANG, RONG & NATIONAL CENTER FOR ATMOSPHERIC RESEARCH STAFF (Eds). Last modified 05 Jun 2021. "*The Climate Data Guide: Atlantic Multi-decadal Oscillation (AMO)*." Retrieved from https://climatedataguide.ucar.edu/climate-data/atlantic-multi-decadal-oscillation-amo. Accessed in 09/05/2021.

VAN DER MEER, J.W., ALLSOP, N.W.H., BRUCE, T., DE ROUCK, J., KORTENHAUS, A., PULLEN, T., SCHUTTRUMPF, H., TROCH, P. and ZANUTTIGH, B., 2016. EurOtop, Manual on wave overtopping of sea defences and related structures. An overtopping manual largely based on European research, but for worldwide application www.overtopping-manual.com.

VOUSDOUKAS, M. I., MENTASCHI, L., VOUKOUVALAS, E., BIANCHI, A., DOTTORI, F & FEYEN, L. 2018. Climatic and socioeconomic controls of future coastal flood risk in Europe. *Nature Climate Change*, 8(9), 776–780. https://doi.org/10.1038/s41558-018-0260-4

WAN, W., Y., FAN, C., DAI, Y., LI, L., SUN, W. & ZHOU, P. 2018. Assessment of the Joint Development Potential of Wave and Wind Energy in the South China Sea, 1–26. *Energies*. https://doi.org/10.3390/en11020398

WANG, G., & CAI, W., 2013. Climate-change impact on the 20th-century relationship between the Southern Annular Mode and global mean temperature. Scientific Reports, 3, 1–6. https://doi.org/10.1038/srep02039

WANG, X. L. SWAIL, V. R. 2000. Changes of extreme wave heights in Northern hemisphere oceans and related atmospheric circulation regimes, *Journal of Climate*, 14, 2204–2221.

WANG, X. L., ZWIERS, F. W. & SWAIL, V. R. 2003. North Atlantic ocean wave climate change scenarios for the twenty-first century, *Journal of Climate*, 17, 2368–2383.

WANG, C., and D.B. ENFIELD., 2001: The tropical Western Hemisphere warm pool, Geophys. Res. Lett., 28, 1635-1638.

WANG, C., LEE, S. K. & ENFIELD, D. B. 2008. Atlantic warm pool acting as a link between atlantic multidecadal oscillation and atlantic tropical cyclone activity. *Geochemistry, Geophysics, Geosystems*, 9(5). https://doi.org/10.1029/2007GC001809

WANG, Y., LI, S. & LUO, D. 2009. Seasonal response of Asian monsoonal climate to the Atlantic Multidecadal Oscillation. 114 (November 2008). *Journal of Geophysical Research*. https://doi.org/10.1029/2008JD010929

WASEDA, T., WEBB, A., SATO, K., INOUE, J., KOHOUT, A., PENROSE, B. & PENROSE, S.

2018. Correlated Increase of High Ocean Waves and Winds in the Ice-Free Waters of the Arctic Ocean. *Scientific Reports*, 1–9. https://doi.org/10.1038/s41598-018-22500-9

WEBSTER, P. J., G. J. HOLOLAND, J. A. CURRY, and H.-R. CHANG., 2005. Changes in tropical cyclone number, duration, and intensity in a warming environment. Science,309, 1844–1846 PubMed, doi:10.1126/science.1116448

YANG, Y. M., AN, S. IL, WANG, B. & PARK, J. H. 2020. A global-scale multidecadal variability driven by Atlantic multidecadal oscillation. *National Science Review*, 7(7), 1190–1197. https://doi.org/10.1093/nsr/nwz216

YOUNG, I. R., ZIEGER, S. & BABANIN, A. V. 2011. Global trends in wind speed and wave height. *Science*, 332, 451–455.

ZHANG, R. & DELWORTH, T.L. 2005. Simulated tropical response to a substantial weakening of the Atlantic thermohaline circulation. *Journal of Climate*, 18(12), 1853–1860, doi:10.1175/JCLI3460.1.

ZHENG, F., J. LI, R. T. CLARK, and H. C. NNAMCHI., 2013. Simulation and projection of the Southern Hemisphere annular mode in CMIP5 models. J. Clim.,26(24), 9860–9879, doi:10.1175/JCLI-D-13-00204.1.